

FINITE ELEMENT ANALYSIS OF DEFORMATION BEHAVIOR OF
CONCRETE FACED KONYA AFŞAR HADIMI DAM AND COMPARISON OF
RESULTS WITH MEASUREMENTS

A THESIS SUBMITTED TO
THE GRADUATE SCHOOL OF NATURAL AND APPLIED SCIENCES
OF
MIDDLE EAST TECHNICAL UNIVERSITY

BY

DOĞUŞCAN KARDEŞ

IN PARTIAL FULFILLMENT OF THE REQUIREMENTS
FOR
THE DEGREE OF MASTER OF SCIENCE
IN
CIVIL ENGINEERING

AUGUST 2019

Approval of the thesis:

**FINITE ELEMENT ANALYSIS OF DEFORMATION BEHAVIOR OF
CONCRETE FACED KONYA AFŞAR HADIMI DAM AND COMPARISON
OF RESULTS WITH MEASUREMENTS**

submitted by **DOĞUŞCAN KARDEŞ** in partial fulfillment of the requirements for
the degree of **Master of Science in Civil Engineering Department, Middle East
Technical University** by,

Prof. Dr. Halil Kalıpçılar
Dean, Graduate School of **Natural and Applied Sciences**

Prof. Dr. Ahmet Türer
Head of Department, **Civil Engineering**

Prof. Dr. Erdal Çokça
Supervisor, **Civil Engineering, METU**

Prof. Dr. M. Yener Özkan
Co-Supervisor, **Civil Engineering, METU**

Examining Committee Members:

Prof. Dr. Tamer Topal
Geological Engineering, METU

Prof. Dr. Erdal Çokça
Civil Engineering, METU

Prof. Dr. M. Yener Özkan
Civil Engineering, METU

Assist. Prof. Dr. Nejan Huvaj Sarıhan
Civil Engineering, METU

Assoc. Prof. Dr. Berna Unutmaz
Civil Engineering, Hacettepe University

Date: 19.08.2019

I hereby declare that all information in this document has been obtained and presented in accordance with academic rules and ethical conduct. I also declare that, as required by these rules and conduct, I have fully cited and referenced all material and results that are not original to this work.

Name, Surname: Dođuşcan Kardeş

Signature:

ABSTRACT

FINITE ELEMENT ANALYSIS OF DEFORMATION BEHAVIOR OF CONCRETE FACED KONYA AFŞAR HADIMI DAM AND COMPARISON OF RESULTS WITH MEASUREMENTS

Kardeş, Doğuşcan
Master of Science, Civil Engineering
Supervisor: Prof. Dr. Erdal Çokça
Co-Supervisor: Prof. Dr. M. Yener Özkan

August 2019, 131 pages

To eliminate the problem of scarcity of appropriate fill material in the vicinity of construction site, concrete faced dam is a commonly preferred alternative for embankment dams. Functioning as an impervious membrane, the concrete face makes it possible to use dumped rockfill, compacted rockfill or sand-gravel fill as the dam body material. In this study, deformation behavior of Konya Afşar Hadimi Dam, which is a concrete faced rockfill dam, was investigated by finite element analyses using Plaxis and Midas GTS NX programs. Hardening soil model was used to account for stress dependence of stiffness, nonlinear behavior and inelastic deformation characteristics of rockfill. Analysis results were compared with the data collected from the instruments placed in the dam body. It was seen that, 2-D and 3-D analyses yield significantly different results concerning the settlements and vertical stresses, although the same material parameters are used. It was observed that arching effect should be considered in the deformation analyses of concrete faced rockfill dams located in narrow and asymmetrical valleys, to reach accurate estimates of the actual behavior.

Keywords: Concrete Faced Rockfill Dams, Settlement, Finite Element Analysis,
Hardening Soil Model

ÖZ

ÖN YÜZÜ BETON KAPLI KONYA AFŞAR HADİMİ BARAJI'NIN DEFORMASYON DAVRANIŞI SONLU ELEMAN ANALİZİ VE BULGULARIN ÖLÇÜMLERLE KARŞILAŞTIRILMASI

Kardeş, Doğuşcan
Yüksek Lisans, İnşaat Mühendisliği
Tez Danışmanı: Prof. Dr. Erdal Çokça
Ortak Tez Danışmanı: Prof. Dr. M. Yener Özkan

Ağustos 2019, 131 sayfa

Ön yüzü beton kaplı baraj tasarımı, dolgu baraj için uygun dolgu malzemesinin yetersizliği sorununu ortadan kaldırmak için sıklıkla tercih edilen bir alternatiftir. Beton ön yüz geçirimsiz bir perde görevi görüp, yığma kaya, sıkıştırılmış kaya ve kum-çakıl dolgu kullanımını mümkün kılmaktadır. Bu çalışmada, ön yüzü beton kaplı kaya dolgu bir baraj olan Konya Afşar Hadimi Barajı'nın deformasyon davranışı sonlu eleman programları Plaxis ve Midas GTS NX ile incelenmiştir. Zeminin doğrusal olmayan davranışı, elastik olmayan deformasyon karakteri ve rijitliğin gerilme bağımlılığını göz önünde bulundurmak için sertleşen zemin modeli kullanılmıştır. Analizlerden elde edilen bulgular baraj gövdesine yerleştirilmiş cihazların ölçümleriyle karşılaştırılmıştır. 2 ve 3 boyutlu analizlerin aynı malzeme parametreleri kullanılmasına karşın farklı sonuçlar verdiği görülmüştür. Buna bağlı olarak, özellikle dar ve asimetric vadilerde yer alan ön yüzü beton kaplı kaya dolgu barajların analizinde, kemerlenme etkisini göz önünde bulundurmanın gerçeğe yakın sonuçlar elde etmedeki önemi gözlemlenmiştir.

Anahtar Kelimeler: Ön Yüzü Beton Kaplı Kaya Dolgu Barajlar, Oturma, Sonlu Elemanlar Analizi, Sertleşen Zemin Modeli

To my family; Çağılsu, Arzu and Ersin Kardeş

ACKNOWLEDGEMENTS

First and foremost, I would like to express my sincere gratitude to my supervisor Prof. Dr. Erdal Çokça, and co-supervisor Prof. Dr. M. Yener Özkan for their guidance, advice and especially patience.

I would like to thank İlker Peker, Gülru S. Yıldız, M.Sc., and Prof. Dr. Yalın Arıcı for their suggestions and interest.

I owe special thanks to Mehmet Kozluca, M.Sc., for his patience and encouragements, and my colleagues in Inpro Engineering for their motivation. I wish to thank my friends, Kemal Işık, Ozan Orhan, and Uğur Duru for their continuous support.

Throughout this study and my professional life, guidance and enthusiasm of Akın Oyat, M.Sc., have been invaluable to me.

Last but not least, I am deeply grateful to my dear family. I would like to thank my parents Arzu and Ersin Kardeş for their endless love and support. Their vision, patience and care help me overcome all the difficulties. I am thankful to Çağılsu Kardeş for being such an amazing sister. Their presence always gave me strength and happiness.

TABLE OF CONTENTS

ABSTRACT	v
ÖZ	vii
ACKNOWLEDGEMENTS	x
TABLE OF CONTENTS	xi
LIST OF TABLES	xiii
LIST OF FIGURES	xv
LIST OF ABBREVIATIONS	xix
CHAPTERS	
1. INTRODUCTION	1
2. CONCRETE FACED ROCKFILL DAMS	3
2.1. General	3
2.2. Design Principles	6
2.2.1. Dam Section	11
2.2.2. Zoning	12
2.2.3. Rockfill Materials	14
2.2.4. Concrete Face	16
2.3. Deformation Analyses of CFRDs	20
2.3.1. Material Models	21
2.3.2. Parameters	28
2.3.3. A Review of Literature on Deformation Behavior of CFRDs	37
2.3.3.1. Alto Anchicaya Dam – Colombia	40
2.3.3.2. Shuibuya Dam – China	40

2.3.3.3. Tianshengqiao-1 Dam – China	41
2.3.3.4. Mohale Dam – Lesotho	42
2.3.3.5. Karahnjukar Dam – Iceland.....	43
2.3.3.6. Kürtün Dam – Turkey.....	45
2.3.3.7. Çokal Dam – Turkey	46
2.3.3.8. Dim Dam – Turkey.....	48
3. KONYA AFŞAR HADİMİ DAM	49
3.1. General Information.....	49
3.2. Instrumentation	57
3.2.1. Total Pressure Gauge.....	62
3.2.2. Vibrating Wire Piezometer.....	63
3.2.3. Hydraulic Settlement Cell	64
3.3. Observed Behavior in Construction Period	65
3.4. Finite Element Analysis of Deformation Behavior.....	73
3.4.1. Deformation Behavior of Afşar Dam in Construction Period.....	79
3.4.2. Effects of the Valley Shape on Deformation Behavior of Afşar Dam.....	94
3.4.3. 3-D Analysis of Afşar Dam in Construction Period.....	99
3.4.4. Deformation Behavior of Afşar Dam at Reservoir Impoundment.....	108
4. SUMMARY AND CONCLUSIONS.....	117
4.1. Conclusions.....	117
4.2. Recommendations.....	119
REFERENCES	121

LIST OF TABLES

TABLES

Table 2.1. Evolution of Concrete Faced Rockfill Dams	4
Table 2.2. Face Slab Properties of CFRDs, Example Projects (Materon, 2008)	19
Table 2.3. Information on CFRDs, Example Projects	39
Table 3.1. Compaction Specifications for Zones of Afşar Dam	53
Table 3.2. Total Stress Monitoring Results and Approximate Overburden Pressures	70
Table 3.3. Model Parameters Used in Finite Element Analysis of Nam Ngum-2 Dam (Sukkarak et al., 2017)	78
Table 3.4. Afşar Dam Deformation Analysis Models.....	80
Table 3.5. Material Parameters Used in Model-1 and Model-2.....	83
Table 3.6. Calculated Settlements in Model-1, Model-2 and Model-3.....	87
Table 3.7. Final Parameters of Zones 3B and 3C for Models 4 and 5	90
Table 3.8. Comparison of Settlement Results of 2-D Plane Strain Analyses	91
Table 3.9. Comparison of Total Vertical Stresses of 2-D Plane Strain Analyses	91
Table 3.10. Comparison of Settlement Results of 3-D Analyses at Km: 0+185	100
Table 3.11. Comparison of Total Vertical Stresses of 3-D Analyses at Km: 0+185	100
Table 3.12. Comparison of Settlement Results of 3-D Analyses at Km: 0+135	103
Table 3.13. Comparison of Total Vertical Stresses of 3-D Analyses at Km: 0+135	103
Table 3.14. Comparison of Settlement Results of 3-D Analyses at Km: 0+270	103
Table 3.15. Comparison of Total Vertical Stresses of 3-D Analyses at Km: 0+270	103
Table 3.16. Comparison of Settlement Results of 3-D Analysis Model-7 at Km: 0+185	115

Table 3.17. Comparison of Total Vertical Stresses of 3-D Analysis Model-7 at Km:
0+185 115

LIST OF FIGURES

FIGURES

Figure 2.1. Section View of a CFRD and Typical Details of Parapet Wall and Plinth	8
Figure 2.2. Zones of a Typical CFRD (ICOLD, 2004)	12
Figure 2.3. Extruded Curb Detail of the Ita Method	18
Figure 2.4. Stress-Strain Relation of an (a) Elastic-Perfectly Plastic Material and a (b) Hyperbolic Material (Ti et al., 2009)	21
Figure 2.5. Stress-Strain Relations of Rock and Soil Samples (Lublinter & Moran, 1992)	24
Figure 2.6. E_i , E_{50} , and E_{ur} represented on q - ε_1 curve (Ti et al., 2009)	26
Figure 2.7. Grain Sizes and Parallel Gradation of a Quarry Rock Sample (Dorador and Urrutia, 2017)	30
Figure 2.8. Arrangement of an In-Situ Large Scale Direct Shear Test (Sowers et al., 1961)	33
Figure 2.9. Representation of the Rockfill Dam and Analysis Model (Deluzarche et al, 2006)	35
Figure 2.10. Numerical Model of a Triaxial Test Sample, Particle Gradations of Laboratory Test Sample and Numerical Test Sample (Shao et al, 2013)	36
Figure 3.1. Upstream View of Afşar Dam (DSİ, 2016)	49
Figure 3.2. Location of Afşar Dam and Plan View of the Reservoir Area	50
Figure 3.3. Plan View of Afşar Dam with Instrumented Stations at Km: 0+135, 0+185, and 0+270	51
Figure 3.4. a) Longitudinal South and b) Upstream Top Views of Afşar Dam, c) Embankment Construction	52
Figure 3.5. Cross Section of Afşar Dam	54
Figure 3.6. Longitudinal Section View of Afşar Dam from Upstream	55
Figure 3.7. Geological Map of Afşar Dam	57

Figure 3.8. Dam Section and Monitoring Devices at Km: 0+135	59
Figure 3.9. Dam Section and Monitoring Devices at Km: 0+185	60
Figure 3.10. Dam Section and Monitoring Devices at Km: 0+270	61
Figure 3.11. Circular and Rectangular Total Pressure Gauges (Roctest, 2016)	62
Figure 3.12. Vibrating Wire Piezometer (Roctest, 2017)	64
Figure 3.13. Hydraulic Settlement Cell (DGSI, 2018)	65
Figure 3.14. Face Slab Normal Deflection vs. Shape Factor for Selected CFRDs (Escobar and Posada, 2008).....	67
Figure 3.15. Total Monitored Settlements at Section Km: 0+135.....	68
Figure 3.16. Total Monitored Settlements at Section Km: 0+185.....	68
Figure 3.17. Total Monitored Settlements at Section Km: 0+270.....	69
Figure 3.18. Total Monitored Pressures at Section Km: 0+135	71
Figure 3.19. Total Monitored Pressures at Section Km: 0+185	71
Figure 3.20. Total Monitored Pressures at Section Km: 0+270	72
Figure 3.21. Zoning and Construction Sequences of Nam Ngum-2 CFRD (Sukkarak et al., 2017)	75
Figure 3.22. Three-Dimensional View and Cross Sections of Nam Ngum 2 Dam (Sukkarak et al., 2017).....	75
Figure 3.23. Reference Points Evaluated in the Analyses	81
Figure 3.24. Finite Element Mesh Used in 2-D Analyses	82
Figure 3.25. Computer Model of Afşar Dam, with only Zone 3B (Model-1).....	82
Figure 3.26. Computer Model of Afşar Dam, with Zones 3B and 3C (Model-2).....	82
Figure 3.27. Calculated Total Settlements of Model-1.....	85
Figure 3.28. Calculated Total Settlements of Model-2.....	85
Figure 3.29. Finite Element Mesh of the Model with 5m lifts (Model-3).....	86
Figure 3.30. Calculated Total Settlements of Model-3.....	88
Figure 3.31. Calculated Total Settlements of Model-4.....	92
Figure 3.32. Calculated Total Settlements of Model-5.....	92
Figure 3.33. Total Vertical Stress Contours of Model-4	93
Figure 3.34. Total Vertical Stress Contours of Model-5	93

Figure 3.35. Representative General Deformation Behavior of an Embankment (Özkuzukıran, 2005)	94
Figure 3.36. Settlement and Total Pressure Recordings on El.1180.0 at Km: 0+18595	
Figure 3.37. Monitored Total Vertical Stress and Settlement Values at the Axis of Afşar Dam	98
Figure 3.38. Defined Sections of Afşar Dam for 3-D Model.....	101
Figure 3.39. 3-D Views of Bedrock, Dam Body and Zoning	102
Figure 3.40. Settlement Results at Km: 0+185 at the End of Construction (Model-6)	105
Figure 3.41. Total Vertical Stress Results at Km: 0+185 at the End of Construction (Model-6)	105
Figure 3.42. Settlement Results at Km: 0+185 at the End of Construction (Model-7)	106
Figure 3.43. Total Vertical Stress Results at Km: 0+185 at the End of Construction (Model-7)	106
Figure 3.44. Frequency Distribution of Settlements Monitored to Calculated at Km: 0+185 (N=9).....	107
Figure 3.45. Frequency Distribution of Settlements Monitored to Calculated at Km: 0+185 (N=7).....	107
Figure 3.46. Settlement Results at Km: 0+185 at the End of Construction (Model-7)	110
Figure 3.47. Settlement Results at Km: 0+185 at Reservoir Impoundment (Model-7)	110
Figure 3.48. Total Vertical Stress Results at Km: 0+185 at the End of Construction (Model-7)	111
Figure 3.49. Total Vertical Stress Results at Km: 0+185 at Reservoir Impoundment (Model-7)	111
Figure 3.50. Horizontal Displacements at Km: 0+185 at the End of Construction (Model-7)	112

Figure 3.51. Horizontal Displacements at Km: 0+185 at Reservoir Impoundment (Model-7)..... 112

Figure 3.52. Shear Stresses at Km: 0+185 at the End of Construction (Model-7).. 113

Figure 3.53. Shear Stresses at Km: 0+185 at Reservoir Impoundment (Model-7) . 113

LIST OF ABBREVIATIONS

- CFRD: Concrete Faced Rockfill Dam
- DEM: Discrete Element Method
- DSI: General Directorate of State Hydraulic Works
- ECRD: Earth Core Rockfill Dam
- EoC: End of Construction
- FEM: Finite Element Method
- ICOLD: International Commission on Large Dams
- RI: Reservoir Impoundment
- USBR: United States Bureau of Reclamation

CHAPTER 1

INTRODUCTION

Throughout the history, the need of water led the humans to construct water storage structures. The primary need to store water for domestic needs is one of many purposes of building dams, including irrigation, industrial uses and hydroelectric energy production. Scarcity of quality materials, difficult construction conditions, budget constraints, combined with the development in science and technology, resulted in alternative dam types; one of which is impervious faced rockfill dams. A concrete faced rockfill dam (CFRD) is a type of impervious faced rockfill dam, relying on the rockfill embankment for stability, providing upstream impermeability by a concrete face slab. Advantages provided in cost, scheduling and performance made the concrete faced rockfill dam a preferable alternative dam type.

With an evolution of about 200 years, the design of CFRD's depend on empirical knowledge, due to modelling and experiment scaling difficulties. Data collection and observations on constructed dams provide engineers experimental knowledge for future projects, making dam instrumentation vital for the improvement of CFRD design. Also, usage of finite element modelling for verification of gathered data for future reference improved the design knowledge for almost 50 years.

This study focuses on the two- and three-dimensional analyses of 127 m high Afşar Dam located in Konya, for construction and reservoir impoundment periods. Construction period calculations are compared to the measurements made; and predictions are made based on the analyses for the reservoir impoundment period. Two-dimensional analyses are made by finite element analysis software Plaxis; using Hardening Soil model as the material model for rockfill embankment to simulate the inelastic, nonlinear and stress dependent behavior of rockfill. Hardening soil model is

a modified version of Duncan-Chang hyperbolic model. Model parameters are derived evaluating previous studies on similar projects. Preliminary parameters are iterated comparing the analysis results with monitored behavior. The estimated parameters from two-dimensional strain analyses are used to study the three-dimensional analyses by finite element software Midas GTS NX. Hardening Soil model is used also in the three-dimensional model; to evaluate the effects of valley shape on the overall deformation behavior of the dam body. Calculated results from the two- and three-dimensional analyses are compared with the instrumentation recordings.

CHAPTER 2

CONCRETE FACED ROCKFILL DAMS

2.1. General

Referring to the definition made in 1939 ASCE Symposium, a rockfill dam is a dam consisting of loose dumped rockfill with slopes on both faces closely approximating natural slopes with an impervious facing on the upstream side (Galloway, 1939). Although usage of rockfill materials in dam construction dates to ancient Egypt; with recorded impervious faced dams, for example La Granjilla dam constructed in 1660's in Spain, origination of modern rockfill dam construction is accepted to be 1850's, in the California gold rush (Cruz et al, 2010). Evolution of rockfill dams with impervious face started with mortar, lime and timber as facing material, followed by concrete and asphalt. Including constructed, under construction and proposed ones, there are known to be more than 600 concrete faced rockfill dams in the World. Cooke states that the CFRDs were not invented but rather developed by contributions of many engineers; keeping in mind that design of CFRDs evolved by empirical knowledge (Cooke, 1984). Following part summarizes improvements starting from the very first rockfill dams.

In the 18th Terzaghi Lecture given by Cooke, the evolution of modern rockfill dam is identified in three periods, as “the early period”, “transition period”, and “modern period” (Cooke, 1984). A summarized representation of the evolution of CFRDs can be seen in Table 2.1. In the early period, from 1850 to 1940, using the know-how gained on blasting and availability of rock, the miners of California built rockfill dams with timber and concrete upstream faces for water storage. Dumped rockfill was used for building the embankment in these dams. Though they performed safely, leakage

problems occurred. This efficiency issue led to the development of earth core rockfill dams.

Table 2.1. *Evolution of Concrete Faced Rockfill Dams*

<i>Early Period</i>	<i>Transition Period</i>	<i>Modern Period</i>
1850 - 1940	1940 - 1965	1965 -
Dumped Rockfill	Compacted Rockfill	Compacted Rockfill
Timber/Concrete Face	Concrete Face	Concrete Face
Leakage Problems	Higher Dams Scarcity of Quality Material	Optimization Improvements

The early period is followed by the transition period, which refers to the transition in embankment construction method from dumped to compacted rockfill. This is a two-decade period initiated by the need for higher dams and scarcity of high-quality rock. As indicated by Cooke, this was a period of aggressive experimentation in both design and construction (Cooke, 1984). Unlike other embankment dam types, limit equilibrium analyses are not applicable to a typically dimensioned concrete faced rockfill dam; as the ratio of vertical loads to horizontal forces is generally higher. Due to this, design of CFRDs is empirical and development only occurred with experiences gained from previous projects. This point of view strengthens the importance of the transition period by changing properties of CFRDs making it possible to use weaker rocks, construction in smaller layers, reducing the leakage rates. This period, although development of earth core rockfill dam (ECRD) projects were realized, resulted at a point which it was indicated that CFRD is a competitive alternative for ECRD in many sites mainly due to cost advantages. Though both CFRDs and ECRDs were improved throughout the periods mentioned, foundation treatment costs, rapid construction and greater freedom in material choice made CFRDs preferable in many cases.

The third period is the modern period, in which the definition of a rockfill dam deserves to be changed to a dam that relies on compacted rockfill as the main structural element. In this period higher dams were built with thinner concrete faces, less

reinforcing and improved joint design. Especially in this period is when CFRD is the most feasible alternative for many dam construction projects because of its superiority over other dam types in overall aspects.

Korkmaz evaluated the selection of CFRD for a dam project on Gökçeler River in Antalya (Korkmaz, 2009). In the study a comparison was made between CFRD and earth core rockfill and roller-compacted concrete dam types. Located in a mountainous terrain with high precipitation rates in the summer and near useful rockfill quarries; Gökçeler Dam project was designed in the preliminary stage at a height of 103,0 m above a schist formation under 2-10 m of alluvium. Korkmaz (2009) prepared a cost comparison considering labor costs, annual expenses to irrigation benefits and internal rate of returns. Also including time as a dimension in the analysis, work schedules were designed for each alternative to reach a more accurate estimation. Regarding the operation and maintenance costs, interest and projected irrigation benefits, the study reaches the conclusion of a CFRD being the most profitable alternative. Although from the perspective of investment expenditures each alternative has similar costs, including the future projection of cost comparison the results show a CFRD is probably the most feasible to be constructed.

Another example for the selection of CFRD as the most feasible dam type alternative is Ilisu Dam in Turkey, which is the largest CFRD by embankment volume in Turkey. In the preliminary studies, Ilisu Dam was planned to be designed as either a clay core rockfill dam or a CFRD. Because the site investigation and trial embankment results showed that basalt, one of the two materials available to be used for the construction of embankment, was angular and had inappropriate compaction ratios, CFRD was not considered to be the preferable alternative. However, clay material amount and the quality of obtained clay was not found to be appropriate to be used for the core construction. Due to scarcity of appropriate clay material, and the estimated cost and time to be lost for processing the clay to better properties, a modified cross section was designed in which marly limestone was to be placed in upstream and basalt to be

placed in downstream; which was selected as the final design of Ilisu CFRD (Yenigun, 2013).

Through the periods of evolution of CFRDs, in contrast to the probable expectation on a design perspective that briefly depends on trial and error, the observed performance is commonly satisfactory; examples from case studies are given in Section 2.3.3. Observed performance of CFRDs reflects the adoption of proper design principles and assumptions in the aspect of engineering. Briefly, the main design principles, the development of the elements of a CFRD, and construction methods implemented to ensure adequate performance are discussed in the following sections.

2.2. Design Principles

Design of CFRDs is mainly empirical, that is, the preliminary design of a CFRD is made based on the conditions of its foundation and valley, deriving data from previous similar projects. Foundation conditions and available construction materials determine the design of CFRDs. Cross sections and zone thicknesses are generally selected based on precedent. Details of the project are prepared based on the results of site investigations and laboratory tests. The advantage in the design of a CFRD is that if the required flexibility of face slab and its connection to the toe slab are assured, standard zoning and construction technique of common practice provide adequate performance.

Stability, displacement behavior and permeability are the main concerns for CFRD design. Stability, which is one of the major points in embankment dam design, is ensured by the rockfill embankment in conventional cross sections. As stated by Cooke and Sherard (1987), rockfills cannot fail along plane or circular surfaces, whenever dumped or compacted, if the external slopes are 1,3H:1,0V or 1,4H:1,0V,

which are the usual slopes in CFRDs, because the friction angle of the rockfills are at least 45° , and this is already a guarantee of stability.

Subsections to be considered in the design of CFRDs can be listed as foundation and ground improvement, zoning, rockfill embankment, toe slab, perimeter joint and concrete face slab.

Excavation for the foundation of a CFRD focuses on removing alluvial deposits roughly, and this preparation is considered more important in the upstream half of the dam due to the assumption that essentially all the water load is transferred to the foundation through the upstream half. Although there are examples of CFRD projects in which except local removals near the plinth, the alluvium was not removed in foundation excavations, such as Alto Anchicaya, Aguamilpa, Golillas and Salvajina dams; it is common practice to remove the alluvium layer to prevent unexpected settlement (Cruz et al, 2010).

The toe slab, also named as plinth, controls the flow through the foundation. It is constructed to provide the bond between the foundation and concrete face. The toe slab has an important role on the performance of the dam, therefore, the dimensioning and stability analysis of the toe slab are key elements of CFRD design. Depending on foundation conditions, the toe slab can be constructed directly above rock foundation or after excavation of a trench reaching acceptable foundation conditions. Stability of the toe slab is a main concern for the design especially in high dams, since it must not fail under the water pressure.

Perimeter joint is a critical element for CFRDs as a poorly designed or constructed perimeter joint expands until failure and this leads to high leakage rates. Perimeter joint is the connection element between concrete face and the toe slab, sealing the impervious upstream face of the dam while providing displacement ability for the concrete face without cracks occurring. As indicated by ICOLD (2004), displacement of the concrete face can occur normal to the perimeter joint, normal to the face slab, and parallel to the perimeter joint. Initial design of the perimeter joint included two

water barriers, a copper waterstop at the bottom of the joint. For higher CFRDs, this design is modified to account for increased pressures and displacements. Mastic application under the copper waterstop, increasing the water barrier quantity to three, improvement of the mastic material used on upper water barriers to reach higher extension capacity can be listed as the measures considered in perimeter joint design for high CFRDs.

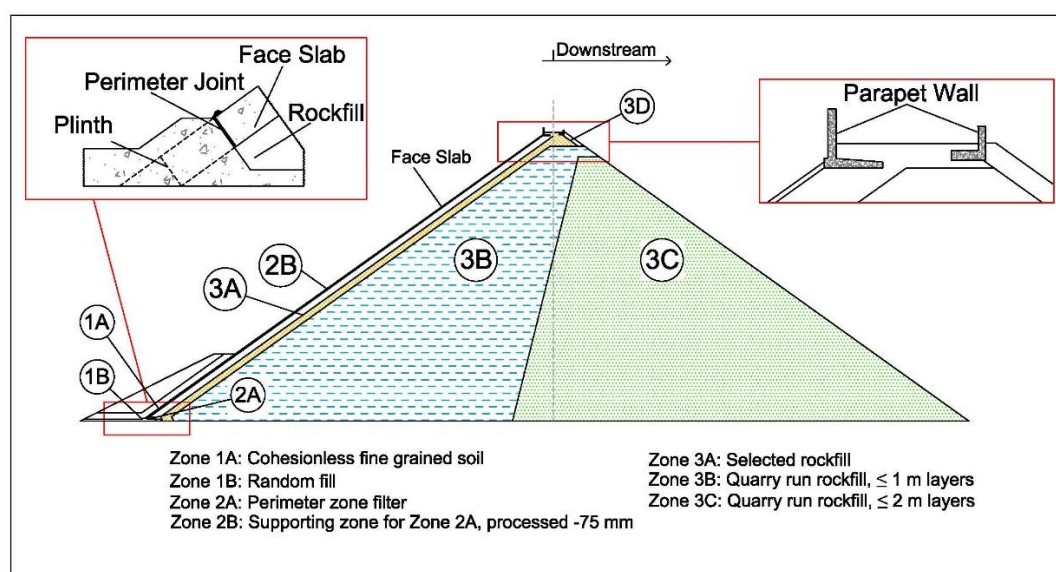


Figure 2.1. Section View of a CFRD and Typical Details of Parapet Wall and Plinth

Cooke states that a parapet wall eliminates the construction of an unnecessary layer of rockfill from the stability point of view, as well as providing a wide working space for slip form concrete pouring works from the crest (Cooke, 1984). It is a preventive measure for maximum water levels at flood events to act as a wave barrier, providing working space for construction of face slab from the crest, access of personnel and delivery of materials. A single parapet wall is commonly constructed at the crest, but depending on the design of the dam, there are projects in which double parapet walls were constructed to provide additional savings in the amount of rockfill used. ICOLD

Committee on Materials for Fill Dams record the height of parapet walls for CFRDs of early period between 1-1,5m, and for CFRDs of modern period up to 8m (ICOLD, 2004). One of the main concerns in design of a parapet wall shall be assuring prevention of leakage at the joint connecting the parapet wall to face slab. Therefore, joint design with usage of a water stop in the middle or at the base of the joint with a mortar pad at the base of the joint are underlined design features of the parapet wall by ICOLD (2004).

The empirical approach underlined for the design of CFRDs has its very reasons present as obstacles even after breakthrough developments in technology and engineering. Deformation of CFRDs has many unknowns so predictions may result in over estimations, but many cracks and ruptures were also observed in previous projects. According to Ma and Chi (2016), main problems in deformation prediction are shortcomings in understanding rockfill behavior and mechanism of face slab rupture, in addition to the scale effects of rockfill material testing. Material models based on continuum mechanics cannot precisely simulate rockfill behavior (Ma et al, 2016). Ma and Chi (2016) also state that tests on rockfill materials generally result in smaller calculated deformations than the measured data for higher dams, whereas larger calculated deformations than the measured data for dams of lower height.

As the empirical approach evolves with every undertaken and monitored project, it is important to point out problems for appropriate revisions and development. Focusing on recent CFRD projects, excessive leakage remains to be a major problem, caused mostly by the cracks in face slab and cushion layer, separation of face slab from cushion layer and concrete rupture along vertical joints. When case studies are investigated in the scope of the mentioned problems; misinterpretation of the general guidelines in design or construction can be observed. Because of the flexibility in rockfill material choice, compaction level and zoning should be examined carefully. Large differences in the compression moduli between upstream and downstream rockfill embankments amplify differential settlement, resulting in afore-mentioned problems. Also concerning the compaction of rockfill, number of vibratory-roller

passes as well as roller weight should be carefully determined, in order not to cause excessive settlements.

From the interaction of concrete face slab and embankment point of view, it is advised to monitor settlements during and after the embankment construction and wait for a plateau period of settlement rate to prevent cracks in concrete face slab due to settlement of embankment. Another point indicated as a possible cause of problems in CFRDs is filling sequence for the rockfill embankment. The filling sequence should be scheduled to prevent height difference between upstream and downstream rockfill as it would cause differential settlement, and scheduling should also focus on flood seasons to take required measures for drainage, water retention and mitigation of possible flood hazards.

Tosun et al (2007), summarized the experience in Turkey on CFRD construction up to 2007 in International Water Power and Dam Construction Magazine, including the design properties of Kürtün, Torul, Atasu, Gördes, Dim, and Marmaris Dams. In the study the general design principles occupied in Turkey in the design of CFRDs were explained. Common side slopes were 1V:1,4H, in addition, five of the mentioned dams were designed to have 1V:1,5H downstream slopes. Quarry rock with maximum particle size of 1000 mm was used in downstream side, and maximum particle size of 600-800 mm was used in upstream side. Fine content and compaction schedules were the same for upstream and downstream sides, 2% and 4-6 passes of 18-20-ton vibratory roller, respectively. Concrete face slab thicknesses of 30-80 cm were used commonly, changing with depth conforming the empirical equation given in the section on concrete face slab design.

In this study, Tosun et al (2007) explained the risk factors for dam structures. Six CFRDs were evaluated in concern of the seismic hazard in a study conducted on the dams in Turkey; Gördes, Marmaris, Dim, Kürtün, Torul and Atasu.

Results of the analyses showed that according to ICOLD classification of risk classes, other than Marmaris Dam, which would be prone to moderate hazard in an earthquake

event, the selected dams were classified with the low hazard rating. Concerning the probability of an earthquake event to occur at a site and its possible consequences, seismic hazard and risk analyses are of importance for critical structures such as dams; approaches and classifications were also evaluated in the study (Tosun et al, 2007).

2.2.1. Dam Section

A typical dam section of a CFRD can be identified in three parts; an impervious upstream face slab of concrete, a transition zone between the concrete face and embankment, and the rockfill embankment body. Though in the history both dumped and compacted rockfill have been used for the embankment, modern CFRD construction relies on compacted rockfill. As it is categorized as an embankment dam, which relies on the materials nearby for the body construction, its large dead weight provides stability, and the structure is safer against deformations and settlements compared to other dam types, as indicated by Yanmaz(2006). Considering limit equilibrium analyses, conventional CFRD design provides side slopes mild and cross section dimensions large enough to provide a stable structure against sliding and overturning.

A CFRD is generally founded on sound rock, above which alluvial deposits of moderate height are scraped. If foundation is composed of weaker rock, the design is revised to adapt to this condition; by means of rockfill compaction criteria, slope and section revisions, and foundation treatment in addition to sealing applications such as cut-off walls where necessary. Upstream and downstream slopes can be as steep as 1,3H:1V, steeper than the slope of typical earthfill dam section of 2,5H:1V.

A typical section of a CFRD is composed of several parts designed to perform for different purposes, and this principle is known as zoning. Zoning provides functioning of the dam with impervious, filter/transition and main rockfill zones. By the usage of

different materials with different compaction schedules in appropriate lifts, the zones are prepared to perform as intended; for the construction of a CFRD to retain water without structural or hydraulic problems.

2.2.2. Zoning

The zones of a dam body are divided according to the aimed purpose of each. The dam body should retain water with adequate impervious layer, deform in a compatible manner throughout the whole body, translate the pore pressure that would accumulate in the voids out of the body. For these generally summarized features, appropriate materials should be defined for each zone. A standard zone design used also for ECRDs is adopted for CFRDs. This divides the CFRD section to three main parts as

Zone 1: impervious

Zone 2: filter/transition zone under concrete slab

Zone 3: main rockfill.

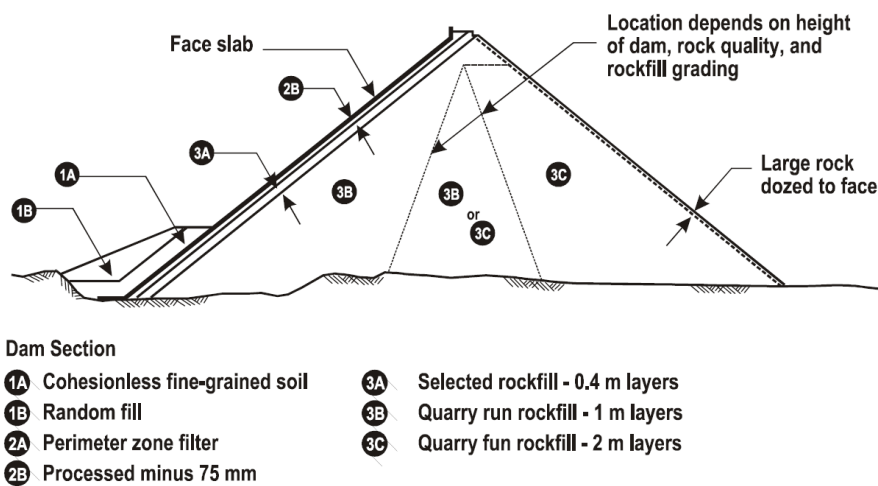


Figure 2.2. Zones of a Typical CFRD (ICOLD, 2004)

Zone 1 is a designated emergency measure; therefore, it is necessary only if a problem develops along the perimeter joint or lower elevations of the face slab. This zone constitutes compacted impervious soil placed upstream of the lower part of face slab. Application of Zone 1 started with Alto Anchicaya dam and had since been adopted in majority of CFRD projects (Cooke et al, 1987). Although dams without this zone are known to perform steadily, it is a preferable element to seal cracks and joint openings with fine impervious soil in case these problems occur. Height and thickness specifications for Zone 1 are not strict due to its remedial nature, but as a guidance it is proposed by Cooke and Sherard (1987), “placing Zone 1 to a level several meters above the original riverbed” to prevent additional load application on the body by debris accumulation. Zone 1 has its subdivisions as Zone 1A and Zone 1B. Zone 1A is constructed using cohesionless materials to avoid brittle cracking; with material of a maximum diameter of 150 mm to migrate through possible cracks in the concrete face. Zone 1B supports Zone 1A and is constructed using a random mix of soil. In several dams, Zone 1 is followed by a sealing concrete application made horizontally through the upstream, to prevent flows through the foundation of the dam.

The initial primary purpose of Zone 2 was to provide a uniform support surface for the concrete face slab (Cooke et al, 1987). Designed as a thin layer of fine rock and sand and constructed in layers with vibratory roller compaction, purpose of this zone has been modified to perform as a filter layer with low permeability to optimize dam design with a smaller concrete face slab thickness. Low permeability provides reliable performance in case a flood occurs before the concrete face construction, and the filter approach for this zone also acts as a remedial measure for leakage, by the finer particles acting as a sealant to fill cracks or openings of any size. Subdivisions of Zone 2 are Zone 2A and Zone 2B. Zone 2A constitutes sand and gravel of similar quality to concrete aggregate, well compacted and protected from erosion during construction. It is constructed at the perimeter joint for 1-3 meters and supported by Zone 2B. Zone 2B also includes material of similar quality to concrete aggregate, and it is constructed to support Zone 2A near the perimeter joint and concrete face for the upper parts.

Main rockfill embankment body is referred to as Zone 3, designed to provide a transition of compressibility and permeability from upstream to downstream, as defined by Cooke et al (1987).

Zone 3 has three main subparts, namely, 3A, 3B, and 3C. Zone 3A is the subpart with the least thickness and least permeability, designed mainly to prevent Zone 2 material from being washed into larger voids in main rockfill body. Its purpose is to minimize the void size, therefore it is placed and compacted simultaneously with Zone 2 in same layer thicknesses. In the design and slope dimensioning of CFRDs, it is aimed that most, if not all, of vertical water load applies on upstream half of the dam. Therefore, the part that transfers this load to the foundation should have its compressibility as low as possible to ensure acceptable settlements. For this objective, Cooke et al (1987) state that in construction of Zone 3B, embankment is placed in 1 m thick layers and compacted with 4 passes of vibratory roller for satisfactory performance. Zone 3C, the downstream rockfill embankment, can be defined as the zone properties of which affects the overall dam performance the least. It takes negligible water load generally, and therefore it can be constructed in thicker layers, with less limitation in rock size, resulting in cost savings.

2.2.3. Rockfill Materials

The rockfill is defined as the structural body of the dam. As previously mentioned, size of rocks to be used in CFRD construction is only limited to layer thickness. Grading of the material to be used is important for the deformation and permeability properties of the dam. Cooke (1984) states the limitations for rockfill material selection rather practically, referring to concrete aggregate specification tests, and in-situ checking of performance. For controlling the rockfill quality and grading, it is underlined that if a layer supports the construction trucks and vibratory rollers, without significant differential deformations, it is considered appropriate. In the absence of

full-scale tests in detailed deformation behavior of rockfill, practical approaches and assumptions have been useful in CFRD design and construction.

Analysis of rockfill materials is traditionally done making use of continuum mechanics approaches; despite the fact that fracturing and crushing are observed in rocks at very low pressures due to the shape and contact point properties, bringing up points in behavior at which continuum mechanics are not applicable. Once the total load applied is high enough to crush the contact between rock blocks, rock strength diminishes, and deformation takes place. As the particle size of the rock increases, so does the probability of fractures inside; thus, deviations in performance compared to laboratory tests and analysis models are observed.

Usage of water in rockfill embankment construction makes use of the loss of strength of the rock. As proved with several tests, water is not a lubricant, on the other hand, wetting reduces the unconfined compressive strength of rock. It was repeatedly proven that the construction of rockfill embankments without application of water results in unexpected settlements in the service period. Increasing the compressibility by reducing the strength of rock, usage of water assures major portion of the settlement of rockfill to occur in construction period. Wetting does not aim to wash the finer particles in between coarser rock. Results of tests done by Terzaghi has shown that sluicing the embankment with pressurized water cannot wash the finer particles as clogging takes place at top layers and prevents jetting fines further (Cooke, 1960). Therefore, sluicing with jets of water is not necessary, and wetting the material by any means is adequate for desired effects. Wetting the rockfill embankment material would ensure more successful compaction and as a result excessive settlement after the construction of embankment body is prevented.

2.2.4. Concrete Face

Main purposes of the concrete face slab are imperviousness and flexibility. For this reason, compressive strength of concrete used does not govern the overall performance; in contrary, concrete with higher 28-day compressive strength can even be avoided due to increased possibility of shrinkage cracks. Concrete with 28-day compressive strength of 20 MPa is generally known to satisfy expected performance.

Commonly used impervious face materials can be listed as concrete, bituminous concrete and steel. Laura and Figene (2008) state that bituminous (asphaltic) concrete face has cost, flexibility and simplicity advantages over other materials, while being easier to repair than concrete or steel and can self-seal the leaks under certain circumstances. On the other hand, asphaltic concrete is less resistant to light and temperature than concrete and steel, and the height of a dam that can be constructed occupying a bituminous concrete face cannot exceed 50 m as indicated by Emiroğlu (2008). Guyer (2018) states that steel faced dams can be rapidly constructed and perform better in deformations of embankment than concrete and bituminous concrete faced dams. Although prone to corrosion, steel face plates can be treated with cathodic protection on both faces to overcome this problem. On the other hand, their applicability is limited in height like bituminous concrete faced dams, with a maximum determined by Emiroğlu (2008) as 40 meters. Performance evaluation of few constructed steel-faced dams show that unlike expected corrosion problems, the impervious faces perform appropriately at projects despite welding problems and maintenance needs. El Vado Dam, located on Rio Chama near Albuquerque with a height of 52,5 m (175 ft) is a steel faced dam, operating since its construction in 1930's. An investigation on its spillway was carried out by U.S. Bureau of Reclamation (2008); observing partially successful repair welds because of post repair cracks in the heat affected zones. In the conducted tests and field investigations, voids, which were commented to occur due to settlement and deformations of the foundation

soil, were observed below the spillway. Although at that time no failure was observed, it was indicated that the spillway rarely operated in the last 50 years to that date, and failure is expected if it did (USBR, 2008). Therefore, significant risk was reported for the spillway of the structure. On the other hand, no negative evaluation results were reported on the steel facing of the dam. Timber planking, although being the most inexpensive alternative, U.S. Bureau of Reclamation suggests it not to be used in permanent dam designs due to the fire danger and very short service life (USBR, 2008).

Generally, the face slab concrete is poured in vertical strips of 12-18 m width, with no horizontal joints. Cold vertical joints commonly constitute waterstops, and continuous horizontal reinforcement through cold joints is considered acceptable practice. Construction of face slab starts after the rockfill body embankment is constructed and preferably a certain amount of time passes for settlement rate of embankment to decline, although there are dams at which due to scheduling, face slab was poured during embankment construction. Pouring the face slab after the completion of embankment is favorable to minimize cracks occurring on the face slab due to settlement of embankment.

In addition, in the literature there is a method defined as the Ita Method; named by Cooke (Resende and Materon, 2000), in which the upstream filter zone materials are placed in berms, and concrete is poured connecting each berm to the upper one, to provide easier placement of the filter zone material, protection from erosion during construction, and supports the compaction of Zone 2 embankment layers. This method was initially used in Ita and Itapebi CFRDs, and then adopted in many succeeding projects. A representative detail of this application is given in Figure 2.3. Ita and Itapebi dams are both in Brazil, with maximum heights of 125m and 120m, respectively. Construction of the extruded curb provided ease of construction of Zone 2B in both projects. In addition, in the construction period of Itapebi Dam, a new construction method was used to keep up with the schedule; by constructing the face slab simultaneously with the rockfill embankment. A temporary platform to support

the slip form was constructed and anchored to blocks poured inside the rockfill. While the Ita Method has the mentioned benefits, it does not eliminate Zone 2, as underlined by Cruz et al(2010), as this zone is necessary for flow control.

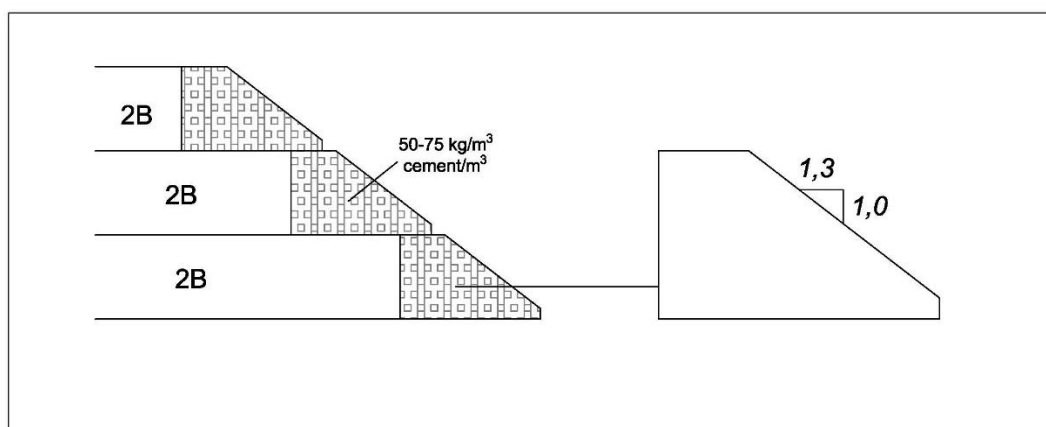


Figure 2.3. Extruded Curb Detail of the Ita Method

Reinforcing in face slab mainly aims to act against shrinkage and temperature, unlike general usage against bending. As the concrete face is under compression despite the vicinity of abutments, positioning of the reinforcement steel at or slightly above slab centerline is considered adequate for appropriate performance of face slab. In the early period, for CFRDs constructed using dumped rockfill, a reinforcement percentage of 0,5 was the common principle. In following periods, for economic optimization, this percentage has been decreased to 0,4 to 0,3, starting from Foz de Areia project.

One layer of reinforcement in each direction has proven to be capable of preventing cracks. However, construction schedule and characteristics of the project may cause different provisions for the reinforcement design of a CFRD. Through the history, different face slab designs were made by engineers, evaluating the preceding projects; properties of selected dams are given in Table 2.2, from the study of Materon (2008) gives key information on face slab designs of some CFRDs. To improve the long-term

performance of CFRD face slabs, as indicated by Arıcı (2013), increasing the reinforcement ratio may prevent crack propagation for CFRDs constructed with rockfill materials of lower quality. Investigating the performance of the face slab during impounding, Arıcı (2013) concluded that increasing the reinforcement ratio would be the most effective way to reduce crack widths.

Table 2.2. *Face Slab Properties of CFRDs, Example Projects (Materon, 2008)*

CFRD Name	Country	Year	Height (m)	Upstream Slope	Downstream Slope	Slab Thickness e_0+kH	Reinforcement ratio (%)
Alto Anchicaya	Colombia	1974	110	1,3	1,3	0,30+0,002H	0,6
Foz do Areia	Brazil	1980	160	1,4	1,25-1,4	0,30+0,0034H	0,4
Aguamilpa	Mexico	1993	187	1,5	1,4	0,30+0,003H	0,3(H)/0,35(V)
Xingo	Brazil	1993	145	1,4	1,3	0,30+0,0034H	0,4
Ita	Brazil	1999	125	1,3	1,3	0,30+0,002H	0,3(H)/0,4(V)
TSQ-1	China	2000	178	1,4	1,4	0,30+0,0035H	0,3(H)/0,3(V)*
Itapebi	Brazil	2002	110	1,25	1,3	0,30+0,002H	0,35(H)/0,4(V)
Mohale	Lesotho	2002	145	1,4	1,4	0,30+0,0035H	0,4
Campos Novos	Brazil	2006	202	1,3	1,4	0,30+0,002H**	0,5***
Barra Grande	Brazil	2006	185	1,3	1,4	0,30+0,002H**	0,3(H)/0,4(V)
El Cajon	Mexico	2006	188	1,4	1,4	0,30+0,003H	0,4
Shuibuya	China	2007	233	1,4	1,4	0,30+0,003H	0,5
Karahnjukar	Iceland	2007	196	1,4	1,4	0,30+0,002H	0,4

*: Double reinforcement at 3rd stage slabs
**: Given is the thickness for $H \leq 100\text{m}$; for $H > 100\text{m}$, $e=0,30+0,005H$.
***: Double reinforcement at 20m from plinth.

Cracks in the face slab occur generally due to shrinkage and temperature effects on concrete and imposed deformations through the interaction with the rockfill embankment. Mori (1999) categorized face cracks in three types, as Types A, B and C. Type A cracks were defined as inevitable horizontal cracks of small widths occurring due to the shrinkage of concrete. Mori (1999) states that these cracks occur commonly in slabs between previously poured segments, and maintenance is not

required for this type of cracks. Type B cracks occur because of the deformations of rockfill embankment. As settlement of rockfill embankment imitates slumping with vertical downward movement and horizontal outward movement, evenly spaced cracks of small widths occur which generally close upon reservoir impoundment; and Mori (1999) suggested maintenance by cement application or application of a rubber membrane over the cracks. Type C cracks were defined by Mori (1999) as structural cracks that occur because of deformation moduli differences or differential settlement. Unlike other types of cracks, these cracks do not self-repair upon reservoir filling, in contrary, the load application induces increased deformation differences. ICOLD (2004) explains the most appropriate precaution for Type C cracks as foundation treatment and construction of a proper transition zone beneath the concrete face.

Thickness of face slab, expressed in an empirical equation, can be calculated as $t = 0,3 + 0,003H$ in meters, H being the dam height (Cooke et al, 1987). CFRDs of constant face slab thickness have been constructed as well as CFRDs with face slab thickness increasing with depth. The thickness formula was modified to $0,3 + 0,002H$, and for dams of moderate height, a constant concrete face thickness of 0,3 m is acceptable practice. Because the main aim of the face slab is providing an impervious membrane; concrete face slab shall be compatible to the deformations of embankment, with minimum crack occurrence. A thinner concrete face slab has advantages both in flexibility and construction economy.

2.3. Deformation Analyses of CFRDs

The nonlinear and stress dependent deformation behavior of the rockfill is one of the reasons why CFRD design depends on engineering judgment rather than numerical analysis. Difficulties in determining material properties may result in inaccurate models for design; given that a wide range of materials, which are not manufactured, are used in construction. Therefore, numerical analyses have served as back analyses

for correlations with estimated or measured behavior and parameters. Numerical analysis of CFRDs have initially been done by linear elastic models. Later, nonlinear analysis has become common using finite difference method or finite element method. Accuracy of a numerical analysis on CFRDs is determined by the accuracy of material properties defined and constitutive model selected to define the model. Considering the behavior aspects of rockfill that cannot be explained by continuum mechanics, the three-dimensional analyses may lead to more reliable results, given that successful assumptions are made, and adequate data are available on the material properties.

2.3.1. Material Models

The relationship between stress and strain is simulated by the use of material models for a certain material. For the soil is composed of soil grains and the water and air between the particles; it is a complex material to be modeled. Behavior in microscopic and macroscopic scales have significant differences in addition to the effects of pore pressure and cohesion. Because of this, certain approaches in describing soil behavior provided different material models.

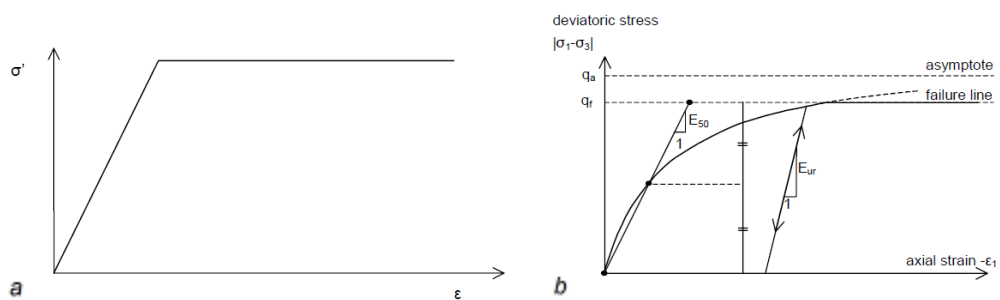


Figure 2.4. Stress-Strain Relation of an (a) Elastic-Perfectly Plastic Material and a (b) Hyperbolic Material (Ti et al., 2009)

Having their roots from Hooke's Law for linear elastic material models, to simulate the highly nonlinear behavior of soils, material models have been improved to provide accurate simulation of stress dependence of the material stiffness (Schanz et al, 1999). In addition, modelling of rock materials have additional difficulties due to modifications of behavior from continuum approach.

Commonly used constitutive material models can be listed as Hooke's Law, Mohr-Coulomb model, Drucker-Prager model, Duncan and Chang hyperbolic model, Cam Clay model, Hoek-Brown model, Soft Soil model and Hardening Soil model. These constitutive material models are generally either based on theory of elasticity or theory of plasticity. Behavior of linearly elastic isotropic materials subject to small deformations are explained by the theory of elasticity. Linear elasticity explains the behavior if the deformation is in the range of elastic deformation limits, namely below the yield point for one dimensional loading, the yield curve for two-dimensional loading, or below the yield surface in the case of three-dimensional loading. When these limits are exceeded, irreversible effects of loading are observed in the materials; such as cracks, crushing or deformation into voids in granular materials; and theory of plasticity aims to explain the behavior exceeding the yield limits. In an elastic – perfectly plastic material model strain hardening is not considered, therefore for stresses exceeding the yield strength, no more resistance is provided for the material.

Mohr-Coulomb model is an elastic-perfectly plastic model, with material behavior defined by Hooke's law in elastic range, and a fixed yield surface defined by model parameters. The relationship between stresses and strains in elastic range is explained as:

$$\dot{\sigma}' = \underline{M} \dot{\epsilon}$$

With \underline{M} being the material stiffness matrix. The matrix representation of the equation is given including the effective Poisson's ratio, ν' :

$$\begin{bmatrix} \dot{\sigma}'_{xx} \\ \dot{\sigma}'_{yy} \\ \dot{\sigma}'_{zz} \\ \dot{\sigma}'_{xy} \\ \dot{\sigma}'_{yz} \\ \dot{\sigma}'_{zx} \end{bmatrix} = \frac{E'}{(1-2\nu)(1+\nu')} \begin{bmatrix} 1-\nu' & \nu' & \nu' & 0 & 0 & 0 \\ \nu' & 1-\nu' & \nu' & 0 & 0 & 0 \\ \nu' & \nu' & 1-\nu' & 0 & 0 & 0 \\ 0 & 0 & 0 & \frac{1}{2}-\nu' & 0 & 0 \\ 0 & 0 & 0 & 0 & \frac{1}{2}-\nu' & 0 \\ 0 & 0 & 0 & 0 & 0 & \frac{1}{2}-\nu' \end{bmatrix}$$

Mohr-Coulomb model modifies the classic theory of plasticity by a plastic potential function in addition to the yield function to prevent overprediction of dilatancy. This is done by a switch-like multiplier to modify the stiffness matrix in case of plastic behavior. Yield condition of this material model is defined in principal stress space, with φ as the internal friction angle, for example at 1 direction as:

$$f_{1a} = \frac{1}{2}(\sigma'_2 - \sigma'_3) + \frac{1}{2}(\sigma'_2 + \sigma'_3) \sin \varphi - c \cos \varphi \leq 0$$

$$f_{1b} = \frac{1}{2}(\sigma'_3 - \sigma'_2) + \frac{1}{2}(\sigma'_3 + \sigma'_2) \sin \varphi - c \cos \varphi \leq 0$$

Also, the model defines the potential functions in principal stress space for 1 direction as:

$$g_{1a} = \frac{1}{2}(\sigma'_2 - \sigma'_3) + \frac{1}{2}(\sigma'_2 + \sigma'_3) \sin \psi$$

$$g_{1b} = \frac{1}{2}(\sigma'_3 - \sigma'_2) + \frac{1}{2}(\sigma'_3 + \sigma'_2) \sin \psi$$

Where the dilatancy angle ψ is introduced into the model structure. The modification from the classic theory of plasticity can be summarized with the case these equations are introduced with “ $f \neq g$ ”, namely non-associated plasticity in contrary to associated plasticity of classic theory of plasticity. Terzaghi comments on the Coulomb theory as

“a working hypothesis for the solution of one special problem of the earth-pressure theory, with its approach on assuming sand as a homogenous mass ignoring the consistence of individual grains; which developed into an obstacle against further progress as soon as its hypothetical character came to be forgotten by Coulomb’s successors” (Terzaghi, 1920).

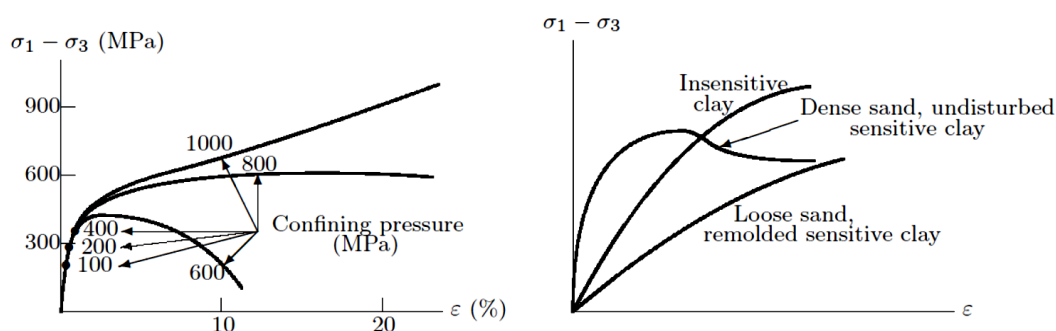


Figure 2.5. Stress-Strain Relations of Rock and Soil Samples (Lubliner & Moran, 1992)

To account for the nonlinear and stress dependent behavior of soils, Duncan and Chang proposed a material model, namely Duncan and Chang hyperbolic model. This model is an incremental nonlinear elastic model based on the stress strain relation in drained triaxial tests on sands and clays; with a failure criterion based on Mohr-Coulomb model (Ti et al, 2009). Mohr-Coulomb model, being an elastic-perfectly plastic model in soil behavior, defines the failure criteria with the friction angle and cohesion of the soil. By the usage of different elastic moduli for loading, unloading and reloading conditions, Duncan and Chang hyperbolic model aims to simulate the difference in behavior of soils in different conditions. Duncan-Chang hyperbolic model defines the elastic modulus (tangent modulus) in loading condition with the equation:

$$E_t = K_e P_{atm} \left(\frac{-\sigma_1}{P_{atm}} \right)^n \left(1 - \frac{R_f (1 - \sin \varphi) (\sigma_1 - \sigma_3)}{2c \cos \varphi - 2\sigma_1 \sin \varphi} \right)^2$$

Where K_e is the modulus number ranging between 350 to 1120, n is the modulus number reflecting the stress dependency of E_t ranging between 0 to 1, R_f is the failure ratio usually ranging between 0,6 to 0,95 and P_{atm} is the atmospheric pressure. Duncan-Chang hyperbolic model defines the unloading/reloading elastic modulus as:

$$E_u = K_u P_{atm} \left(\frac{-\sigma_1}{P_{atm}} \right)^n$$

Where K_u is the unloading modulus number. Ti et al (2009) summarizes the model behavior, as loading, if the state of stress is on the yield surface, leading to plastic deformation, and when the state of stress drops below the yield value, elastic deformations occur which represent the unloading. The model uses Mohr-Coulomb failure criterion describing the failure of material, however, not being formulated properly in theory of plasticity prevents this model from considering dilatancy. Although a widely used material model, the hyperbolic model is not suitable for collapse load computations in fully plastic range, as stated by Ti et al. (2009). In addition, this model cannot distinguish between loading and unloading (Schanz et.al, 1999).

Hardening soil model, which can be defined as an improved version of Duncan and Chang hyperbolic model; describes the yield surface as expandable due to plastic straining. With this approach, Hardening Soil model uses theory of plasticity unlike the hyperbolic model which uses theory of elasticity. Plastic straining provides the ability of the yield surface to expand in Hardening Soil model. Considering the common soil loading phenomena, Hardening Soil model accounts for shear(friction) hardening to model irreversible strains due to deviatoric loading; and for compression(cap) hardening to model irreversible strains due to primary compression loading (Schanz et al, 1999). Like Duncan-Chang hyperbolic model, Hardening Soil model defines the failure with Mohr-Coulomb failure criterion. Considering dilatancy, Hardening Soil model overcomes the shortcomings of Duncan-Chang hyperbolic model in this aspect.

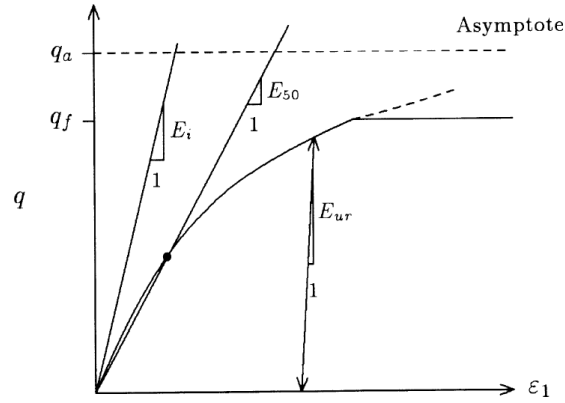


Figure 2.6. E_i , E_{50} , and E_{ur} represented on q - ε_1 curve (Ti et al., 2009)

Hardening Soil model uses the failure parameters of Mohr-Coulomb model, internal friction angle φ , cohesion c , and dilatancy ψ . To define the soil stiffness, E_{50}^{ref} is used as secant stiffness in standard drained triaxial test, E_{oed}^{ref} as tangent stiffness for primary oedometer loading, E_{ur}^{ref} as unloading/reloading stiffness, ν_{ur} as Poisson's ratio for unloading/reloading, p^{ref} as reference stress for stiffness, K_0^{NC} as K_0 value for normal consolidation, m as the power parameter for stress dependency of stiffness and R_f as failure ratio. As the stiffness of the material is stress dependent, the reference values of deformation moduli defined are modified according to the ratio of applied pressure to the reference pressure σ^{ref} . The amount of stress dependency is presented with power parameter m . For the software used in this study the default reference pressure is 100 kPa. The model uses E_{50} , which is the deformation modulus corresponding to the mobilization of 50% of the maximum shear strength, instead of E_t used in Duncan-Chang hyperbolic model as the confining stress dependent stiffness modulus because as stated by Schanz et al (1999), tangent modulus is more difficult to determine experimentally.

$$E_{50} = E_{50}^{ref} \left(\frac{\sigma_3 + c \cot \varphi_p}{\sigma^{ref} + c \cot \varphi_p} \right)^m$$

Similarly, the stiffness modulus for unloading/reloading is defined as

$$E_{ur} = E_{ur}^{ref} \left(\frac{\sigma_3 + c \cot \varphi_p}{\sigma^{ref} + c \cot \varphi_p} \right)^m$$

It is stated in the Plaxis Manual for material models that in practical cases defining the $E_{ur}^{ref} = 3E_{50}^{ref}$ is acceptable.

For the Poisson's ratio in unloading/reloading ν_{ur} , values about 0,2 are recommended. K_0^{NC} is suggested to be assumed equal to $1 - \sin \varphi$, as used practically. In addition, the oedometer stiffness E_{oed} is given by the equation

$$E_{oed} = E_{oed}^{ref} \left(\frac{\sigma_1 + c \cot \varphi_p}{\sigma^{ref} + c \cot \varphi_p} \right)^m$$

Regarding the triaxial case, plastic volumetric strains ε_v^p are negligible, based on their comparison to axial strain. Therefore, plastic shear strain γ^p to be used in yield equations, and the two yield equations are defined as

$$\gamma^p = \varepsilon_1^p - \varepsilon_2^p - \varepsilon_3^p = 2\varepsilon_1^p - \varepsilon_v^p \sim 2\varepsilon_1^p$$

$$f_{12} = \frac{q_a}{E_{50} q_a - (\sigma_1 - \sigma_2)} - \frac{2(\sigma_1 - \sigma_2)}{E_{ur}} - \gamma^p$$

$$f_{13} = \frac{q_a}{E_{50} q_a - (\sigma_1 - \sigma_3)} - \frac{2(\sigma_1 - \sigma_3)}{E_{ur}} - \gamma^p$$

The relationship between volumetric and shear strain rates is defined with the equation

$$\dot{\varepsilon}_v^p = \sin \psi_m \dot{\gamma}^p$$

Where ψ_m is the mobilized dilatancy angle. Dilatancy angle depends on the mobilized internal friction angle φ_m and the critical state friction angle φ_{cv} . Critical state is defined by Schofield and Wroth (1968) as the state which soil or other granular materials would reach when continuously distorted until they flow as a frictional fluid.

$$\sin \psi_m = \frac{\sin \varphi_m - \sin \varphi_{cv}}{1 - \sin \varphi_m \sin \varphi_{cv}}$$

$$\sin \varphi_m = \frac{\sigma_1 - \sigma_3}{\sigma_1 + \sigma_3 - 2c \cot \varphi_p}$$

$$\sin \psi_{cv} = \frac{\sin \varphi_p - \sin \psi_p}{1 - \sin \varphi_p \sin \psi_p}$$

These equations correspond to Rowe's stress dilatancy theory. Rowe (1962) refers to Reynolds' findings on deformation of sands. Reynolds (1885) states that dense sands expand at failure whereas loose sands contract during shear to failure. This behavior of dense sands was named by Reynolds (1885) as dilatancy. Rowe (1962) conducted experiments with regular steel rods to model a two-dimensional stress system and regular steel spheres to model a three-dimensional stress system.

Dilatancy cut-off is another characteristic introduced by the Hardening Soil model, which aims to define the behavior of the soil after extensive shearing. As summarized by Schanz et al (1999), after extensive shearing the dilatancy comes to an end when a state of critical density is reached. By defining the maximum void ratio, a limit is set for dilation in a switch-like manner to set dilatancy angle to zero when the material reaches this maximum void ratio. To sum up, Hardening Soil model considers the effects of plastic deformations on the properties of the soil, preconsolidation effects on the deformation behavior, and irreversible plastic strains.

2.3.2. Parameters

For a representative model of a structure, behavior of materials has to be modelled accurately; and this requires the correctness of parameters as much as the accuracy of material models. Modelling of rockfill has its difficulties in both aspects. Engineering properties of rockfill are difficult to determine since it requires testing of the materials. In addition to being variable in gradation and content, rockfill behavior is also affected by the specimen size used; therefore, scale effects must be considered.

Main parameters necessary to estimate the behavior of rockfill materials are the ultimate shear strength and deformation modulus. Load carrying capacity of the material used shall be known to assure the stability of the structure to be constructed. Although CFRDs provide considerable flexibility in material selection, as economy is a concern in the construction industry in addition to safety, information on the ultimate strength of the material to be used can improve optimization in design. Deformation characteristics of rockfill materials shall be known to manage adequate zoning, and construction scheduling. Unexpected deformation of the rockfill affects the concrete face and problems in the concrete face cause leakage problems which may end up in both structural and performance related problems to dams. However, randomness of distribution of particles as well as fractures in rocks in combination with the very coarse particle sizes of rocks require significant method development both in testing and modelling.

Dorador and Urrutia (2017) summarize material subset preparation approaches for specimens including the most commonly used ones, the Matrix method, Scalping method and Parallel Grain Size method. The Matrix method assumes the coarser particles in a soil matrix to float into the matrix (Siddiqi, 1984). As increasing the coarser content of the specimen would result in contacts between these particles thus eliminating the primary assumption of the approach, Fragaszy et al (1990) modified this method to include an upper bound of 30% for oversize particle content. The Scalping method which was introduced by Zeller and Wullimann (1957) was developed for triaxial tests on materials to be used in Göschenenalp Dam in Switzerland. From the sample material particles coarser than 10 cm were sieved out and then specimens were prepared with gradations of 0-10 cm, 0-3 cm, 0-1 cm, and 0-0,1 cm particle diameters. Zeller et al (1957) explain that grain size distribution and particle shape remained unchanged to a certain extent. After conducting triaxial tests on these specimens, the defined relationships between shear strength, porosity, and grain size distribution were used to extrapolate to define the parameters for actual material (Zeller et al, 1957). This method provides specimens with more uniform

gradations; therefore, estimations may tend to have unexpected differences from the actual performance. The parallel grain size method scales the original particle size distribution to a smaller size distribution, with a semi-logarithmic scale. This method is assumed to keep the particle characteristics of original material with the specimen. Although accepted as a reliable method, Dorador et al (2017) explain points of concern; for example, the sample including a maximum of 10% fines content, parallel gradation as the name of the method implies, and similar minimum and maximum density.

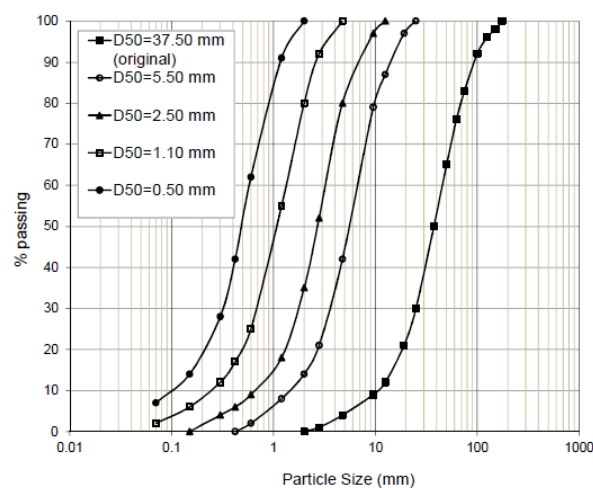
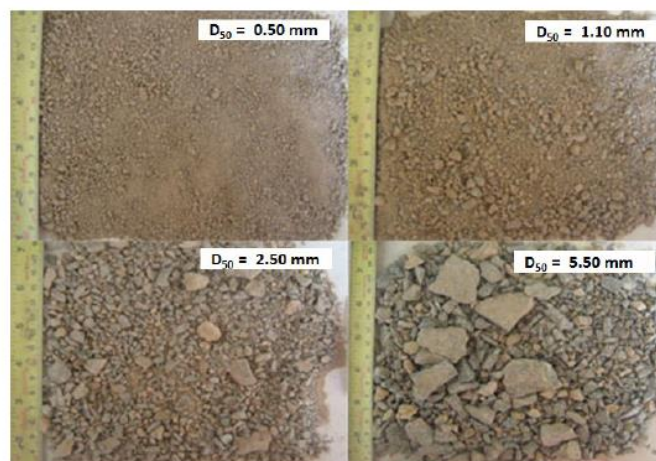


Figure 2.7. Grain Sizes and Parallel Gradation of a Quarry Rock Sample (Dorador and Urrutia, 2017)

Hoek (2000) underlines the deficiency of laboratory testing on rock specimens due to limitations in size, as the specimen can represent only a very small fraction of the rock which has various size, shape and fracture combinations in the field.

Several studies were made on large scale testing of rockfill materials to obtain mechanical parameters. Indraratna et al (1993) set experiments on rockfill specimens in parallel gradation to greywacke rockfill used in Chiew Larn Dam in Thailand with 99,5m height. Sample size ratio was defined regarding two rockfill gradations determined for the dam; by dividing the mean diameter of maximum particle size to the triaxial specimen diameter, which is 30 cm. Specimen height was 60 cm, limited by the triaxial compression test apparatus. This division resulted in size ratios of 8 and 12 for the used gradations. Indraratna et al (1993) indicate that although particle breakage may occur even at lower stresses due to concentrated stresses at contact surfaces, these breakages are negligible compared to the ones that would occur under higher pressures. In the experiments, initial water content, compacted density, particle breakage and effect of angularity on shear strength were neglected. Specimens were prepared by compaction in layers of 5-6 cm, with a hand vibrator. Indraratna et al (1993) refer to the past experiments conducted on large scale specimens by Marsal (1973), Marachi, Chen and Seed (1972); with confining pressures ranging between 2,5 to 4,5 MPa and states these confining pressures may cause misleading results as even at the highest dams, normal stresses are not likely to exceed 1 MPa. Isotropically consolidated drained triaxial tests with varying effective confining pressures between 100-600 kPa were conducted on the specimens. Expected results were obtained in the tests as increasing peak stresses with increasing confining pressure. It was observed that dilation is pronounced for lower confining stresses whereas it is suppressed at higher confining pressures. Evaluating the effect of particle size, in lower confining pressures the gradation with coarser particles showed more dilation than the one specimen with finer particles; however, at higher confining pressures the results tended to become similar. Therefore, Indraratna et al (1993) conclude that confining pressure is more significant in volumetric strain than the particle size, unless the

difference in maximum particle sizes is considerable. Comparing the results obtained in two representative gradations, it was concluded that influence of particle size may even be neglected if the initial porosity of test specimen is similar to the compacted field porosity. According to test results, in increasing confining pressures regardless of the particle size, the internal friction angle reached similar values with a large reduction; it was explained by the crushing of angular particles in high confining pressures; noting that the effect of particle size distribution on the internal friction angle could not be obtained in this experiment. Considering the Mohr-Coulomb criterion for failure of rockfill, Indraratna et al (1993) state that for lower confining pressures less than 500 kPa, the failure envelope has a nonlinear behavior, whereas at much higher confining stresses at about 1-5 MPa, the linear Mohr-Coulomb criterion is acceptable.

In addition to large scale laboratory testing of rockfill specimens, in-situ tests are also conducted to determine material properties. Field tests that are applicable to rocks can be categorized as shear test, deformability tests, strength and internal stress tests. Also, test fills can be constructed to model the overall behavior. In the preconstruction works for Lewis Smith Dam in Alabama, United States; Sowers and Gore (1961) explain an in-place permeability test and a direct shear box test conducted to predict the behavior of materials and plan the construction. Designed as a combined earth and rockfill dam of 90m height, Lewis Smith Dam body is located above a geological profile dominated by sandstone and shale. Two test areas were constructed for the core and shell materials. Test areas were designed in regions with a grid approach to observe the effects of different combinations of material properties and compaction methods. For the core material, regions were constructed in combinations of different water contents, layer thicknesses, and relative weathered rock amounts with compaction methods listed as disc harrow followed by a 50-ton rubber-tired roller, 50-ton rubber-tired roller, 4800 kPa (700 psi) sheep-foot followed by 50-ton rubber-tired roller, and 4800 kPa (700 psi) sheep-foot. Three different relative water amounts were applied in the shell material test area, at field moisture, $\frac{1}{2}$ water to rock ratio by volume, and 2

water to rock ratio by volume; compacted with a 50-ton 4-wheel rubber-tired roller in two different pass amounts, 4 passes and 8 passes (Sowers et al, 1961). Comparing the field permeability test results to the results obtained from laboratory specimens, permeability coefficient obtained in field tests ranged from 2 to $2,5 \times 10^{-4}$ cm/s for the areas compacted with sheep-foot; whereas laboratory tests conducted on large undisturbed samples gave permeability coefficient ranging from $2,2 \times 10^{-4}$ cm/s to $3,3 \times 10^{-4}$ cm/s; and tests on samples compacted in the laboratory gave permeability coefficient about 1×10^{-5} cm/s. Sowers et al (1961) state that the differences may be caused by cracks occurring in the laboratory specimens in sampling in addition to the lack of rock fragments in laboratory samples.



Figure 2.8. Arrangement of an In-Situ Large Scale Direct Shear Test (Sowers et al., 1961)

For the direct shear test, the bottom half of the shear box was placed in the test area during construction of the fill and after the appropriate amount of fill was placed, the top half was placed. The buried box was then uncovered by digging and the shear test was conducted on this sample, Figure 2.8. Considering the results, the internal friction angles measured in this field test and laboratory test gave similar results, 45° from the field test and 42° from the laboratory test were obtained. The difference was predicted to be due to the lack of the larger angular particles in the laboratory test samples.

Sowers et al (1961) underline that laboratory tests alone would be misleading in determining material properties and predicting the fill behavior; and the fill testing program would eliminate uncertainties in the choice of compaction equipment and method.

With the advancement of material modelling methods, simulating the behavior of rockfill including the particle interactions is possible by using discrete element methods. Ma et al (2016) refer to the studies made in numerical experiments on rockfill behavior. Luding (2008) defines the discrete element method as modeling of particles with the approach towards the microscopic understanding of macroscopic particulate material behavior. Assuming the rock materials to behave as a continuum has shortcomings in the aspect that it neglects cracks occurring under the stress applied on a rock body, resulting in deformations and a new rock body formation. Instead of using constitutive relationships to overcome this, DEM simulates the motion and interactions of particles in steps. Initially introduced by Cundall and Strack (1979) in the name of Distinct Element Method, discrete element method was explained as the analysis of the interactions, contact by contact; and the motion of the particles, particle by particle. The calculation was defined to be an alternation between Newton's second law which states that the acceleration of an object depends on the net force acting upon it and its mass; and a force-displacement law to derive contact forces from displacements (Luding, 2008). A general challenge which was studied by many researchers has been the complex shape distribution of rockfill materials and its effects on the behavior. To study the crushing mechanism of rockfills neglected in DEM, random distribution models (Ma et al, 2011), overlapping spheres (Lu and McDowell, 2007) were examples of approaches in simulating the distribution of particle shapes in a rockfill.

In a study carried out by Deluzarche and Cambou (2006) it was stated that to model the rockfill using DEM in two dimensions one should provide the representation of the three-dimensional behavior by a two-dimensional model using a phenomenological approach, which is, the defined parameters may not be

representative of the material individually, but the whole set of parameters shall represent the modelled material realistically. Deluzarche et al (2006) further explain in this approach the parameters shall be evaluated to have no clear physical meaning. Occupying blocks made of spheres linked together to consider the irregular shape and distribution of different shaped materials in a rockfill, Deluzarche et al (2006) modelled clusters of these blocks using breakable bonds to consider particle breakage.

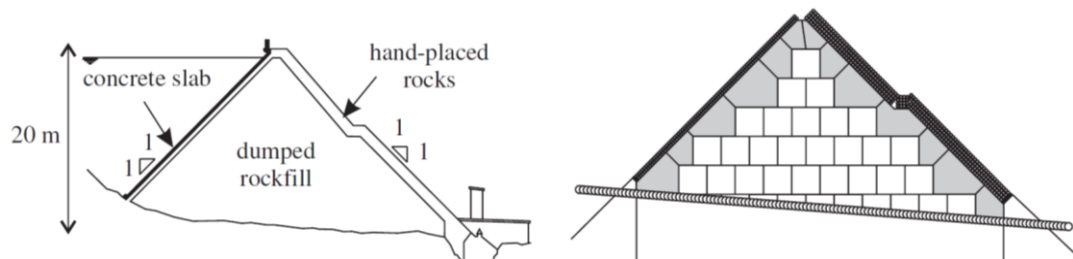


Figure 2.9. Representation of the Rockfill Dam and Analysis Model (Deluzarche et al, 2006)

In the study the two-dimensional model of a 20m high CFRD in Pyrenees mountains was analyzed using DEM, Figure 2.9. The evaluated dam was constructed in 1950's, using granite rockfill dumped with almost no compaction, and has side slopes close to 45° . the dam model was generated using three main types of rockfill assemblies, differing for the central zone, close to dam faces and hand-placed rock on the downstream face. Safety factors were achieved by the usage of reduced characteristic deformation parameters derived from actual test results (Deluzarche et al, 2006). Stability of the dam was analyzed in global and local scales, in end of construction and reservoir impoundment stages. End of construction analysis was performed twice with and without the hand-placed rock on faces; and it was observed that the hand-placed layer improves the stability of the dam. According to the results obtained, Deluzarche et al (2006) underlined the importance of reducing particle breakage in construction of rockfill dams, as even at small breakage rates, settlement values for

the model increase significantly, referring to the observed 5-times increase in crest settlement with an increase of 10% in particle breakage.

Shao et al (2013) studied on the numerical modelling of triaxial tests on rockfill samples using DEM. To assure an acceptable particle shape and size distribution, in the model irregularly shaped clusters of regular spheres were defined limited in the initial state from overlapping as a precaution for maximum tensile stress state of particles, to prevent the release of strain energy at maximum tensile stresses that may result in a large amount of kinetic energy to lead to disturbance of adjacent particles. To consider crushing, particles that reach a predefined tensile failure criterion were deleted and replaced by a new group of particles that follow the rules defined in arrangement according to experimental observations.

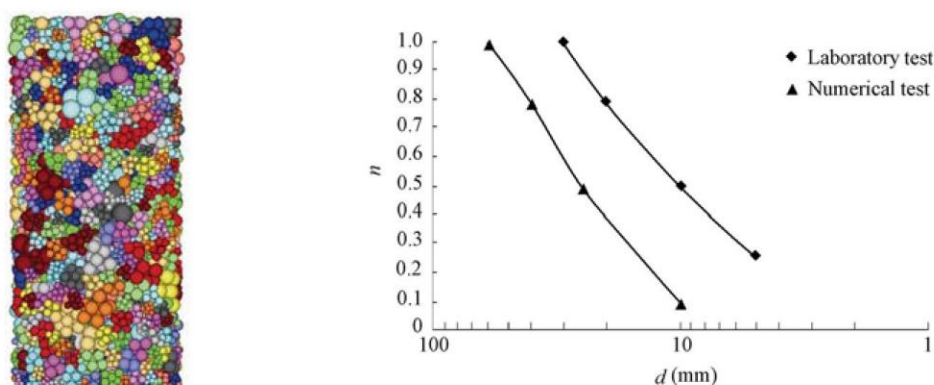


Figure 2.10. Numerical Model of a Triaxial Test Sample, Particle Gradations of Laboratory Test Sample and Numerical Test Sample (Shao et al, 2013)

Consolidated drained triaxial tests made by Gong (2005) on rockfill materials of Sujiahekou Dam in China were simulated by this approach. The conducted triaxial tests were made on samples of 302mm diameter and 655mm height, so the model sample dimensions were designed, Figure 2.10. The model elements were summarized by Shao et al (2013) as 1062 initial clusters including 8617 small spheres with 17522 contact bonds. Loading was simulated by specifying the velocities of top and bottom

walls, and confining stress was kept constant by adjusting the velocity of the side wall with a soft confinement level of a stiffness that is 0,1 of that of the particles. Deriving the macroscopic parameters of the material from the conducted experiments, microscopic parameters which are normal contact stiffness, shear contact stiffness and friction coefficient were defined considering experimental data. Behavior of the sample was investigated from the aspect of energy. The relationship between the energy dissipation and behavior of the rockfill sample was evaluated in four stages in the study. In the first stage where particle crushing did not occur, the elastic strain increased rapidly. The second stage showed an increase in friction energy dissipation much more significantly than the elastic strain energy, governing the behavior of particles. In the third stage rapid growth was observed both in friction and crushing energy dissipations. Voids were filled with smaller cracked particles. In the fourth stage, more particles were crushed at a stable high rate, causing deformation and movement of particles leading to structural changes in material composition and lower carrying capacity, while observing relatively stable frictional and crushing energy dissipations (Shao et al, 2013). Comparing the numerical results with experimental results, Shao et al (2013) noted that because the particle amount in the numerical experiment was far less than that in the laboratory experiment, the difference in behavior increased with increasing confining pressure due to the insufficient compactness of the numerical sample. However, considering the overall comparison of results, the proposed tensile failure criterion was generally appropriate.

2.3.3. A Review of Literature on Deformation Behavior of CFRDs

The performance of a CFRD is evaluated on its vertical and horizontal deformations, creep behavior, leakage rate and deflection of the concrete face. Except two reported failure cases, problems occurred in CFRDs have been practically repairable as mentioned below in several case studies. The two failures belong to Gouhou and Taum

Sauk dams (Qian, 2008). Gouhou Dam, located in China, failed due to leakage in 1993, 6 years after the end of construction. The other case of failure occurred in Taim Sauk CFRD in USA, because of overtopping in 2005, 42 years after the completion of the dam (Cruz et al, 2010).

Vertical deformation behavior of the rockfill body follows a logarithmic manner, with high settlement rates in the initial phases after being constructed, decreasing in time to long term deformation due to secondary breakages of rockfill, namely creep. The impoundment causes a step of increasing settlements, however, after the impoundment period generally creep governs the settlement of CFRDs.

Expected settlement of a CFRD can be summarized with maximum values occurring near the central area about the mid-height, decreasing towards the upstream and downstream faces. For a homogenous dam at which the largest settlements occur about the mid-height; Cruz et al (2010) propose a formula to predict the vertical deformation as

$$R = \frac{\gamma H^2}{4E}$$

Where R is the settlement, γ is the unit weight of rock material, H is the height at the midsection and E is the modulus of compressibility of rock material. Surely, for a CFRD with non-homogenous material, with variable moduli of compressibility, behavior may show differences. The valley shape as well as the rock type used in embankment affects the vertical deformation of a CFRD. Lower compressibility moduli lead to higher settlements; and CFRDs constructed in open valleys undergo larger vertical deformations than those in narrower valleys.

Horizontal displacements during construction period are generally towards the upstream and downstream faces as expected of an ordinary embankment construction, depending on the construction schedule of the rockfill. During impoundment, because of the application of the hydraulic pressure, the embankment deflects horizontally towards the downstream; and after the impoundment period the horizontal

deformations also reach a state of creep with smaller deformation rates. One problem of monitoring horizontal displacements is that providing certain reference points by sealing and fixing monitoring devices reduce the precision of measurements.

Leakage through CFRDs is critical in the aspect of efficiency, but commonly not as critical in the aspect of stability. Even leakage rates reaching thousands of liters per second were reported that do not cause instability. In many cases leakage rates reach the maxima in impoundment periods, but there are CFRDs at which the leakage rates increased in years after the impoundment. Commonly, leakage rates between 30-400 l/s depending on the characteristics of the project are acceptable for CFRDs. In the literature, rates exceeding 800-2000 l/s were reported to require investigation and remedial measures. Reinforcing the rockfill, placement of fine material, application of sand-mortar mixtures are examples of solutions preferred in several cases.

Face slab deflection of a CFRD in which the required bond with the rockfill is assured generally depends on the behavior of rockfill. In the impoundment period, as observed in many dams, movements cause the perimeter joint to open. Creep behavior is also more significant in the face slab than in the rockfill, especially if the construction gets interrupted or is made in stages taking long periods of time.

Table 2.3. *Information on CFRDs, Example Projects*

CFRD Name	Crest Length (m)	Max. Height (m)	A/h^2	Max. Sett. (cm) - EoC	Max. Sett. (cm) - RI
Alto Anchicaya	260	140	1,14	63	6
Shuibuya	660	233	2,21	214	28
TSQ-1	1104	178	5,68	332	-
Mohale	600	145	4,14	130	35
Karahnjukar	700	196	2,42	153	40
Kürtün	300	133	-	215,5	36,5
Çokal	605	83	-	-	-
Dim	365	134,5	2,24	87	-

2.3.3.1. Alto Anchicaya Dam – Colombia

Built in Western Andes in Colombia, Alto Anchicaya Dam was constructed in 4 years, 1970-1974, for a hydroelectric plant project (Cruz et al, 2010). With its 140 m height, and 1,4H:1V slopes; Alto Anchicaya has similar properties to Afşar Dam in Turkey. However, Alto Anchicaya Dam is located on a very narrow valley considering its ratio of face width to height. Rockfill embankment was built using mainly hornfels, and the dam was instrumented with inclinometers, strain gauges, jointmeters, settlement cells and external monuments.

Construction schedule of the dam is different from the conventional due to rainy climate of the region; the face slab was poured simultaneously with the rockfill embankment construction. Deformations during the initial impoundment caused cracks along the perimeter joint; which were repaired using a mastic covered by a mixture of asphalt, sand and impervious material after the drawdown of water for investigation. Although recorded leakage rates were as high as 1,8 m³/s initially, after repair works, leakage rates as well as deformations proved the adequate performance of the dam. Materon (1985) listed the maximum crest settlement values for Alto Anchicaya as 6 cm after the second filling, 11 cm one year later, and 15 cm ten years later. Materon (1985) stated these values are “typical of a very well-graded and well-compacted rockfill”.

2.3.3.2. Shuibuya Dam – China

The highest CFRD in the World, Shuibuya Dam, with a height of 233 m, was constructed in a 5-year period starting in 2002 and ending in 2007 (Zhou et al, 2011). Located above a foundation constituting shale and limestone, settlement recordings show that a significant portion of total settlement occurred during construction, with

a decreasing settlement rate then. It is stated that more than 85% of total settlement of dam body occurred in construction period. At reservoir impoundment, while the water level was rising, settlement rate was increasing more rapidly near the upstream face and slowly near the downstream face due to the low rate of infiltration.

Considering the unexpected effects of having a very high embankment body, settlement results match with observations made on dams of moderate height; higher settlement values near the center and about the middle zone, than top and low layers or upstream and downstream faces. Settlement analysis of Shuibuya Dam using FEM was carried out by Zhou et al (2011), making use of Duncan-Chang E-B Model, and a constitutive model of rock creep following the data derived by creep tests on rockfill materials. Monitored settlements, with a cumulative maximum of 248 cm, 1,06% of dam height; match roughly with analysis results, differences explained with variables of construction stages for the comparison in construction period; on the other hand, results of service period show a better agreement with observations. Considering the highest dam in the World is Jinping-1 Dam in China with a maximum height of 305 m, an arch dam; and the highest embankment dam is Nurek Dam in Tajikistan with a height of 300 m, Shuibuya Dam stands as a successful example for future super high CFRDs to be constructed.

2.3.3.3. Tianshengqiao-1 Dam – China

Located in China, Tianshengqiao-1 Dam has a maximum height of 178 m and its construction was completed in 2000. The dam with an A/H^2 ratio of 5,68, was built on Nanpanjiang River. Ma et al (2007), (2016) suggest that there are several reasons which resulted in deformation problems for this dam. Firstly, the compaction schedule, which was six passes of a 10-ton vibratory roller for upstream lifts of 80 cm, and six passes of an 18-ton vibratory roller for downstream lifts of 160 cm, was not

enough to provide an adequate compaction density. In addition, compressive modulus of upstream fill was 45 MPa whereas that of downstream fill was 22 MPa.

In construction period, to overcome flood problems, upstream rockfill embankment was constructed to a larger height than downstream embankment, and after the flood season the downstream embankment construction was carried out with a fast schedule to reach the level of upstream. Also, observing the cracks occurred in the face slab during construction, engineers revised the reinforcement design of the face slab in the last stage using double reinforcement. These problems listed above resulted in excessive deformation and differential settlement in dam body; with cracks in concrete face and separation of concrete face from cushion layer. Maximum displacement reported in the dam body was 2,92m. These mentioned structural problems also resulted in increased leakage rates. After the repair works on the joints that ruptured 3 years after the impoundment, TSQ-1 Dam continued service with adequate performance (Ma et al, 2016).

2.3.3.4. Mohale Dam – Lesotho

Constructed above a basalt foundation using basalt rockfill material, Mohale Dam is in Lesotho, South Africa. The dam has a 145,0 m height with symmetrical side slopes of 1,4H:1V in upstream and downstream faces. During the impoundment period, cracks were observed in the concrete face slab of the dam. Gamboa (2011) investigates the formation of these cracks with deriving parameters by back analysis and conducting a three-dimensional analysis of the dam. To derive the parameters for materials, a two-dimensional model occupying Hujoux's material model was prepared, preferring a two-dimensional model to reduce the computational time spent in back analysis. The back analysis focused on the end of construction stage with

models involving variable number of zones with explained assumptions. Gamboa (2011) underlines that by using an increased number of parameters, an increased similarity is reached between the simulations and measurements. Using the parameters derived from the back analysis, deformation of the upstream face was modelled in a three-dimensional model. Firstly, comparing the construction stage deformation calculations of the 2-D and 3-D models, Gamboa (2011) observes that the effect of abutments in deformation limitation due to arching effect influences the results of the 3-D model. Concerning the deformations of the concrete face, perfect bond was assumed between the rockfill and concrete face neglecting additional modelling of a concrete slab above the upstream face, aiming to do the calculations using the upstream face strain values.

The results obtained from the three-dimensional analysis in the impoundment stage reveal tensile deformations near the lower end of the upstream face, and compressive strains in the lower third part of the upstream face. Gamboa (2011) indicates that the obtained results do not give insight on the cracks occurred in the midsection of the crest; explanation of which can be made by the complex interaction between the rockfill and the face slab or a progressive failure initiated at the lower third part of the face. Based on the results of the analyses, Gamboa (2011) suggests using magnification factors in two-dimensional back analysis of deformations for more accurate representation of three-dimensional behavior; giving examples such as assuming a magnification factor of 1,35 for V-shaped valleys with abutment slopes of 1H:1V, or a magnification factor of 1,25 for valleys with abutment slopes 1,6H:1V and a horizontal flat bottom, like in the case of Mohale Dam.

2.3.3.5. Karahnjukar Dam – Iceland

Karahnjukar Dam is the highest CFRD in Europe, with a maximum height of 196m. Located on the Jökulsa River, it is the main dam of the Karahnjukar project which

aims to generate electricity energy using Halslon reservoir basin with a joint cascade design. Karahnjukar and Desjarar Dams were constructed in Halslon reservoir, in addition to two smaller dams named Desjararstifla and Saudardalsstifla, to the east and west of Karahnjukar respectively (Gardarsson et al, 2015). A tunnel translates the water from Halslon reservoir to join another tunnel from Upsarlon pond and reaches the intake at the northwest of the joint in Valbjofsdadafjall in Fljotsdalur Valley, where the electricity energy is generated by turbines.

The A/H^2 ratio of the dam located in a deep valley is 2,42; main rockfill material is basalt and designed slopes for upstream and downstream faces are 1,3H:1V. Due to reported ruptures in central joints in similar dams during the construction of the dam, several protective measures and revisions were made in the compaction specifications, joint details and reinforcement (Cruz et al, 2010). Also, a self-healing fill on the upstream was specified as reported by Modares and Quiroz (2015), to protect the face slab and repair the body in case of crack development. In the study carried out by Modares et al (2015), a three-dimensional analysis model of Karahnjukar Dam was prepared to observe the effects of valley shape in addition to two-dimensional section behavior. In the analysis material model of Mohr-Coulomb was used for the rockfill, and as the foundation of rock has adequate stiffness to neglect the settlements, it was assumed to be rigid. Modares et al (2015) considered the construction in lifts by defining different material parameters at different elevations, in addition to making a staged construction analysis. The settlement results monitored on Karahnjukar Dam were used to calibrate the rockfill material parameters of the model. In the study, analysis results show a settlement of 130cm at the end of construction, and the monitored maximum value for settlement was 153cm. Modares et al (2015) therefore considers the assumptions made to be acceptable. In addition, the afore mentioned mitigation measures of possible risks were evaluated in the study regarding the performance of the dam. As explained above, preventive measures were taken against face slab rupture. Comparing the calculations on the performance of the initial design to the revised design, it was observed that the horizontal stresses on concrete face slab

were calculated to be considerably larger in the initial design. Therefore, it was stated that the design revision improved the performance and safety of the concrete face. The overall performance of Karahnjukar Dam was reported to be successful, with low settlement values and leakage below 200 l/s; which is normal in glacial areas.

2.3.3.6. Kürtün Dam – Turkey

With a height of 133 m, Kürtün Dam is the first CFRD constructed in Turkey. Located on Harşit River, Kürtün Dam has the purpose of energy production. Özkuzukıran (2005) indicates that tender/preliminary project determines ECRD type for Kürtün Dam, however, due to climatic conditions and scarcity of available impervious soil in vicinity, dam type was revised to CFRD. After the construction of rockfill embankment, a period for settlement was waited for 1,5 years to start the construction of concrete face. Özkuzukıran (2005) states the general geological profile as granadiorite, diabase, andesite and limestone. Maximum observed settlement for the construction period was 215,5 cm, and for the reservoir impoundment period the maximum observed settlement was 36,3 cm.

The analysis model studied by Özkuzukıran (2005) investigates the dam performance in both periods making use of FEM in 2-D. Deriving the model parameters from previous studies, Özkuzukıran (2005) carried out an analysis using the material model of Hardening Soil. Due to its structure, arching has significant effect on the behavior of Kürtün Dam; therefore, Özkuzukıran (2005) used correction factors for arching effect suggested by Hunter and Fell (2003) to increase the accuracy of analysis results. Analyses of Özkuzukıran (2005) indicated a maximum settlement of 205,13 cm for end of construction, and 54,10 cm for reservoir impoundment.

Results of stress calculations at the end of construction show similar stresses in upstream and downstream halves of the dam, because both sides were modelled with

the same material, and in reservoir impoundment condition horizontal, vertical and shear stresses increase in the upstream half whereas the increase of stresses near the downstream face are negligible. Comparisons of settlement and deformation show general agreement between calculated and observed results, despite differences which can be explained with construction method such as the practical efficiency of compaction, or macroscopic structural effects such as the real behavior of rockfill during impoundment and the bond between concrete face and the embankment.

2.3.3.7. Çokal Dam – Turkey

Çokal Dam, constructed in Turkey, has a height of 83 m and is located at a distance less than 10 kilometers to the North Anatolian fault. Arıcı (2013) evaluated the deformation behavior of the dam during construction, impoundment periods and in an earthquake event. The face slab was modelled in the construction stage with a linear elastic material model to investigate the effect of embankment body behavior on the behavior of face slab. It was observed that, the face slab is under compression in construction period, however, at reservoir impoundment period as the water level rises these compression stresses transform to tension, causing separation from the plinth at maximum water level. Observing the tensile stresses above 4 MPa, which exceeds the tensile strength of concrete, Arıcı (2013) made further analysis with a nonlinear material model for concrete. With this nonlinear model, tensile stresses at concrete were again observed to cause separation from plinth, but calculated tensile stresses were approximately 1 MPa. Arıcı (2013) stated portions of face slab between cracks were still able to undergo tension. Using Gergely-Lutz method, the width of cracks in the face slab was determined, with the formula

$$w_{max} = 2,2\beta_{GL}\varepsilon_{scr}\sqrt[3]{d_c A}$$

With w_{max} being the maximum crack width, β_{GL} being strain rate factor, ε_{scr} being the strain in reinforcement at cracking region, d_c being the section effective depth, and A being the effective area of concrete around the reinforcement. Calculating force demands converging to yield capacity of reinforcement, Arıcı (2013) observed crack widths about 1 mm in the analysis.

In the study of Özel (2012), Çokal Dam was analyzed with 2-dimensional and 3-dimensional finite element models to observe the differences in results calculated. Regarding the deformations in construction and impounding periods, 2-D and 3-D models do not provide significantly different results. Özel (2012) stated that 2-D analysis has its shortcomings in determining the state of stress near valley boundaries in the face plate. Seismic analyses for earthquake events with 144, 475, 975, 2475-year return periods were carried out; and the results of 2-D and 3-D models match for the events with smaller return periods, however, for the earthquake events with 975- and 2475-year return periods, significance of 3-D effects increase. Larger strains were derived from the 2-D model. On the other hand, for these events with 975- and 2475-year return periods, deformations of the face slab resulting in hitting of slab strips to each other in the 3-D model led to local crushing on the face slab. Özel (2012) suggested increasing the thickness or concrete strength of face slab to prevent this from occurring and suggested this type of a problem can be repaired after an earthquake event. Erdoğan (2012) studied on the effects of soil-structure interaction on an earthquake event; assuming the foundation soil to be a stiff soil according to classification of NEHRP and reservoir full condition neglecting hydrodynamic effects of the hydraulic pressure. Results of calculations gave 0,8- and 1,7-mm crack widths for impoundment and earthquake cases (Erdoğan, 2012). Regarding the soil-structure interaction, as the soil gets deeper, increase in crest deformations were observed in the earthquake event despite observing decrease of axial tensile stresses on the face slab in the impoundment case.

2.3.3.8. Dim Dam – Turkey

Constructed in Antalya on Dim River between years 1997-2006 and analyzed by Ayvaz (2008); Dim Dam has a height of 134,5 m with an upstream slope of 1V:1,4H and a downstream slope of 1V:1,5H. Designed with a concrete face area of 40521 m² the dam has a shape factor of 2,24; which can be considered as narrow. Ayvaz (2008) studied the deformations and stresses occurring on the dam for the end of construction. Analysis model was prepared using Hardening Soil model in a finite element analysis software, including zones 2A, 2B, 3B, and 3C on model embankment body. Evaluating the monitoring results, Ayvaz (2008) noted that some monitoring data on deformations may be unreliable, due to re-calibrations of the instrumentation and deviations in measurements. Obtaining a maximum settlement value of 1,74 m, Ayvaz (2008) comments that the results are in agreement with the analysis results of similar dams in the literature. A study by Keskin et al(2009) carried out on the safety of Dim Dam focuses on the performance of the dam in case of an earthquake event. Keskin et al (2009) modelled the dam in another finite element analysis software as a three-dimensional model with constant section dimensions of the maximum cross section along the body, assuming fixed connection of the dam body to the foundation, and a damping coefficient of 5%. Three scenarios in which the reservoir is empty, half-full and full were evaluated in the analysis model in an earthquake event, using linear elastic materials in a dynamic analysis with the earthquake records of 1999-Düzce earthquake. Commenting on the results, Keskin et al (2009) stated that the dam would be safe in the case of the simulated earthquake because of the observed small deflections and stresses, however, for a precaution against earthquakes of higher magnitudes, suggested construction of wider crests, milder slopes on the upstream and downstream faces in addition to the selection of appropriate compaction methods.

CHAPTER 3

KONYA AFŞAR HADİMİ DAM

3.1. General Information

Afşar Dam is a concrete faced rockfill dam located in Taşkent, Konya on the river Ilıcapınar, Turkey. With a maximum height of 127 m and a total length of 720 m, it is intended to serve for irrigation and drinking water supply of the region. It is constructed as a part of “Konya-Çumra Project” which is in the scope of “Konya Lowlands Irrigation Project”. This project aims to supply water for irrigation, domestic uses, industrial uses and hydroelectric energy production. Konya-Çumra Project constitutes the largest area of irrigation among the subprojects of Konya Lowlands Irrigation Project, with 343850 hectares. The objective in construction of Afşar Dam is to regulate the derived water from Göksu Basin to Bağbaşı Dam through the Afşar-Bağbaşı Tunnel, by the designed derivation system with a total length of 24 kilometers. Location of the dam and relevant information are given in Figures 3.1, 3.2, 3.3, 3.4, 3.5 and 3.6.

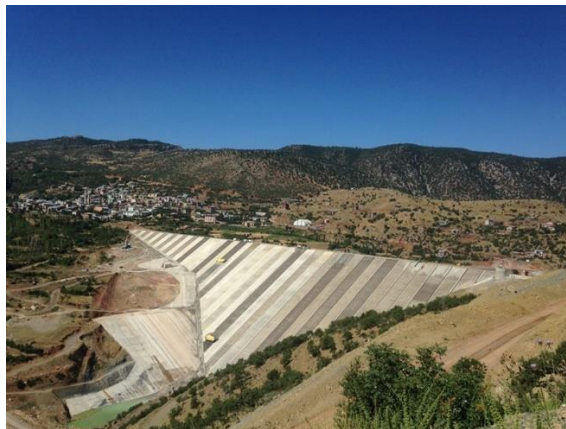


Figure 3.1. Upstream View of Afşar Dam (DSİ, 2016)

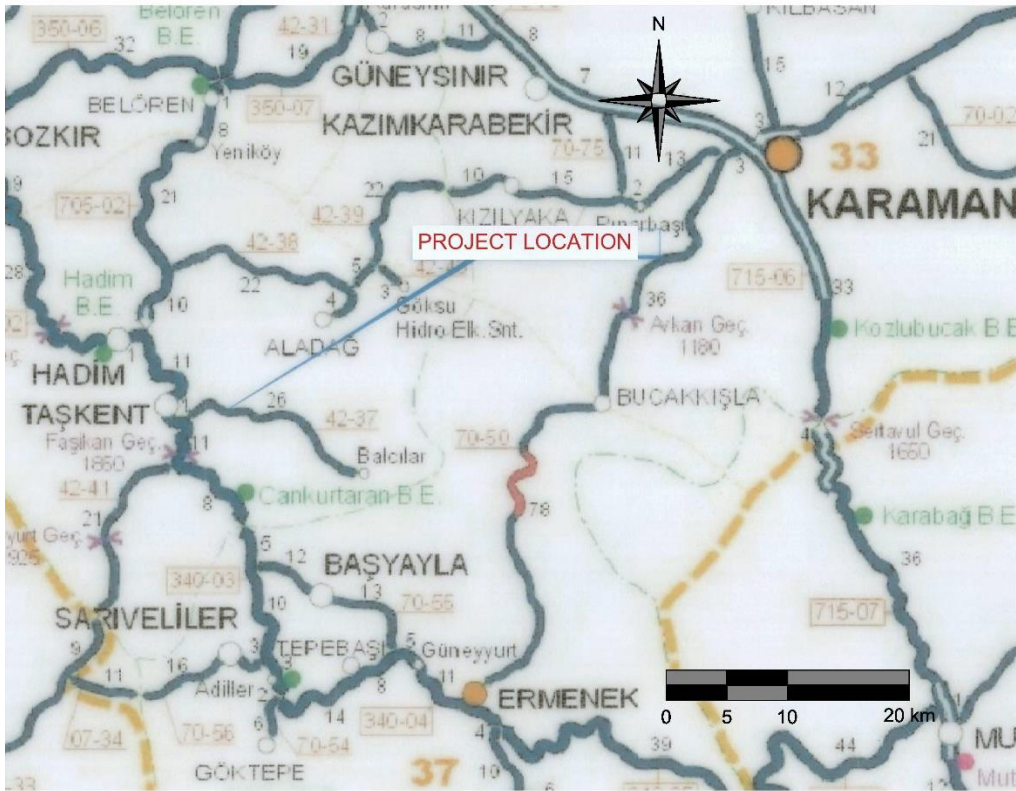


Figure 3.2. Location of Afşar Dam and Plan View of the Reservoir Area

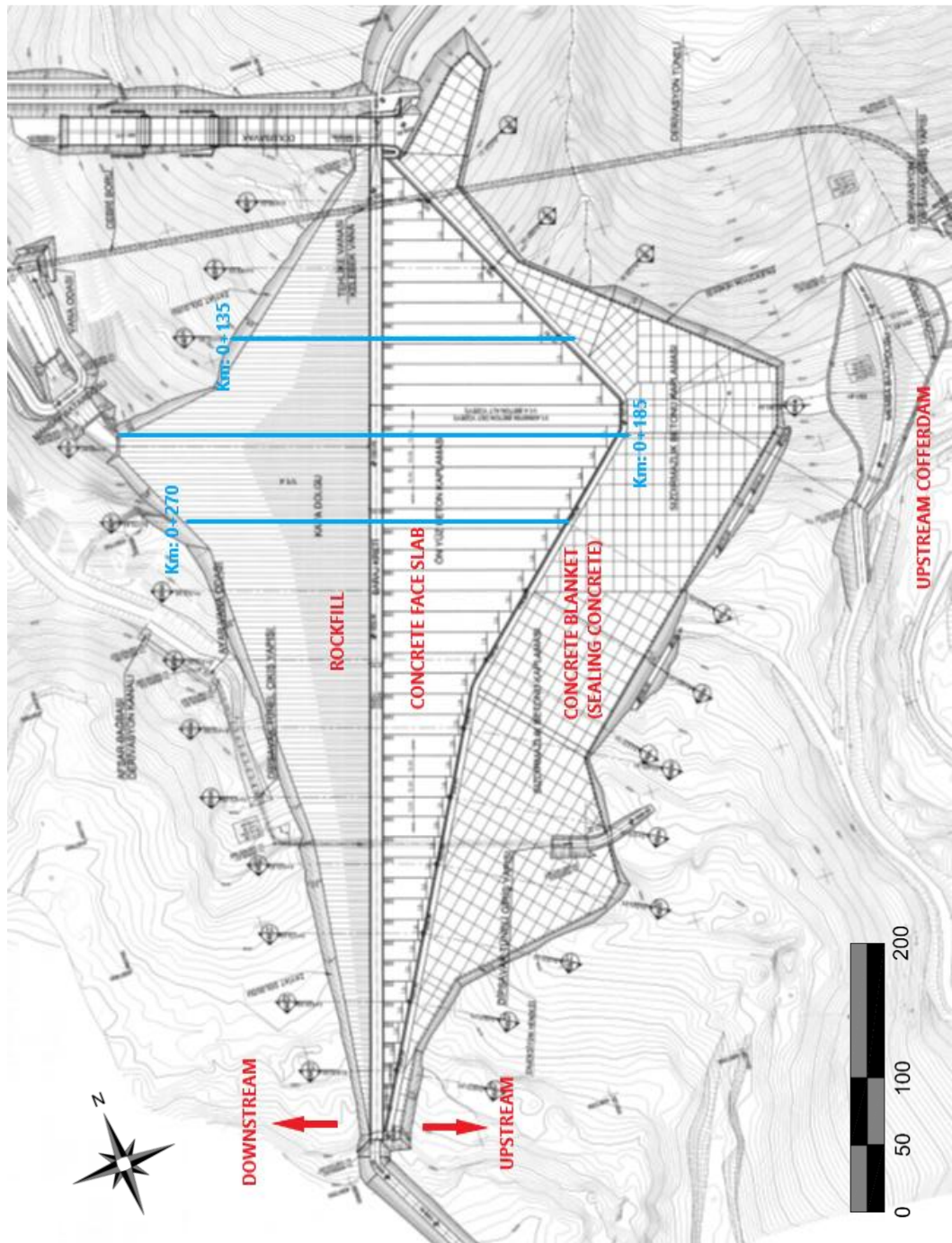


Figure 3.3. Plan View of Afşar Dam with Instrumented Stations at Km: 0+135, 0+185, and 0+270

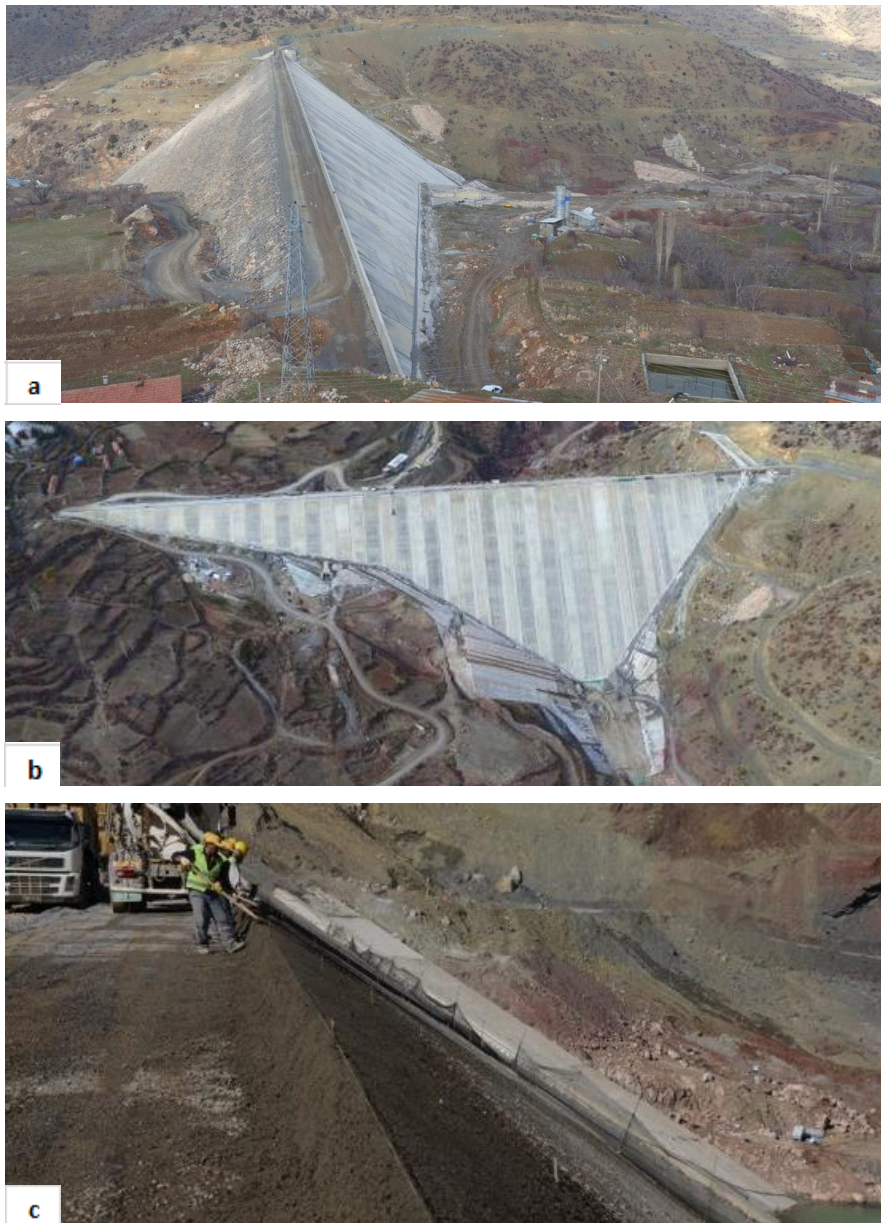


Figure 3.4. a) Longitudinal South and b) Upstream Top Views of Afşar Dam, c) Embankment Construction

Construction of the dam body started in December 2013, and 95% realization was indicated in July 2016 by DSI General Directory of State Hydraulic Works (DSI, 2016). With a height below that of Alto Anchicaya Dam (140 m, Colombia) which was built in 1970s, Afşar Dam can be categorized as a medium height dam when

compared with the highest; Shuibuya Dam (233 m, China) or Campos Novos (202 m, Brazil); but given that design and construction of concrete faced rockfill dams are closely related to experience; Afşar Dam has a considerable height, considering the previous examples from Turkey, Kürtün (133 m), and Dim (135 m) dams.

Dam zones occupied in Afşar Dam were placed according to the common zoning definition. Zones 1A, 1B, 2A, 2B, 3A, 3B, 3C, and 3D were positioned as shown in a representative cross section given in Figure 3.5. Compaction specifications indicated in construction drawings are given in Table 3.1.

The dam has a slope of 1,4H:1V on both upstream and downstream faces. Impervious upstream concrete face of Afşar Dam was designed to have a thickness increasing from 30 to 70 cm with depth. The common practical formula of $t = 0,3 + 0,003H$ was adapted in this project. In the construction drawings, concrete characteristic strength of 20 MPa was specified; with covers of 7,5 cm for the rockfill facing end, and 5 cm for the water facing end. Concrete face strips of 15 m were designed with construction joints in between. It was specified in the construction drawings that the placement of material for embankment shall be made from upstream towards downstream using material ascending in particle size providing regular appropriate side faces.

Table 3.1. *Compaction Specifications for Zones of Afşar Dam*

Zone	Material	$D_{max}(cm)$	Layer	
			Thickness (cm)	No. of Passes
1A	Cohesionless fine sand+silt fill	5	15	4
1B	Unsorted pervious fill	40	40	4
2A	Perimeter joint filter zone	2	30	4
2B	Cushion layer zone	8	30	4
3A	Select rock	30	40	6
3B	Quarry rock	60	90	6 + 250L/m ³ water
3C	Quarry rock	80	100	6 + 250L/m ³ water
3D	Quarry rock	100	Placed by Machine	

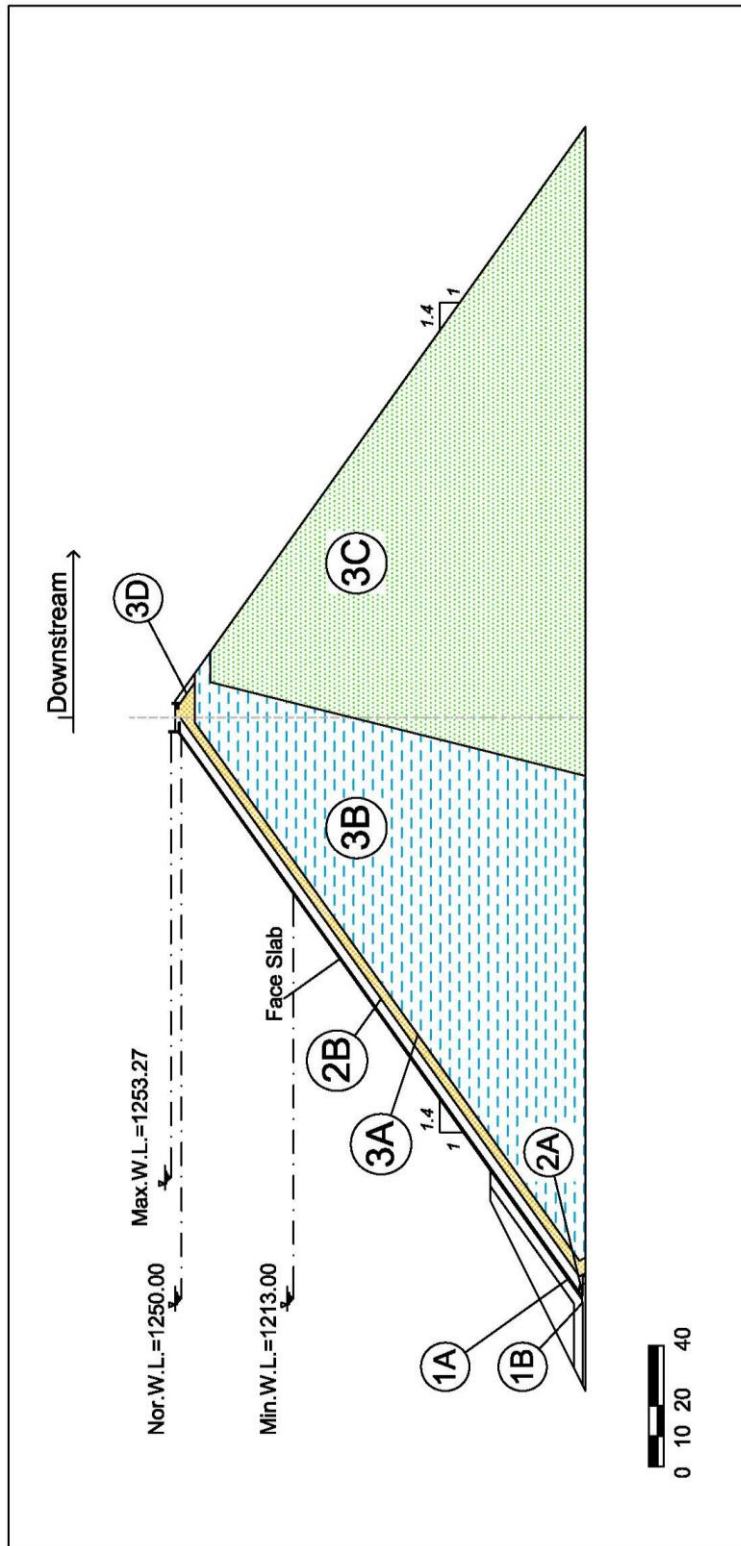


Figure 3.5. Cross Section of Afşar Dam

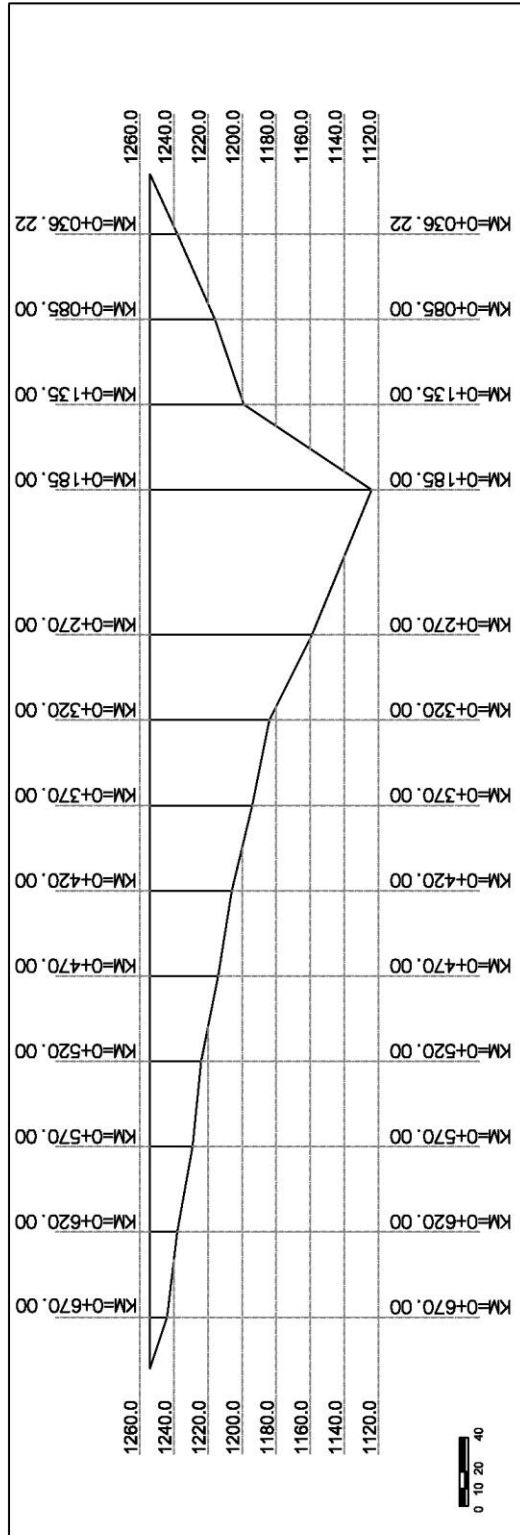


Figure 3.6. Longitudinal Section View of Afşar Dam from Upstream

Design notes on Zone 3B specified the maximum particle size as 60 cm, with a maximum percentage of particles passing 5 mm sieve of 2%, and particles with a smaller diameter than 2,5 cm was limited to 30%. Zone 3B was specified to be constructed in 90 cm lifts with minimum 6 passes of a 10-ton vibratory roller. Design notes on Zone 3C specified the maximum particle size as 80 cm, with a maximum percentage of particles passing 5 mm sieve of 2%. Zone 3C was specified to be constructed in 100 cm lifts with minimum 6 passes of a 10-ton vibratory roller. Sluicing during the construction was specified as 250 L of water per m³ of rockfill for both Zones of 3B and 3C.

Specified in the construction drawings with a maximum reservoir level on elevation of 1253,27 m, a normal reservoir level on elevation of 1250,0 m, and a minimum reservoir level on elevation of 1213,0 m; Afşar Dam has a foundation level lowest near the elevation of 1120,0 m. The dam was built on a limestone formation, by scraping the above alluvium layer of approximately 5 m in thickness. The dam site also contains talus, which is considerably weak from the stiffness point of view; however, the thickness of talus layer is smaller than 5m. The dam is located in an area where the main limestone layer dips into the Döngelli formation, which is defined as a formation consisting of flysch, conglomerate, sandstone, siltstone and shale.

The geological map of the dam site is given in Figure 3.7. For the treatment of the foundation, grout curtain applications were made about the plinth and at the end of concrete blanket following the plinth. Cap grout with 3 m spacing was applied at a depth of 5 m in 2 rows below the plinth. Seaming grout of 15 m depth was applied at the end of concrete blanket in 1 row with 3 m spacing. As it was stated by ICOLD (2004), hydraulic gradients as high as 20 can develop along the plinth; therefore, possible erosion and piping shall be prevented by foundation treatment with grouting. Grouting was specified to be made by filling the holes drilled with grout at a pressure of 22,5 kPa for cap grout and 33 kPa for seaming grout.

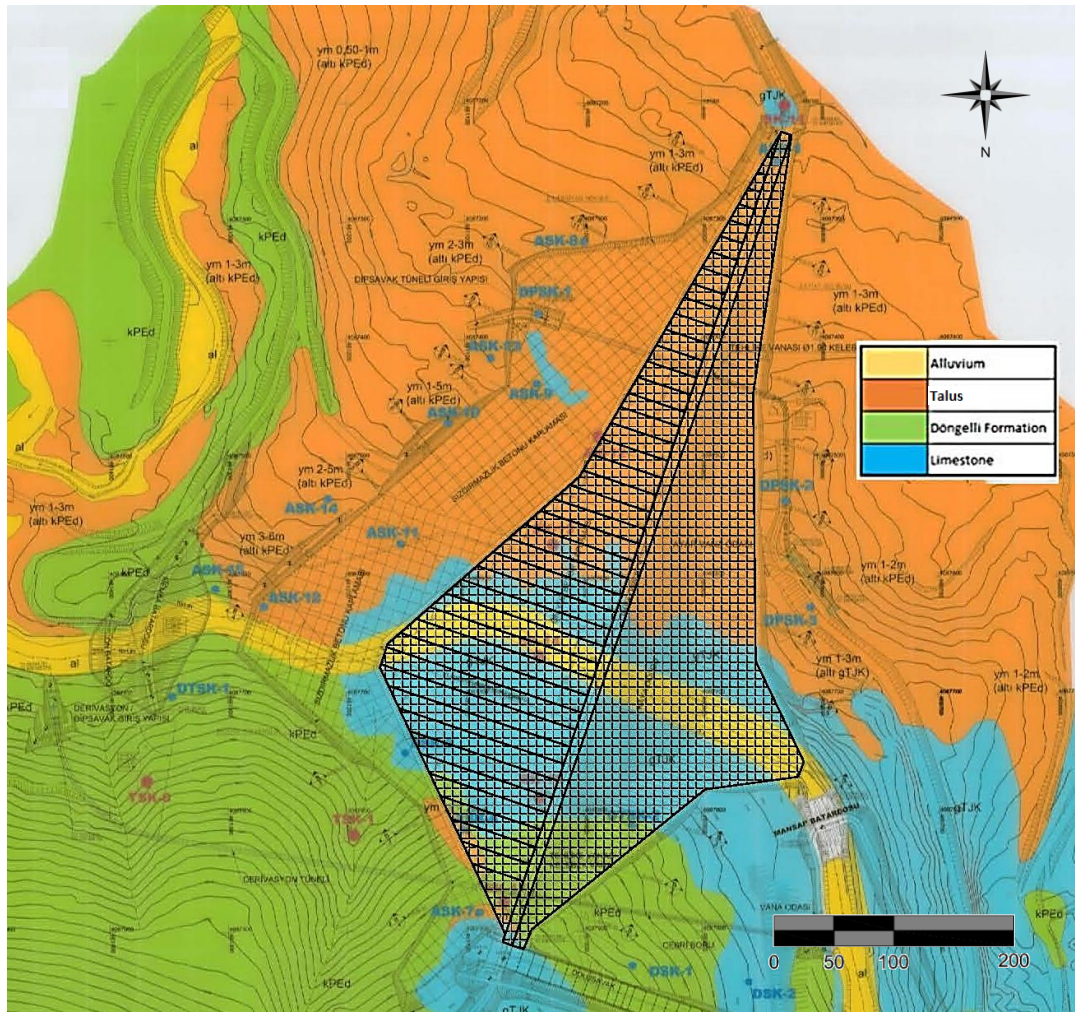


Figure 3.7. Geological Map of Afşar Dam

3.2. Instrumentation

For operational safety and providing data for future projects, instrumentation of CFRD behavior is vital. Instrumentation is placed in dam bodies to observe the performance of the dam, verify the expectations in design, find out possible problems, check the success of remedial measures applied and collect data for future projects. A useful instrumentation is the one in which data collection is done regularly, calibration and replacement of instruments are done in case of instrument failure, and the collected data are evaluated for operation and maintenance.

As indicated by Arı (2016), lifetime monitoring of a CFRD may provide essential data for observing the dam behavior and for taking remedial measures when necessary. In Turkey, it is specified by the State Hydraulic Works (DSİ) that pressure cells, hydraulic settlement cells, in-place and servo inclinometers, jointmeters, and vibrating wire piezometers should be placed in the construction of CFRDs. The numbers and positions of dam instrumentation are project-specific, but the Authority specifies the placement and instrument precision requirements (DSİ, 2014).

In Afşar Dam, it is indicated in the project drawings that 20 total pressure gages, 20 hydraulic settlement cells, 16 1D jointmeters, 11 3D jointmeters, 8 strainmeters, 18 vibrating wire piezometers, 1 magnetic plate inclinometer were planned to be installed and 43 embankment measuring points were planned to be established. The geotechnical instruments are located in three stations, at Km: 0+135, Km: 0+185, and Km: 0+270. Cross sections of the dam at these stations are given in Figures 3.8, 3.9, and 3.10, with the instruments indicated on the prescribed locations. Embankment measuring points were established along the longitudinal axis of the dam body as well, at stations, Km: 0+036, Km: 0+085, Km: 0+320, Km: 0+370, Km: 0+420, Km: 0+470, Km: 0+520, Km: 0+570, and Km: 0+620. As it is the cross section with maximum height and displacements, the station at Km: 0+185 is selected for the two-dimensional analyses. This study is based on the data collected by 20 total pressure gauges, and 18 hydraulic settlement cells, for the period between February 2014 and February 2016. Brief information on the instrumentation of Afşar Dam is given below.

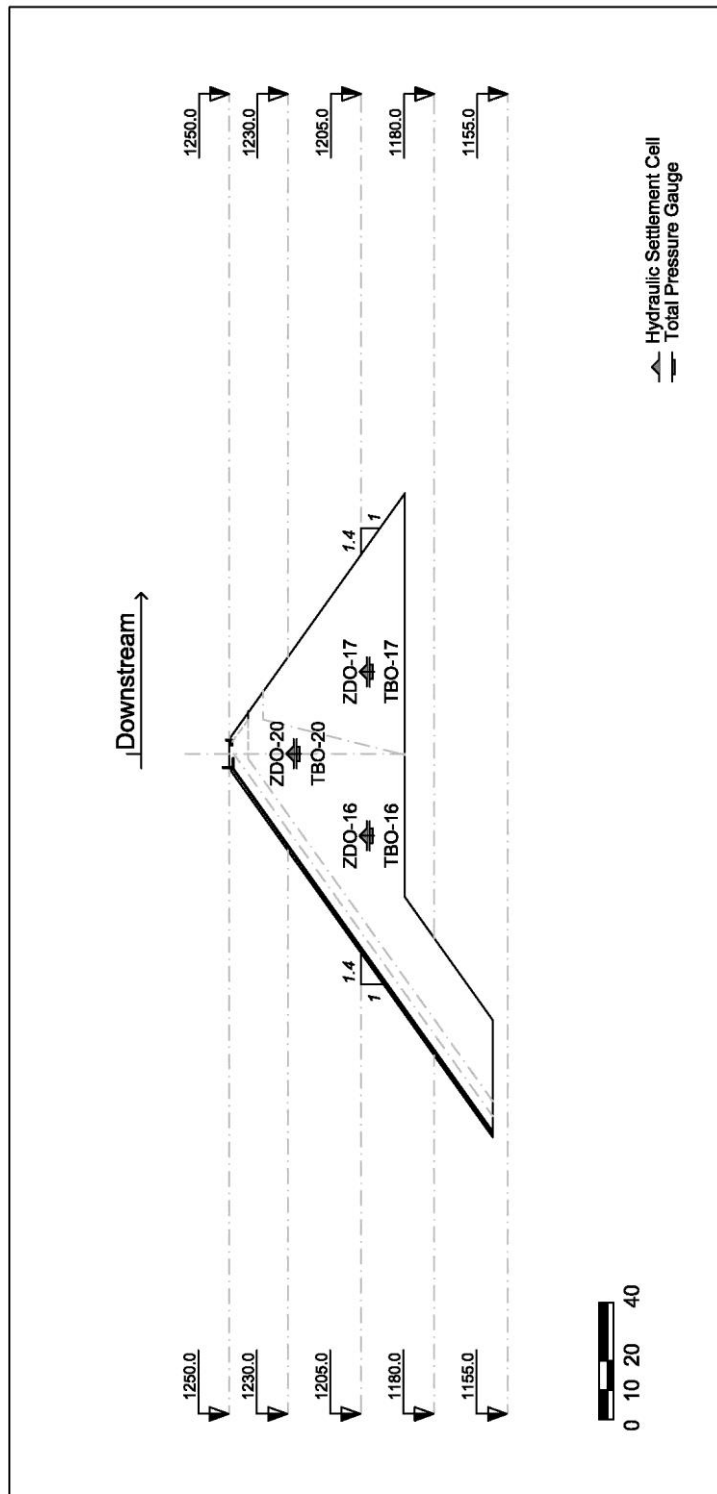


Figure 3.8. Dam Section and Monitoring Devices at Km: 0+135

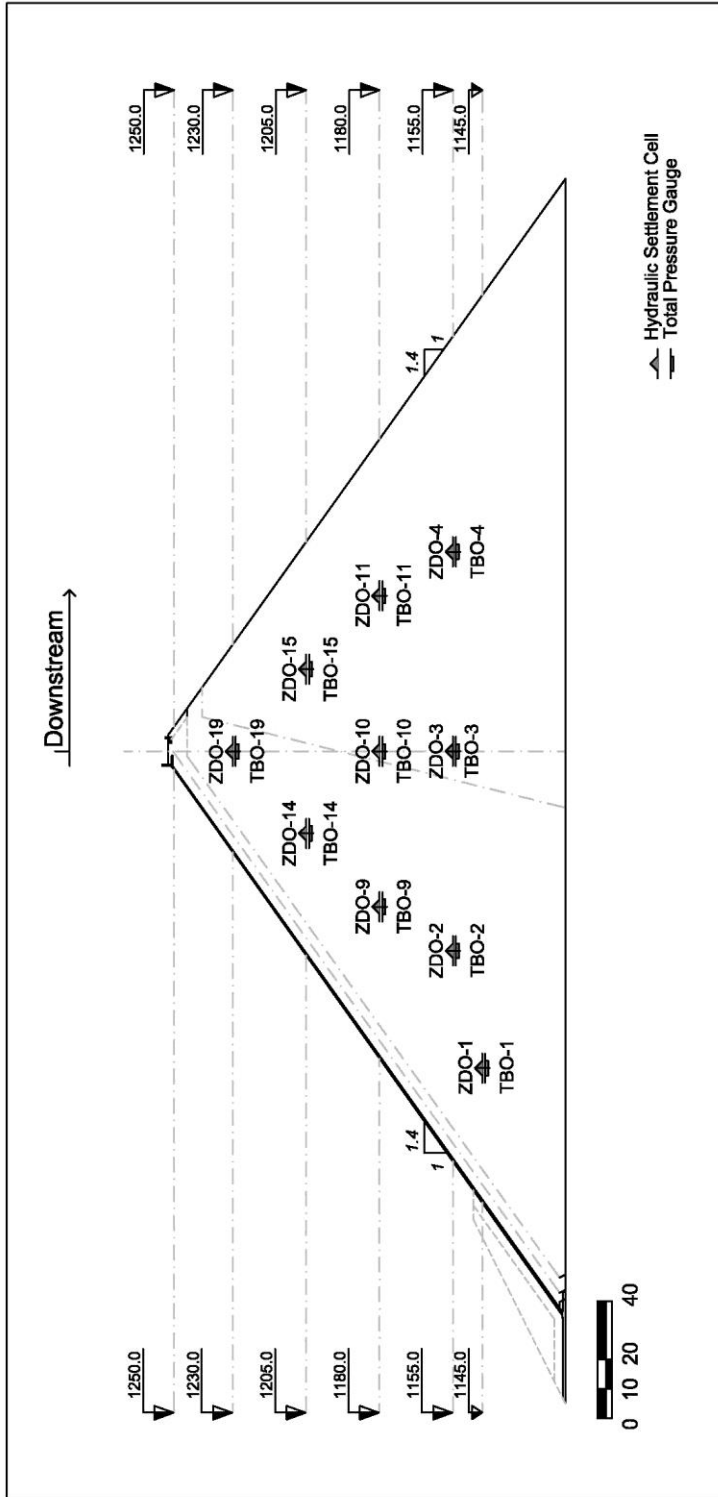


Figure 3.9. Dam Section and Monitoring Devices at Km: 0+185

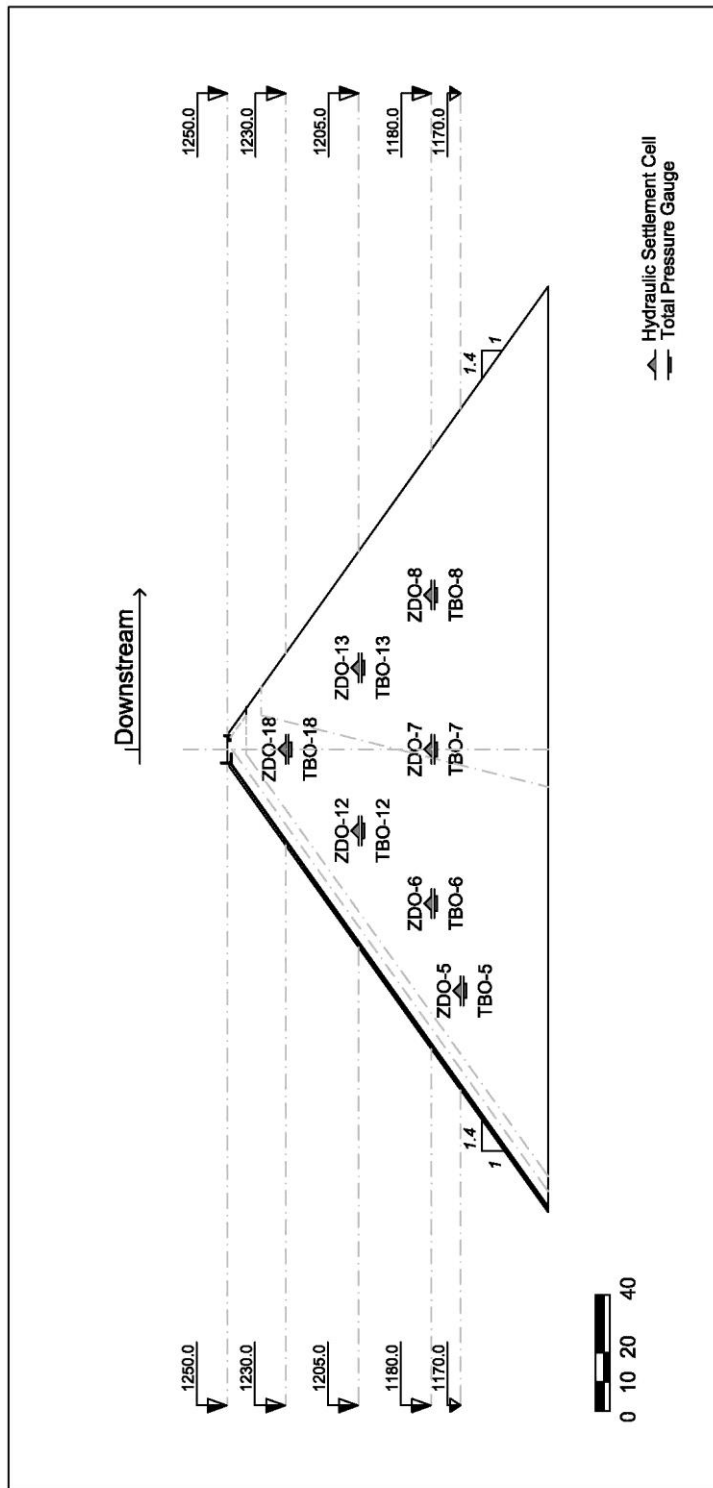


Figure 3.10. Dam Section and Monitoring Devices at Km: 0+270

3.2.1. Total Pressure Gauge

Monitoring the pressure on certain locations throughout the dam body provides data for evaluation of dam behavior; as well as observation of the overall rock skeleton performance. Total pressure gauges are installed inside the dam body; therefore, to measure the internal stresses accurately, stiffness of the gauge must be similar to that of the embankment material. It was indicated by Elmi and Mirghasemi(2013) that possible difference in stiffness between the installation trench of pressure cells and embankment may cause local arching which may result in underestimations in stress measurements; because the pressure cells are installed within finer grained fills, and the compaction of the installation trenches generally should be made using lighter weights than used in embankment compaction. Therefore, proper installation and calibration of pressure cells are vital for proper performance (Elmi and Mirghasemi, 2013). Regarding the local arching phenomenon that may occur about the geological instrumentation placed inside dam bodies, Elmi and Mirghasemi (2013) stated that local arching may occur by the transfer of stresses from the installation trench to the main dam body material, and the investigating local arching may be possible by following the first 15 m of overburden to be loaded upon the instrument elevation.

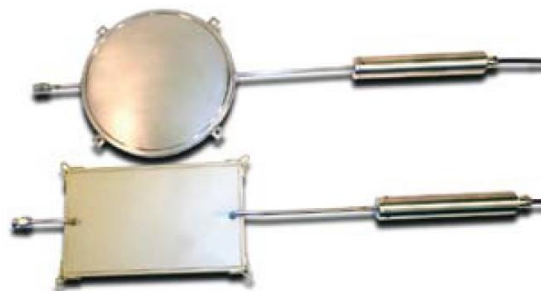


Figure 3.11. Circular and Rectangular Total Pressure Gauges (Roctest, 2016)

Measurements of the cell are transmitted via a vibrating wire transmitter; and as the gauge is installed during the embankment construction, it should be covered adequately to operate safely.

20 total pressure gauges were installed in Afşar Dam; 3 of which located in station at Km: 0+135.00 (TBO-16, 17, 20), 10 in station at Km: 0+185.00 (TBO-1, 2, 3, 4, 9, 10, 11, 14, 15, 19), 7 in station at Km: 0+270.00 (TBO-5, 6, 7, 8, 12, 13, 18). All of the installed total pressure gauges were reported to be operational, except TBO-1 at Km: 0+185 and TBO-6 located at Km: 0+270, on which incompatible values were recorded, therefore these were not considered in the analyses. Measurements of the total pressure gauges installed in Afşar Dam body were recorded weekly starting from the installation dates of each.

3.2.2. Vibrating Wire Piezometer

Seepage is an important indicator of the overall performance of a dam. Seepage and leakage under the dam foundation and through the dam body are monitored by piezometers. Piezometers are used for recording the groundwater table level and measuring pore water pressures.

Piezometers can be categorized into two types, as hydraulic piezometers and electrical piezometers. Hydraulic piezometers directly measure the water level; observation wells and standpipe piezometers can be listed as examples. Electric piezometers provide higher precision, by measuring the pore pressure with acoustic gauges, manometers or pneumatic sensors.



Figure 3.12. Vibrating Wire Piezometer (Roctest, 2017)

As specified by State Hydraulic Works (DSI) in Dam Instrumentation Technical Specifications, for CFRDs of height higher than 50 m, vibrating wire piezometers with 0,5% accuracy and 0,1% precision shall be installed (DSI, 2014).

18 piezometers were installed in the body of Afşar Dam, two of which (P06, P11) failed therefore could not provide data. Because piezometers were installed inside the dam body, embankment deformation can cause problems in operation and signaling; preventing monitoring. 5 piezometers were installed in station at Km: 0+135.00 (TP-14, 15, 16, 17, 18); 6 piezometers were installed in station at Km: 0+185.00 (TP-8, 9, 10, 11, 12, 13); and 7 piezometers were installed in station at Km: 0+270.00 (TP-1, 2, 3, 4, 5, 6, 7).

3.2.3. Hydraulic Settlement Cell

For an embankment structure, settlements are inevitable, due to the mass of the body; on the other hand, these deformations have to be in acceptable range for a structure to be considered safe. Hydraulic settlement cells are installed in CFRDs to monitor the rate and amount of settlements. Like total pressure gauges, hydraulic settlement cells are installed inside the dam body, covered appropriately with the transmitter cables

placed inside pipes to prevent harm from water or embankment material. Criteria which are also specified by the State Hydraulic Works for hydraulic settlement cells as regard to the corrosion resistance, accuracy and precision since these devices are planned to be used for the service life of the dam (DSI, 2014).

A total of 20 hydraulic settlement cells were installed in Afşar Dam, one of which (ZDO-18) failed. Hydraulic settlement cells were installed in the three sections mentioned above; and elevations where these cells were installed were listed as 1205 and 1230 m for Km: 0+135; 1145, 1155, 1180, 1205, 1230 m for Km: 0+185; 1170, 1180, 1205, 1230 m for Km: 0+270.

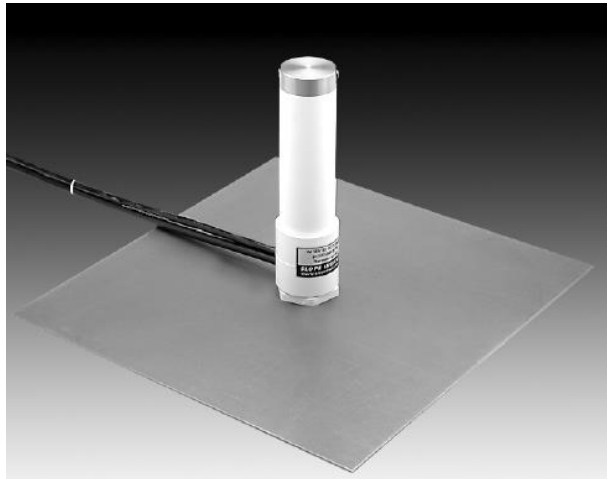


Figure 3.13. Hydraulic Settlement Cell (DGSI, 2018)

3.3. Observed Behavior in Construction Period

For a dam with level foundation, that has symmetrical dimensions about the centerline, expected deformation behavior is larger vertical displacements near the central section with decreasing values about the upstream and downstream ends. This occurs mainly due to the sloped geometry of rockfill embankments. Generally upstream zone, Zone

3B, has a higher deformation modulus than that of Zone 3C, the downstream zone. However, if this difference is not significant or combined with an uneven embankment construction schedule, it does not amplify the deformation difference in construction period. These expectations on deformation of CFRDs neglect the effects of 3-dimensional behavior and as Özel (2012) states, especially at sections near the abutments, deformations are affected by the valley shape by the support provided by the abutments decreasing the expected deformation to some extent near the valley ends.

A study carried out by Escobar and Posada (2008) gives a graphical representation on deformation behavior of CFRDs regarding the valley shape, Figure 3.14. A non-dimensional shape factor of A/H^2 , A being the area of concrete face and H being the height of the dam, reflects the different situations with lower values for narrow valleys and higher values for wider ones. With an approximate concrete face area of 53620 m² and a maximum height of 127 m, Afşar Dam has a shape factor of 3,32, and according to the study being mentioned the valley can be classified as narrow. As seen in Figure 3.14, although height and side slopes of Afşar Dam were mentioned to be similar to that of Alto Anchicaya Dam, this dimensionless representation may give a general indication regarding the effects of three-dimensional behavior within the analysis, nevertheless, behavior of two dams should have differences.

Data available on the monitoring of Afşar Dam are limited to the construction period, with a time span between 03.12.2013-29.02.2016. Monitoring results give insight on the construction period of embankment, and the settlement rates for a period of 9 months after the completion of embankment; although the data for impoundment was not available.

Regarding the study made by Escobar and Posada (2008), the behavior including impounding can be estimated to be similar to Cajon Dam optimally or similar to Barra Grande as a worst-case scenario. Cajon Dam, with a height of 188 m and shape factor of 3,1 was constructed in Mexico. Monitoring results reflect a very successful

performance with seepage values below 150 l/s. Barra Grande Dam, on the other hand, located in Brazil at a height of 185 m, is in a very narrow valley. Several problems occurred in dam performance due to cracks and ruptures on the concrete face. It was reported that seepage values between 600-1300 l/s were experienced.

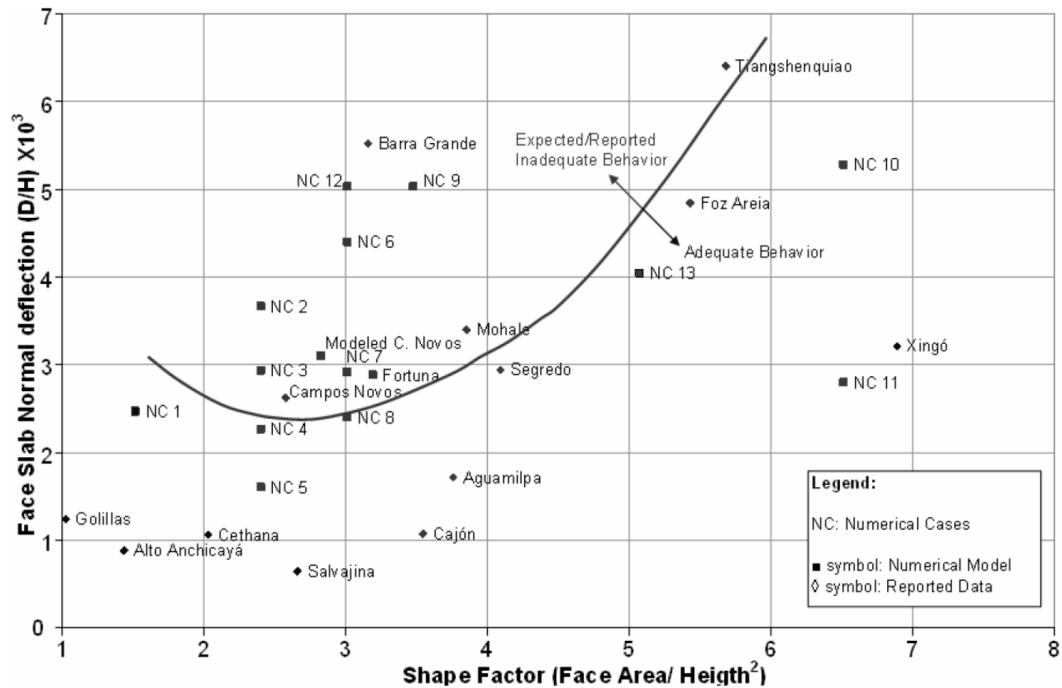


Figure 3.14. Face Slab Normal Deflection vs. Shape Factor for Selected CFRDs (Escobar and Posada, 2008)

Deformations of Afşar Dam (Figures 3.15, 3.16, 3.17) have differences from general expectations on CFRD behavior during construction period. Firstly, unlike the common behavior of higher displacements near the central portion decreasing through the upstream and downstream ends, when the section with the maximum height is observed for Afşar Dam, it is seen that higher displacements occur about the upstream end, and the displacement values are decreasing through the downstream end. The geology with dips of the main layer into the local formations, affects the design as the dam height on the upstream and downstream sides differ significantly which is

assumed to affect the observed results of the settlement behavior. After the completion of the embankment construction approximately in May 2015, settlement rate through the dam body got slower, yet having monthly rates as large as 9,87 cm.

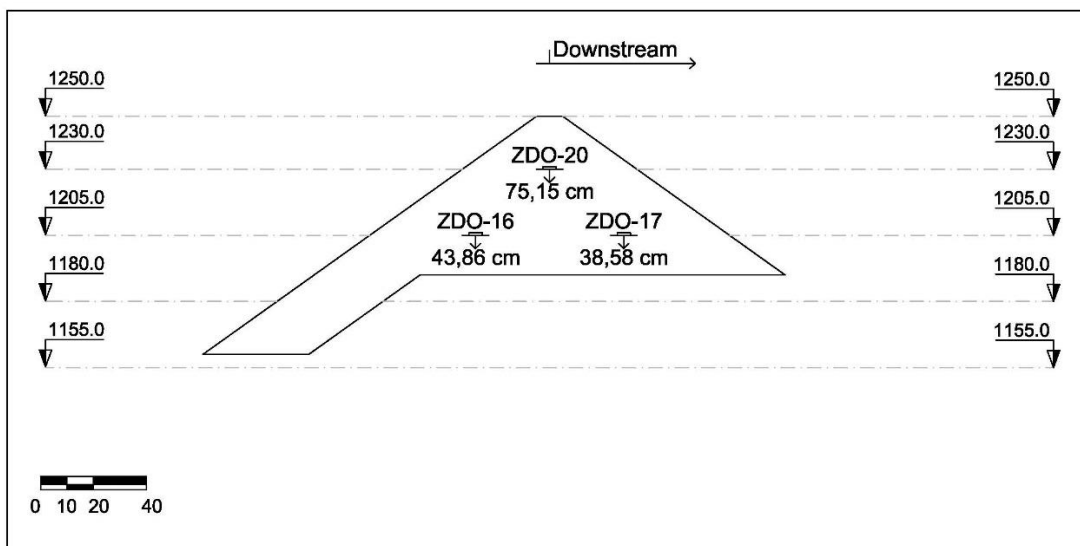


Figure 3.15. Total Monitored Settlements at Section Km: 0+135

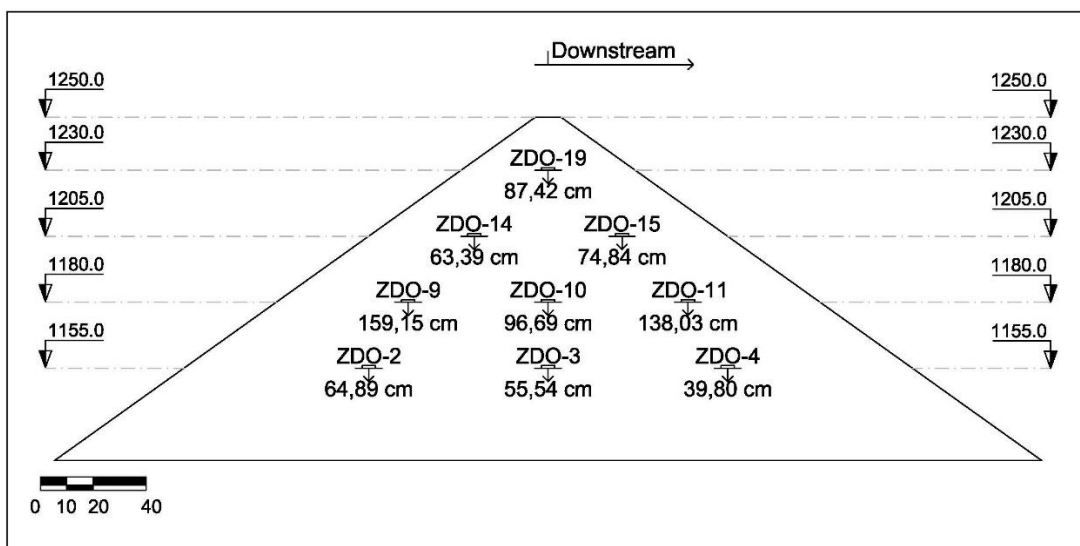


Figure 3.16. Total Monitored Settlements at Section Km: 0+185

Table 3.2. Total Stress Monitoring Results and Approximate Overburden Pressures

Section	Elevation (m)	Total Pressure Gauge	Average Fill Height Above (m)	Average Total Stress (kPa)	Monitored Total Stress (kPa)
Km: 0+135	1230,0	TBO-20	20	420	294
	1205,0	TBO-16-17	22	462	494-506
Km: 0+185	1230,0	TBO-19	20	420	229
	1205,0	TBO-14-15	22	462	512-436
	1180,0	TBO-9-11	32	672	650-635
		TBO-10	70	1470	1138
	1155,0	TBO-2-4	46	966	1305-857
		TBO-3	95	1995	1072
Km: 0+270	1230,0	TBO-18	20	420	228
	1205,0	TBO-12-13	22	462	570-719
	1180,0	TBO-6-8	32	672	153-1015
		TBO-7	70	1470	779

Simply comparing the total stress results at instrumentation points with average fill pressure calculations, the expected behavior of increasing stresses towards the center was verified; especially for the section with the maximum height, that is at Km: 0+185. Monitoring results at the instrumented sections for total stresses are given in Figures 3.18, 3.19, 3.20. On the other hand, this verification is in contradiction with the monitored settlement results; which leads to a requirement to assess the valley shape effects on the deformation behavior of Afşar Dam. Comparing the deformation monitoring results to recorded stress measurements, especially for the section with the maximum height, which is the main analysis section of this study, incompatible results were observed for the ratio of displacements to occurring stresses. For the central zone of dam at elevation 1180 m, displacement results decrease from upstream and downstream ends towards the dam center, whereas the vertical stresses increase in the same direction. This incompatibility may be a result of problems in displacement

monitoring devices since the stress results match with general expectations. On the other hand, to reach reliable conclusions regarding the behavior analysis; the results and causes shall be properly identified.

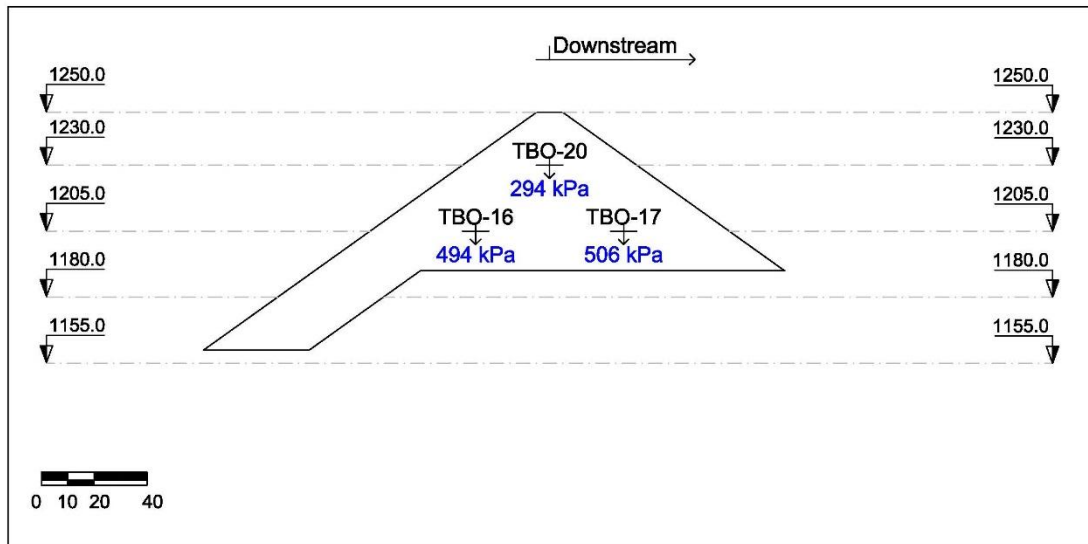


Figure 3.18. Total Monitored Pressures at Section Km: 0+135

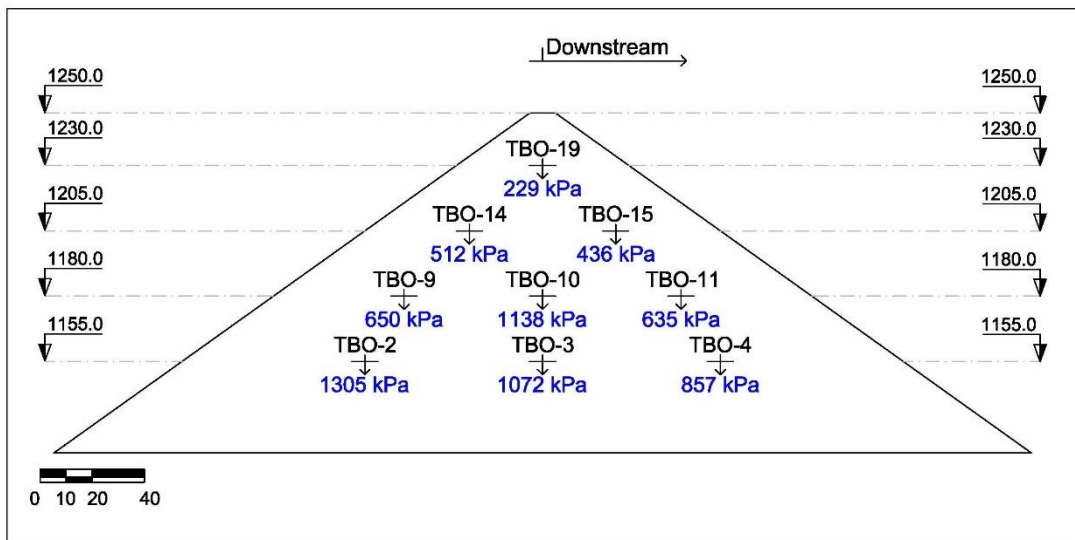


Figure 3.19. Total Monitored Pressures at Section Km: 0+185

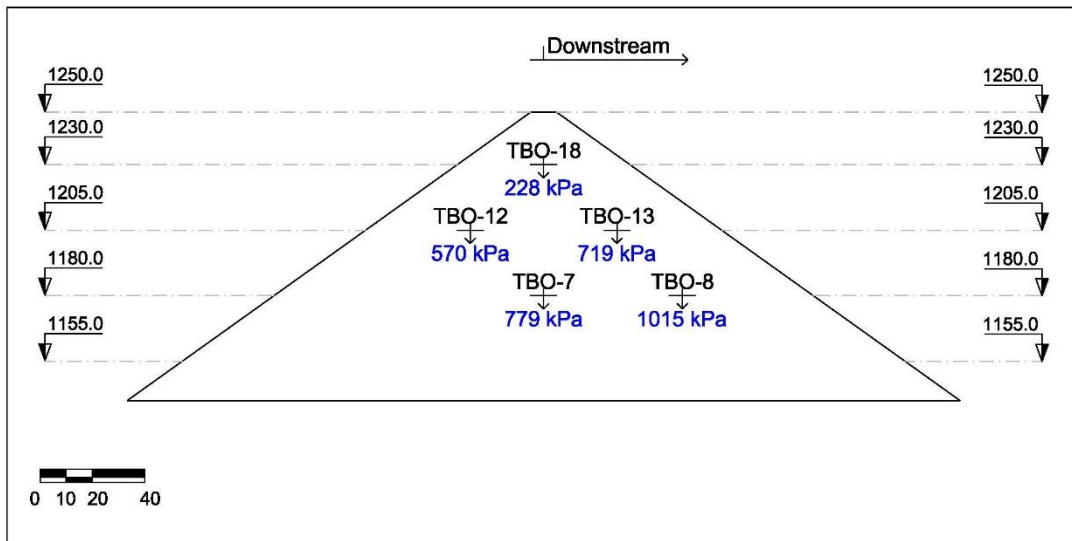


Figure 3.20. Total Monitored Pressures at Section Km: 0+270

The valley shape plays an important role in the deformation behavior of a dam. As stated by Da Silva and Assis (2014), especially for dams constructed in narrow valleys with varying geology; the effects of valley shape on the mechanical behavior of the dam have to be considered. Therefore, observations on sections should be evaluated considering the overall shape and location of the dam. The length of Afşar Dam is nearly 700 m, however, the deep valley sections occupy less than 1/3 of this length. Because of this, the deformation behavior of Afşar Dam is predicted to be affected by the arching force provided by the dam-valley connections. Although monitoring problems and failure of devices are commonly recorded in the instrumentation reports; a simple cross check between the deformation and stress results, or the expected overburden stresses and stress results, may provide more insight on the selection of reliable monitoring data. In this study, in addition to this comparison, effect of valley shape in the behavior of Afşar Dam was also investigated; to reach more reliable conclusions regarding the actual conditions of the dam.

3.4. Finite Element Analysis of Deformation Behavior

It should be remembered that when modelling is made, material properties and model parameters determine the likelihood of the model to simulate realistic results. However, it is not always possible or feasible to determine the properties of the rockfill embankment with field or laboratory tests. Therefore, in this study, previous studies on CFRD deformation behavior were taken into account, considering dam projects with similar height and shape properties, and material parameters used in previous studies were considered as preliminary parameters for the deformation analysis of Afşar Dam; iteratively reaching analysis parameters by comparing the model results with monitoring results.

Instrumentation results were available for the construction period, and although the recordings of impoundment period were not available, finite element analyses were made for the impoundment condition. Two-dimensional plane strain analysis of the dam body was studied on software Plaxis 2D. The staged construction of the embankment body was modelled, assuming groundwater level to be further below the foundation. Settlements of each construction stage were calculated independently and then the overall results were evaluated. Like the afore mentioned studies, the two-dimensional deformation analyses of the dam were used to calibrate the model material parameters to be used in the three-dimensional analyses. Because the monitored deformation results of the dam deviated from the expected results, an investigation of the effect of valley shape on the overall behavior was considered necessary. Three-dimensional analyses of Afşar Dam were studied by software Midas GTS NX. Different cross sections at stations given in construction drawings were used to model the dam body, to take into account the foundation geometry. Similar to the two-dimensional analyses, the foundation bedrock was assumed to be incompressible; therefore, the parameters selected for the bedrock material were checked to ensure no deformation occurs below the foundation of the dam body.

Determination of the model material parameters stand as the most important step in the deformation analysis; in a drained scenario using Hardening Soil model, cohesion, internal friction angle and deformation moduli are required by the engineer; and deformation moduli shall especially be defined by judgment. In the deformation analysis of a CFRD the only material with prescribed parameters is the concrete face; therefore, initial rockfill material parameters should be selected for the back analyses by surveying the previous studies and the data given in construction drawings.

Initial parameters to be used in the deformation analyses of Afşar Dam were derived from previous research on the deformation analyses of Nam Ngum 2 Dam in Laos. Observing the cross sections, Nam Ngum 2 Dam is located on a site with deviating natural ground level. Cross sections and the three-dimensional view of the dam are given in Figures 3.21 and 3.22. Also, upstream and downstream slopes, although in the downstream there exist two berms; are equal to the side slopes of Afşar Dam. In addition, because this study is a recent analysis including three-dimensional behavior analysis, the preliminary parameters to be used in the analyses of Afşar Dam for materials of Zones 3B and 3C were derived from the study of Sukkarak et al (2017). Comparing the values defined for zones 3B1, 3D, 3B2, 3C1 and 3C2, to ensure the difference in deformation behavior of zones, preliminary analyses were made using the values defined for zones 3B1 and 3C1 in the study of Sukkarak et al (2017).

In the study carried out by Sukkarak et al (2017), deformation of Nam Ngum 2 CFRD was analyzed by using a modified approach on Hardening Soil model. Nam Ngum 2 Dam was designed to have a height of 182 m, with side slopes of 1,4H:1V in the upstream face, 1,4H:1V in the downstream face with two berms. Face slab thickness was designed to be variable with height determined by the equation $T = 0,3 + 0,003H$ in meters. With a concrete face slab area of 88000 m², the dam has a shape factor of 2,65; which can be categorized as narrow. Construction schedule of the dam was planned so that after reaching a height of about 94m upstream, first stage of face slab was to be constructed and after reaching the total height, second stage of face slab was

to be constructed. Therefore, construction of rockfill embankment in upstream and downstream halves were not realized simultaneously.

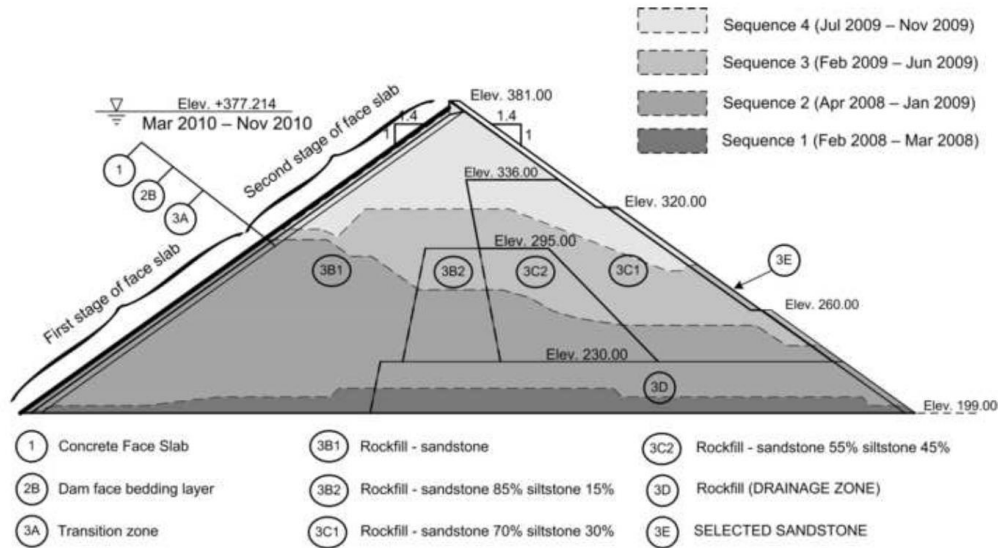


Figure 3.21. Zoning and Construction Sequences of Nam Ngum-2 CFRD (Sukkarak et al., 2017)

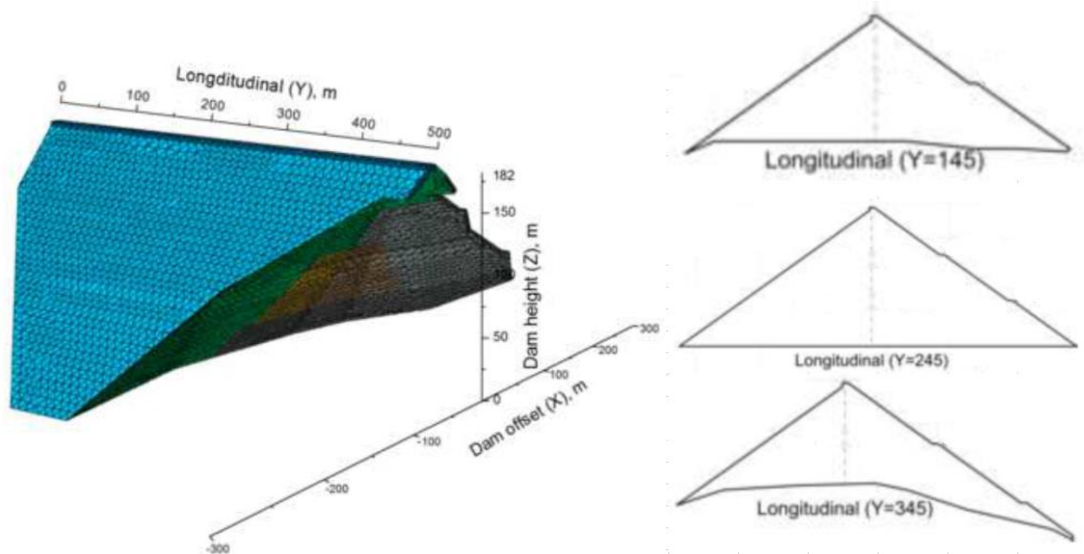


Figure 3.22. Three-Dimensional View and Cross Sections of Nam Ngum 2 Dam (Sukkarak et al., 2017)

Sukkarak et al (2017) aimed to reach an improved version of Hardening Soil model appropriate for rock behavior; by considering the effect of compression under high

confining pressures, causing stress dependent stiffness of material; and particle breakage using a modification of Rowe's dilatancy equation. Particle breakage index by Einav (2007) was used to define the occurrence of particle breakage. Einav (2007) defined the particle breakage factor, B_g , with the equation

$$B_g = \frac{\int_{d_m}^{d_M} [F_u(d) - F_0(d)] d(\log d)}{\int_{d_m}^{d_M} [F_c(d) - F_0(d)] d(\log d)}$$

Where F_0 , F_c , and F_u are the initial, current and ultimate gradation curves; and d , d_m , and d_M are the particle diameter, minimum particle diameter and maximum particle diameter, respectively. Einav (2007) defined these curves with α_0 , α_c , and α_u , fractal dimensions for the initial, current and ultimate gradation curves, respectively, as

$$F_0(d) = \left(\frac{d}{d_M}\right)^{3-\alpha_0}$$

$$F_c(d) = \left(\frac{d}{d_M}\right)^{3-\alpha_c}$$

$$F_u(d) = \left(\frac{d}{d_M}\right)^{3-\alpha_u}$$

Yang and Juo (2001) suggested assuming 2,7 value for α_u is appropriate. Particle breakage was related to plastic work W_p and is defined as

$$B_g = \frac{W_p}{\chi + W_p} \text{ with } W_p = \int p' d\varepsilon_v^p + q d\varepsilon_s^p$$

In the principal stress space. The modification to Hardening Soil model was studied due to the results reached comparing the test results to model results for deformation. Differences in volumetric strain were reported to be much larger than the model results. Therefore, the power parameter m which represents the stress dependency of stiffness was modified as different values to be used for primary compressive and deviatoric stresses. It was estimated in the study that power parameter m for primary compressive stress can be assumed as 0,651 times the power parameter for deviatoric

stress. This suggestion was based on the tests conducted on rockfill materials of Nam Ngum 2 Dam, observing the data collected in the experiments on test samples under deviatoric stresses between 0,5 to 2 MPa, and a maximum stress of 3,2 MPa. To consider different degrees of evolution of stress dependent stiffness, n , to represent the power parameter m for cap yield surface in oedometer stiffness E_{oed} was used in the equation

$$E_{oed} = E_{oed}^{ref} \left(\frac{c \cos \varphi - \frac{\sigma'_3}{K_0^{NC}} \sin \varphi}{c \cos \varphi + p^{ref} \sin \varphi} \right)^n$$

In the study dilatancy with respect to particle breakage was defined by the equation

$$\sin \psi_{m,bg} = \frac{(\sin \varphi_m - \sin \varphi_{cv})(1 - B_g^\lambda)}{1 - \sin \varphi_m \sin \varphi_{cv}}$$

Where φ_m is the mobilized friction angle, φ_{cv} is the critical-state friction angle, and λ is the power parameter for breakage. This modification creates a small difference in pre-peak case, but the significant change in behavior is observed in post-peak case, where Rowe's dilatancy approach results in dilatancy fully mobilizing, while in the modified approach dilatancy decreases at a decreasing rate. Dependence of friction angle on the confining pressure was defined by the equation,

$$\varphi = \varphi_0 - \Delta\varphi \log\left(\frac{\sigma'_3}{p_a}\right)$$

Where φ_0 is the reference friction angle, $\Delta\varphi$ is the reduction factor, $\Delta\varphi$ is the reduction factor, and p_a is the atmospheric pressure. Using this modified approach on Hardening Soil model, Sukkarak et al (2017) prepared a model analysis of three-dimensional deformation behavior of Nam Ngum 2 Dam. In the model, the face slab was modeled with three-dimensional shell elements. Rock foundation and abutments were assumed to be linearly elastic. Model parameters for rockfill materials are given in Table 3.3.

Table 3.3. Model Parameters Used in Finite Element Analysis of Nam Ngum-2 Dam (Sukkarak et al., 2017)

Parameter	Zone					
	2B	3A	3B1&3D	3B2	3C1&3E	3C2
$\varphi_0(\text{deg})$	43,23	46,08	47,09	42,60	42,00	43,30
$\Delta\varphi$	1,16	2,59	2,99	2,55	2,45	3,95
$\Psi_0(\text{deg})$	3,2	3,2	3,2	0,5	-5,0	-5,0
$E_{50}^{\text{ref}}(\text{MPa})$	65	65	80	32	20	12
$E_{\text{oed}}^{\text{ref}}(\text{MPa})$	50	52	55	24	17	10
m	0,45	0,34	0,29	0,69	0,68	0,70
n	0,25	0,24	0,14	0,42	0,32	0,26
R_f	0,74	0,75	0,78	0,82	0,68	0,65
Other	$E_{\text{ur}}^{\text{ref}}=3E_{50}^{\text{ref}}, p^{\text{ref}}=100\text{kPa}, c=1\text{kPa}, \text{OCR}=1, K_0^{\text{NC}}=1-\sin\varphi, v_{\text{ur}}=0,3$					
Breakage Parameter	$\chi=993, \lambda=0,268$					

Results of the study proved that the maximum settlements are occurring in Zones 3C1 and 3C2, which have lower stiffnesses than other zones. Maximum calculated settlement was 1,9 m, and a particle breakage factor of 4 was reached in the model. Comparing the analysis results to measurements on the dam, calculated results were generally lower but in agreement with the measurements regarding the distribution of deformations. It was stated that the differences may be due to creep behavior of rockfill, which was not considered in model calculations.

In Afşar Dam project, an average unit weight of 21 kN/m^3 was assumed both for Zones 3B and 3C as it was stated that the quarries were to be used to supply material for both. Referring to the afore mentioned specifications on construction drawings, despite using the materials from same quarries, Zones 3B and 3C may be assumed to have different final stiffness moduli and internal friction angles, due to different

compaction schedules specified. Effects of defining different zones in the analysis model were also evaluated in the following section.

3.4.1. Deformation Behavior of Afşar Dam in Construction Period

The method and assumptions used in the analyses of deformation behavior of Afşar Dam in construction period are summarized in this section. Preliminary two-dimensional analyses performed for calibration of material parameters and three-dimensional settlement analyses of Afşar Dam are explained. Calculation results are compared to the monitoring results.

Results of the instrumentation show that in embankment construction period, despite negligible deviations, pore water pressure remains as zero, therefore, the deformations in construction period are computed assuming drained condition, with groundwater table further below the lowest elevation of the foundation. Parameters defined for each analysis were kept constant through the construction stages; and the bedrock was assumed to be infinitely rigid to focus solely on the deformations of dam body.

Preliminary two-dimensional analyses of the deformation behavior were carried out to calibrate the selected parameters for rockfill materials, to assess the significance of different zones in overall behavior, to evaluate the effects of assumed lift heights in construction stages and to observe the importance of valley shape in distribution of deformations along the dam body. The aim of these analyses was to reach settlement values at the end of construction period similar to the monitoring results on the maximum cross section at Km: 0+185. Assuming a thickness increasing linearly from 30 to 70 cm with depth for the face slab through the upstream face and a unit weight of 25 kN/m^3 for concrete, the total concrete face weight to act on a width of 1m is approximately 2775 kN. The concrete face slab was preferred to be included in the analyses following the calibration of the main model assumptions; as the predicted behavior of the embankment body directly determines the deformation estimates of

the concrete face. Finite element analyses of the deformation behavior of Afşar Dam were studied in 7 models; assumptions of which are given in Table 3.4.

Table 3.4. Afşar Dam Deformation Analysis Models

Model	Analysis	Lift Height(m)	Zones	Material Parameters (MPa)			
				Zone 3B		Zone 3C	
				$E_{50,ref}$	$E_{oed,ref}$	$E_{50,ref}$	$E_{oed,ref}$
1	2-D	10	3B	80	55		
2	2-D	10	3B-3C	80	55	20	17
3	2-D	5	3B-3C	80	55	20	17
4	2-D	5	3B-3C	52	35,75	30	25,5
5	2-D	5	3B-3C	24	17	20	17
6	3-D	5	3B-3C	52	35,75	30	25,5
7	3-D	5	3B-3C	24	17	20	17

For the calibration analyses 9 points were selected; given in Figure 3.23; at points of embankment body where the instruments were installed; as:

- Top center (A): 20 m below the crest elevation at the center of dam body
- 45-m Upstream (B): 45 m below the crest elevation, 40 m towards the downstream from upstream face
- 45-m Downstream (C): 45 m below the crest elevation, 40 m towards the upstream from downstream face
- Mid-height Upstream (D): 70 m below the crest elevation, 50 m towards the downstream from upstream face
- Mid-height Center (E): 70 m below the crest elevation, at the center of dam body
- Mid-height Downstream (F): 70 m below the crest elevation, 50 m towards the upstream from downstream face
- Bottom Upstream (G): 95 m below the crest elevation, 70 m towards the downstream from upstream face

- Bottom Center (H): 95 m below the crest elevation, at the center of dam body
- Bottom Downstream (I): 95 m below the crest elevation, 70 m towards the upstream from downstream face

Initially, significance of modelling dam zones with different material parameters was evaluated. Given in Figure 3.5, major zones the dam body constitutes are Zones 3B and 3C. In the construction specifications of Afşar Dam, it was stated that the same quarry rock to be used for both zones with different compaction schedules. Therefore, two alternative plane strain analyses were studied to observe the significance of these two zones with different deformation moduli and internal friction angles on the overall behavior.

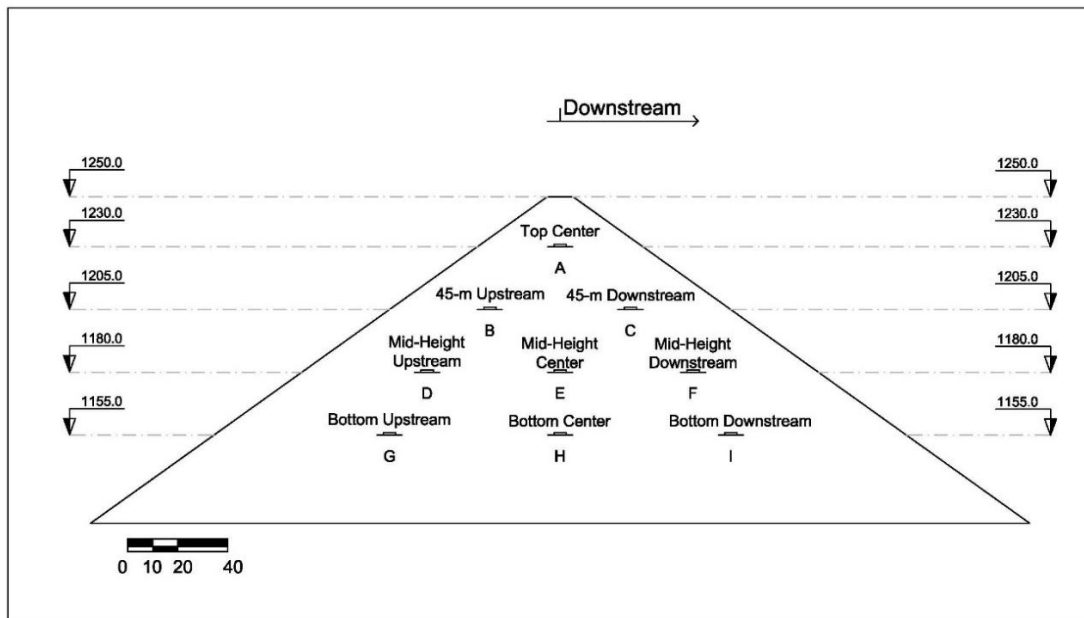


Figure 3.23. Reference Points Evaluated in the Analyses

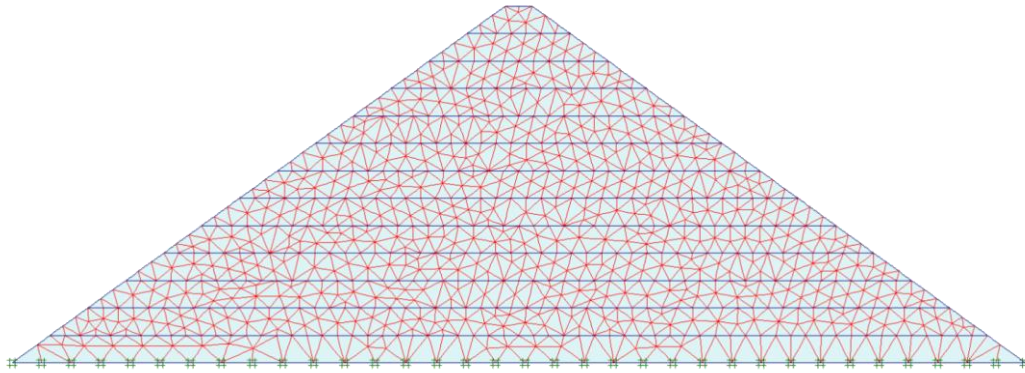


Figure 3.24. Finite Element Mesh Used in 2-D Analyses

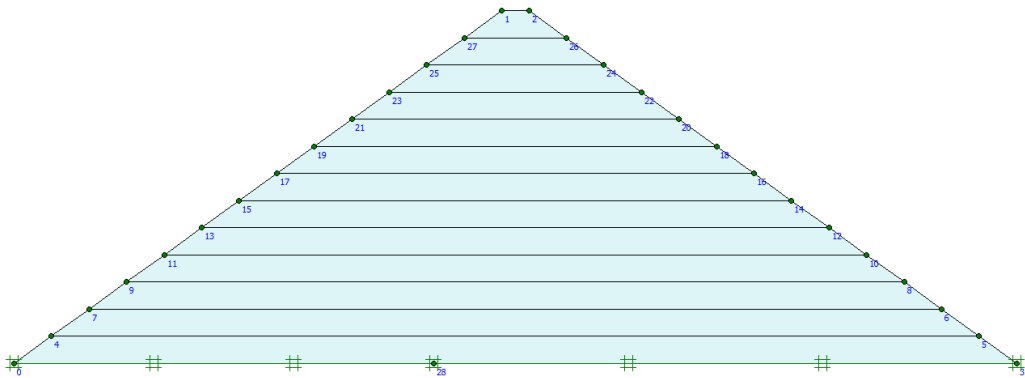


Figure 3.25. Computer Model of Afşar Dam, with only Zone 3B (Model-1)

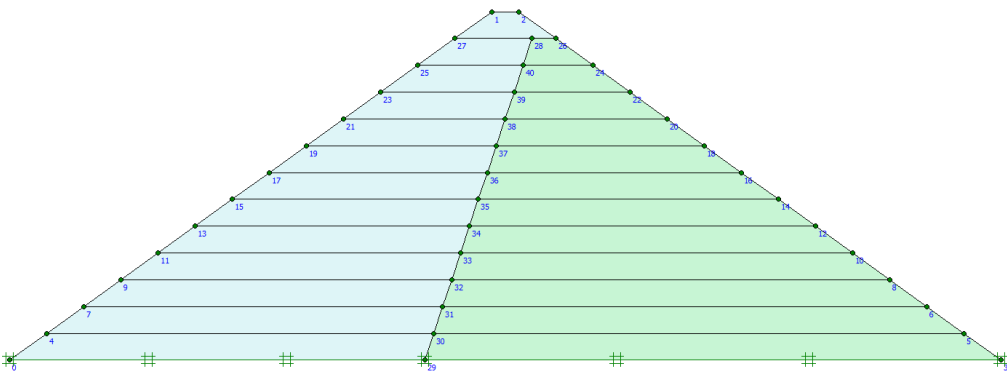


Figure 3.26. Computer Model of Afşar Dam, with Zones 3B and 3C (Model-2)

Computer models of the alternatives were prepared assuming construction stages in 10-m lifts. In the first case, the material properties of Zone 3B were assigned to the whole dam body. In the second case, both zones 3B and 3C were modelled separately using different material properties and appropriate section proportions. Material parameters used in the analyses were the ones used by Sukkarak et al (2017). The parameters assigned to zones 3B and 3C are listed in Table 3.5.

Table 3.5. *Material Parameters Used in Model-1 and Model-2*

Material	3B	3C
$\gamma(\text{kN/m}^3)$	21	21
$E_{50,\text{ref}}(\text{MPa})$	80	20
$E_{\text{oed,ref}}(\text{MPa})$	55	17
$E_{\text{ur,ref}}(\text{MPa})$	240	60
m	0,5	0,5
$c_{\text{ref}}(\text{kPa})$	1	1
$\varphi(^{\circ})$	47	42
$\psi(^{\circ})$	0	0
ν	0,3	0,3

The model using only Zone 3B was named as Model-1; and the one using both zones was named as Model-2 in the following sections. As previously mentioned, the bedrock was assumed to be infinitely rigid; therefore, the foundation of the dam was modelled with simply supporting boundary conditions, restraining deformations below foundation level with full fixity of deformations horizontally and vertically. Simultaneous construction was assumed for zones 3B and 3C. To prevent lateral pressure calculation errors that may occur due to sloping ground, i.e., for the sloped faces of the dam; initial conditions were not calculated according to the K_0 procedure defined in the analysis software Plaxis 2D. Instead, with the Gravity Loading method, the initial condition calculations were by-passed by defining a coefficient of zero, and then calculating an initial stage where the first 10-m lift was constructed. Following stages were calculated using the construction stage inputs. This modification in

calculating the initial stage was made because of the calculation method of software. In the K_0 -procedure of calculating initial stresses, the assumption for the horizontal stresses is as the equation implies:

$$\sigma'_{h0} = k_0 * \sigma'_{v0}$$

Which is applicable for horizontal ground surfaces but may result in unbalanced horizontal stresses for sloping surfaces. In the preferred calculation method explained above, shear stresses were calculated according to the modelled ground surface; to prevent calculation errors on the sloped faces of embankment. In the preliminary analysis models, the concrete face was not modelled, as the major load to be considered in the analyses was the weight of embankment lifts.

The dam body in Model-1 has a higher rigidity resulting in smaller deformations than the monitored values due to the strength properties defined for Zone 3B; however, the properties of Zone 3C result in higher deformations in Model-2 than those calculated in Model-1, at all reference points. Including Zone 3C in the analysis model directly decreases the rigidity provided by Zone 3B to the total dam body behavior. In Model-1 due to the symmetrical dimensioning of embankment, the maximum deformation value was observed at the mid-height center reference point, as expected. However, material parameters assigned to Zone 3C resulted in a more deformable behavior in the downstream zone; which causes the maximum displacement to be calculated at the mid-height downstream reference point. Comparing the maximum settlements obtained from Models 1 and 2, the effect of stiffness parameters may easily be observed; as the maximum settlement calculated in Model-1 was 53,15 cm, whereas in Model-2 a maximum value of 163,04 cm was obtained. Although observed results at Km: 0+185 differed in distribution of settlements from the results of both models, it was seen that zones with different strength characteristics cause considerable differences in the overall behavior. Therefore, it may be concluded that both zones 3B and 3C should be included in the analyses. In addition to observing comparatively low deformations when the parameters of Zone 3B were assumed representative for the

whole dam body, using a single material for the dam body caused negligence of the differences in deformation about upstream and downstream ends; which may result in errors. Deformation results of the analyses are given in Figures 3.27 and 3.28. In addition, except the results of points A and B obtained in Model-2, it was observed that none of the results are within $\pm 10\%$ range of the monitored settlements. This difference in behavior proves that the selected parameters should be calibrated.

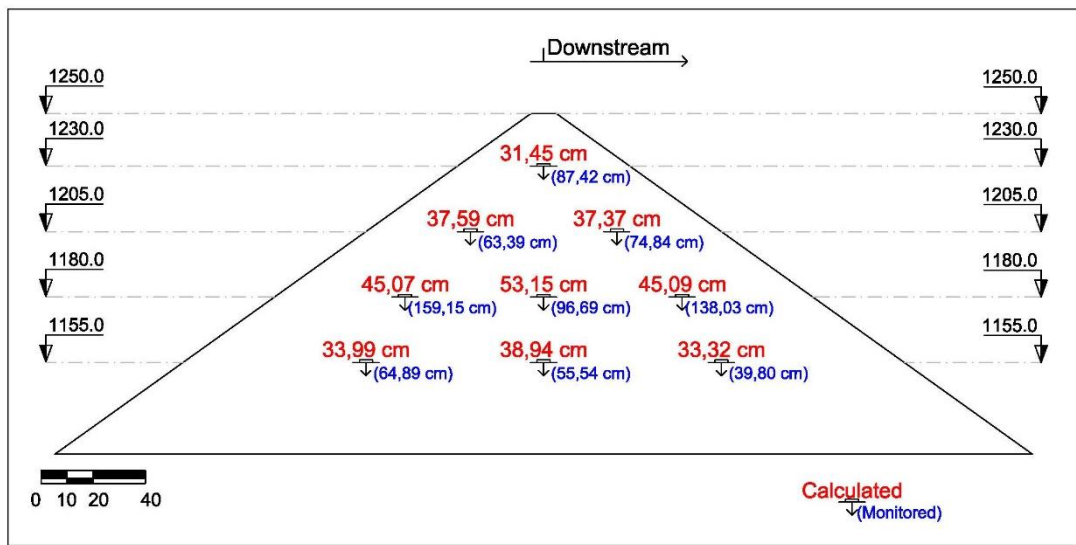


Figure 3.27. Calculated Total Settlements of Model-1

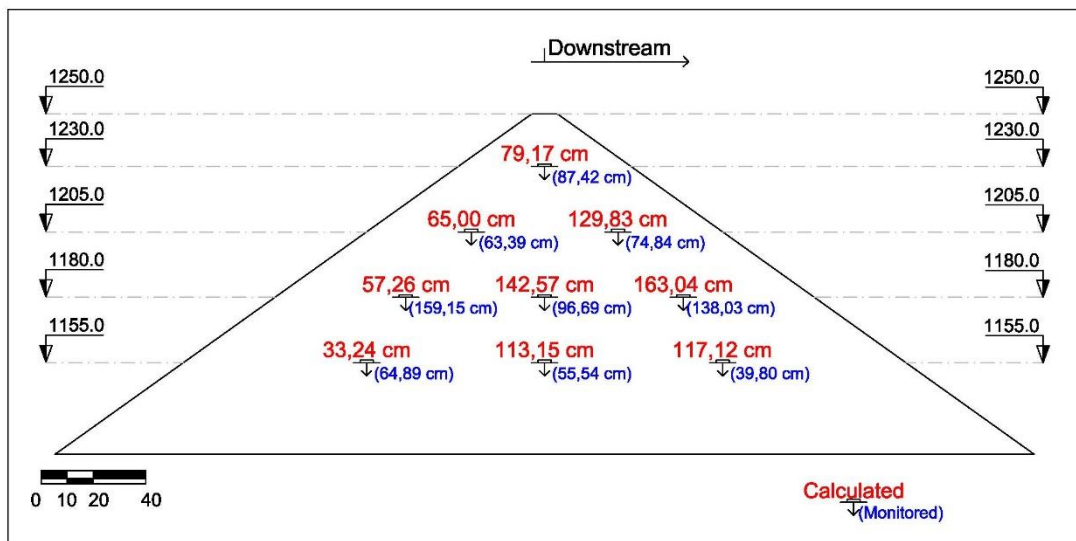


Figure 3.28. Calculated Total Settlements of Model-2

Construction of the rockfill embankment was modelled in stages; and trials were carried out to select a certain lift height for each construction stage. Considering the results of Model-1 and Model-2, it was decided to model the dam body using both zones 3B and 3C. Models 1 and 2 were studied to analyze the significance of different zones in overall behavior. Also, two analyses with different lift heights were compared to observe the differences in final results caused by lift height assumptions. Results of Model-2 were used as the reference for 10-m lift analysis. Later, 5-m lift construction scheme was studied (Model-3).

In Model-3, the bedrock was idealized with simple supports, similar to the aforementioned analyses. The K_0 -procedure was by-passed also in calculations of Model-3; same material parameters are used with Model-2, and because of the change in lift height definitions, construction stages were increased from 13 to 26. Cross section view with the finite element mesh of Model-3 is given in Figure 3.29.

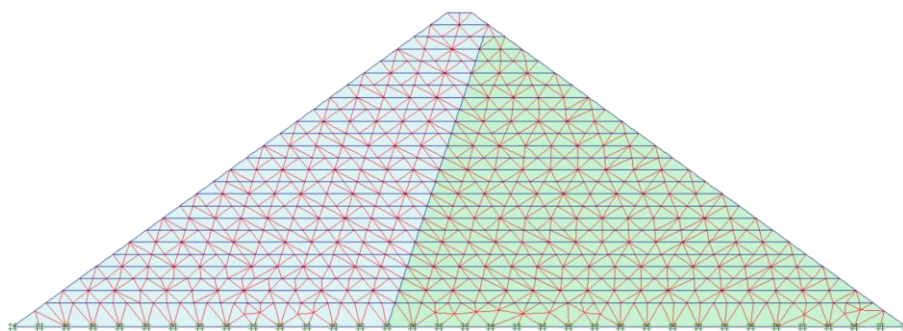


Figure 3.29. Finite Element Mesh of the Model with 5m lifts (Model-3)

Model-3 analysis with the assumption of 5-m lifts resulted in settlements similar to the values obtained in Model-2 at certain points; namely, the 45-m upstream and downstream points, and the points located at the bottom, given in Figure 3.30.

However, the maximum settlement values, as well as the top-center measurements differed by more than 10% from the calculated values for Model-2. Considerable differences were observed at reference points A, D, E and F. Especially D, E and F are at the elevation where the maximum settlements were expected. Therefore, it may be concluded that the assumed lift height in construction stage analyses may considerably change the final settlement values obtained. Settlement results obtained in the three models and the differences with monitoring results in percentages of measurements are given in Table 3.6.

As the difference is more pronounced at mid-height reference points where the maximum settlement values were recorded, modelling the construction stages in 5-m lifts may be considered to provide more accurate results. On the other hand, calculated deformation and stress distributions clearly differ from the monitoring results, therefore, using the preliminary parameters, a revision was made to obtain more compatible results with the measurements. Calibration of the parameters was performed by using Model-3.

Table 3.6. *Calculated Settlements in Model-1, Model-2 and Model-3*

Instrument	Monitored(cm)	Model-1 (cm)		Model-2 (cm)		Model-3 (cm)	
		Sett.	Diff. (%)	Sett.	Diff. (%)	Sett.	Diff. (%)
ZDO-19(A)	87,42	31,45	-64,02	79,17	-9,44	60,17	-31,17
ZDO-14(B)	63,39	37,59	-40,70	65,00	2,54	63,17	-0,35
ZDO-15(C)	74,84	37,37	-50,07	129,83	73,48	129,99	73,69
ZDO-9(D)	159,15	45,07	-71,68	57,26	-64,02	49,03	-69,19
ZDO-10(E)	96,69	53,15	-45,03	142,57	47,45	125,20	29,49
ZDO-11(F)	138,03	45,09	-67,33	163,04	18,12	142,02	2,89
ZDO-2(G)	64,89	33,99	-47,62	33,24	-48,77	34,31	-47,13
ZDO-3(H)	55,54	38,94	-29,89	113,15	103,73	110,07	98,18
ZDO-4(I)	39,80	33,32	-16,28	117,12	194,27	117,35	194,85

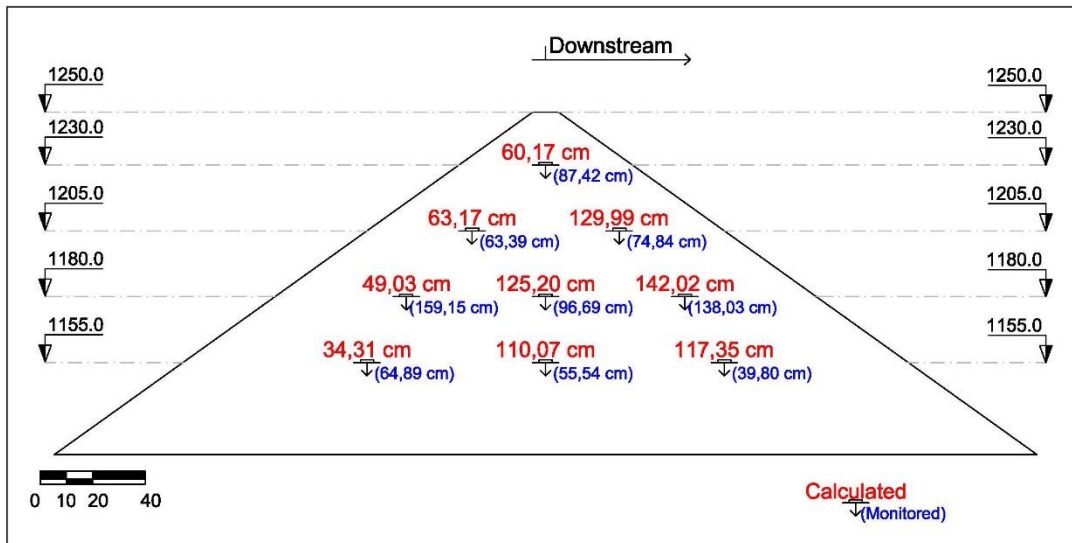


Figure 3.30. Calculated Total Settlements of Model-3

Using the material parameters selected from the study of Sukkarak et al (2017), it was seen that the parameters for Zone 3B result in smaller deformations than the observed ones, in addition, due to the stiffness difference between Zones 3B and 3C, considerable settlement differences were observed between upstream and downstream points at the same elevations. Because of these observations, selected values for dam body material parameters were modified, with lower stiffnesses for Zone 3B and higher stiffnesses for Zone 3C. As previously mentioned, distribution of recorded settlements in the dam contradict with the expected behavior of an embankment body, therefore, two approaches were used for calibration of parameters in two-dimensional analyses, as given below:

- Calibrating material parameters to obtain total settlement results similar to the monitored values on mid-height center reference point in the station Km: 0+185 (Model-4)
- Calibrating material parameters to obtain total settlement results similar to the monitored values on mid-height upstream reference point (maximum recorded value) in the station Km: 0+185 (Model-5)

By studying these two models, two different material parameter sets were obtained. Using the parameters obtained by the calibration on two-dimensional plane strain analysis models, three-dimensional deformation analyses were made; and results were compared with each other. Referring to the previously discussed settlement measurements at Km: 0+185, target settlement value of Model-4 was 96,69 cm as recorded on hydraulic settlement cell ZDO-10. Model-5 was studied with the maximum settlement value of 159,15 cm, as recorded on the hydraulic settlement cell ZDO-9. Because the dam body material was obtained from the same quarry for both zones 3B and 3C, construction technique was critical to provide the expected material behavior. Therefore, it was considered that the recorded maximum value should be considered in the analyses. Also, for comparing and integrating the results obtained from these analyses, arching effect was investigated to observe the distribution of settlements along the longitudinal axis of the dam, so it may be concluded that the valley shape significantly affects the deformation behavior of Afşar Dam.

The trial analyses for the calibration of parameters were carried out by the two models summarized above. Considering the preliminary analyses on Models 1,2, and 3, in determining lift heights and zones in the model, material parameters were iterated in different approaches to reach the deformation results to the maximum displacement values. In Model-4, stiffness parameters of Zone 3B were decreased while increasing the parameters of Zone 3C. In Model-5, stiffness parameters of Zone 3B were iterated while the parameters of Zone 3C were kept constant. Because the two-dimensional analyses consider only the general embankment behavior in deformations, reaching results totally similar to the values monitored at Km: 0+185 was not possible; given the recorded settlements on ZDO-9, ZDO-10, and ZDO-11, in Figure 3.16. Considering the monitoring results at Km: 0+135 and Km: 0+270; it was also observed that the settlements were not uniform along the longitudinal axis. Therefore, the plane strain assumption would be too approximate to reach acceptable results. The maximum settlement value of Model-5 was approximately 165% of the maximum settlement value of Model-4, therefore, the final parameters selected for the stiffness

characteristics were significantly different in the two models. In addition, when lower stiffness parameters were estimated for both zones, settlement results exceeded 1 meter at all points except the top reference point. However, results obtained in Model-4 two-dimensional analysis provided more similar settlement values especially at points 45 m below the crest level and at the bottom level. The smaller settlement results obtained in the two-dimensional plane strain analysis for Model-4 showed that a three-dimensional analysis using these parameters would yield much smaller settlements. A comparison of results is discussed in the following section.

For Models 4 and 5, material parameter sets were calculated in iterations; modifying the stiffness parameters in multiples of 5% of the initial values; aiming to reach the target settlement within $\pm 2,5\%$ range. Final values obtained for the material parameters of Zones 3B and 3C are given in Table 3.7.

Table 3.7. Final Parameters of Zones 3B and 3C for Models 4 and 5

Material	Model-4		Model-5	
	3B	3C	3B	3C
$E_{50,ref}$ (MPa)	52	30	24	20
$E_{oed,ref}$ (MPa)	35,75	25,5	17	17
$E_{ur,ref}$ (MPa)	156	90	72	60
m	0,5	0,5	0,5	0,5
φ (°)	47	42	47	42
c_{ref} (kPa) = 1, ψ (°) = 0, ν = 0,3, γ (kN/m ³) = 21				

Calculated deformation and vertical stress results are given for the models 4 and 5 in Figures 3.31, 3.33 and 3.32, 3.34, respectively. Parameters used in Model-4 resulted in a maximum settlement value of 97,11 cm, whereas the maximum settlement obtained with Model-5 parameters was 158,43 cm. Except the top point, the distribution and magnitudes of settlements calculated in Model-4 were closer to the recorded values. On the other hand, Afşar Dam is located in a narrow and stepped valley, therefore the valley shape effect should be evaluated. Since the three-

dimensional effects of the bedrock on the dam body may result in a decrease in the calculated settlements significantly, both parameter sets should be evaluated. The settlements and total vertical stresses calculated at various points are listed together with the observed results in Tables 3.8, and 3.9, respectively. The differences between calculated and monitored values in percentages of measurements are given in the tables.

Table 3.8. Comparison of Settlement Results of 2-D Plane Strain Analyses

Instrument	Monitored(cm)	Model-4(cm)		Model-5(cm)	
		Result	Diff. (%)	Result	Diff. (%)
ZDO-19	87,42	49,97	-42,84	86,45	-1,11
ZDO-14	63,39	62,94	-0,71	119,17	87,99
ZDO-15	74,84	89,54	19,64	137,28	83,43
ZDO-9	159,15	61,12	-61,60	123,77	-22,23
ZDO-10	96,69	97,11	0,43	158,43	63,85
ZDO-11	138,03	94,23	-31,73	140,60	1,86
ZDO-2	64,89	52,05	-19,79	109,31	68,45
ZDO-3	55,54	80,60	45,12	126,98	128,63
ZDO-4	39,80	77,76	95,38	115,98	191,41

Table 3.9. Comparison of Total Vertical Stresses of 2-D Plane Strain Analyses

Instrument	Monitored(kPa)	Model-4(kPa)		Model-5(kPa)	
		Result	Diff. (%)	Result	Diff. (%)
TBO-19	229	375	63,76	369	61,14
TBO-14	512	637	24,41	642	25,39
TBO-15	436	614	40,83	605	38,76
TBO-9	650	836	28,62	842	29,54
TBO-10	1138	1110	-2,46	1152	1,23
TBO-11	635	858	35,12	851	34,02
TBO-2	1305	1166	-10,65	1302	-0,23
TBO-3	1072	1510	40,86	1550	44,59
TBO-4	857	1139	32,91	1137	32,67

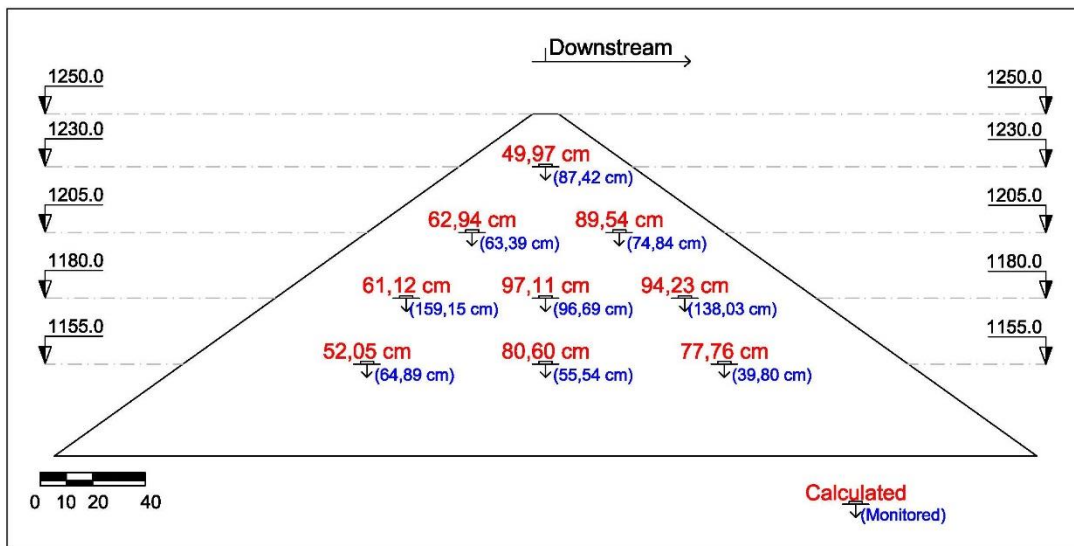


Figure 3.31. Calculated Total Settlements of Model-4

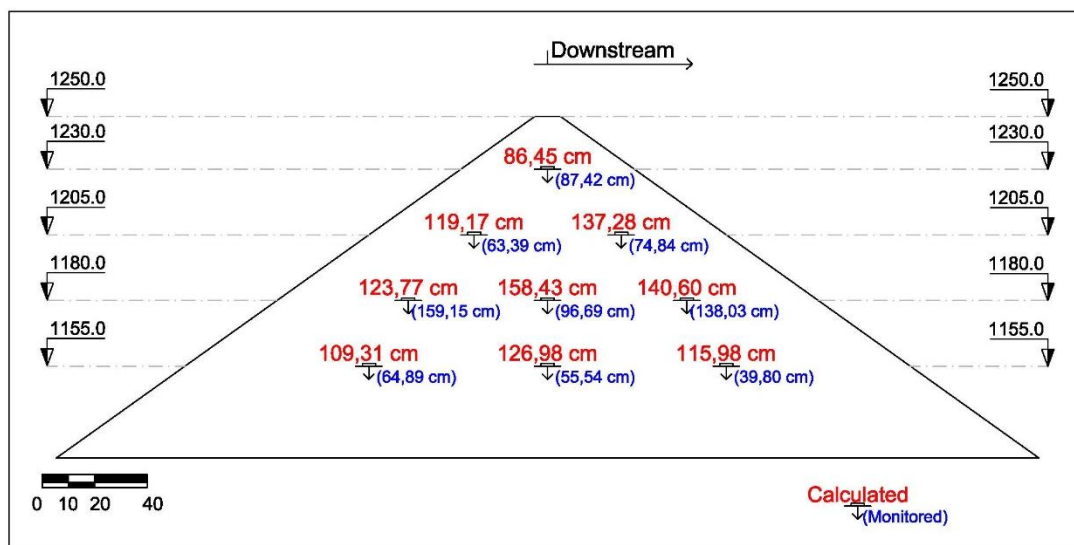


Figure 3.32. Calculated Total Settlements of Model-5

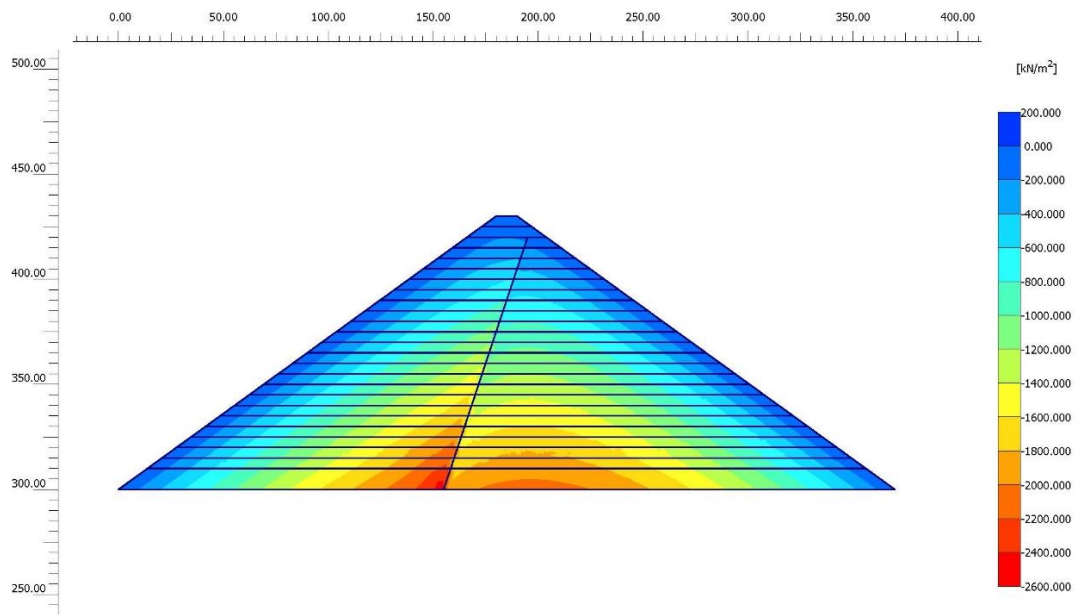


Figure 3.33. Total Vertical Stress Contours of Model-4

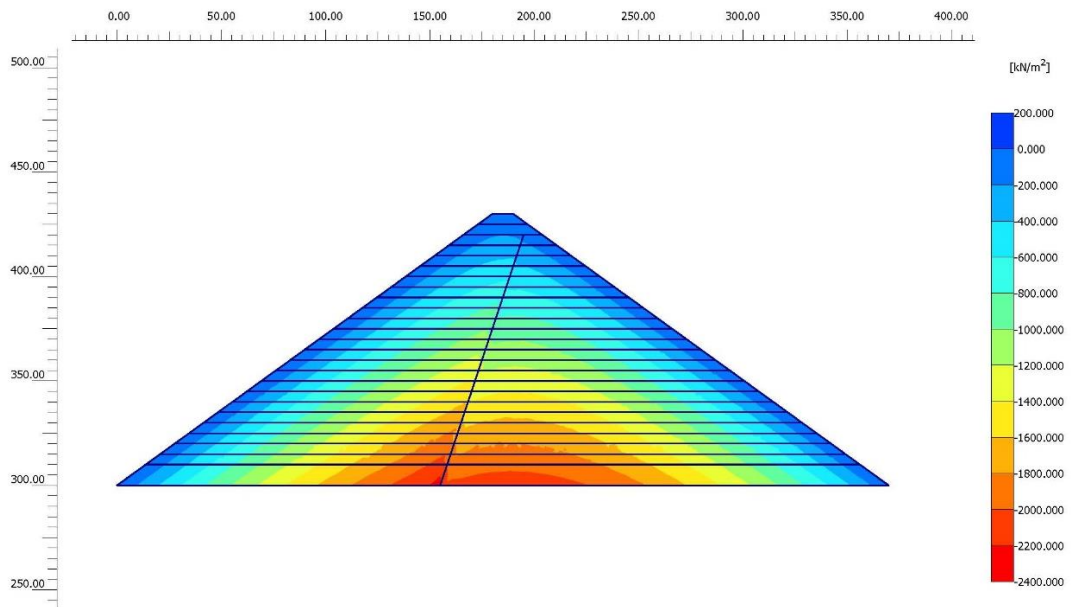


Figure 3.34. Total Vertical Stress Contours of Model-5

3.4.2. Effects of the Valley Shape on Deformation Behavior of Afşar Dam

In the construction period, the major load acting upon the embankment body is its own weight. The generalized deformation behavior of an embankment body with equal slopes on both side faces is as given in Figure 3.35. Maximum vertical deformations occur about the center of the body near the mid-height, and it decreases towards the faces of embankment. A deviation from this behavior is possible if the body is not symmetrical about its vertical axis, material used is not homogenous, construction schedule is different than common practice, or support conditions concerning three-dimensional behavior result in deformations different than the expected.

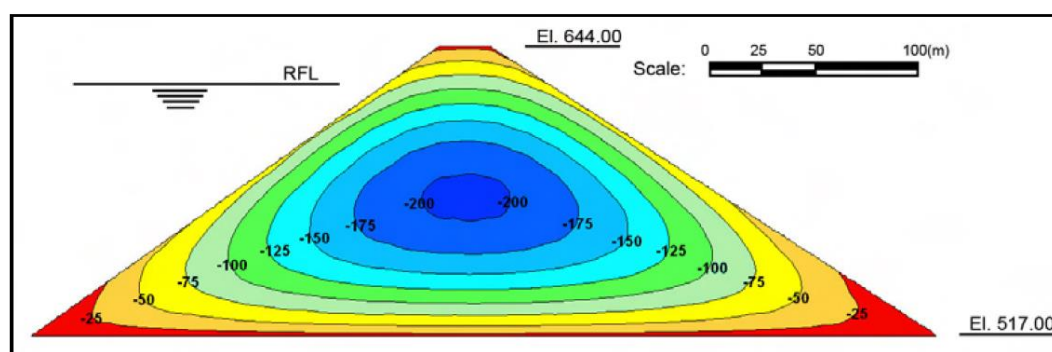


Figure 3.35. Representative General Deformation Behavior of an Embankment (Özkuzukıran, 2005)

Monitoring results on Afşar Dam show that settlement behavior in construction period is different than the common expectations. Concerning the material properties given previously in the results of calibration analyses, even if major differences are assumed for dam body zones, the generally expected behavior is still present in two-dimensional analyses. In addition, it was stated that the same quarry material is used for construction of both Zones 3B and 3C, only following different compaction schedules; therefore, the deviation of behavior due to non-homogeneity was

considered unlikely to be the cause of the monitored deformation behavior. Settlement results at upstream and downstream mid-height reference points may have been affected by construction problems or calibration errors. Although the records on ZDO-9 and ZDO-11 do not include extraordinary rates of change to prove some problems occurred, given in Figure 3.36, the results cannot be attributed to embankment behavior even when arching effect is also considered. The contradictory settlement values obtained on these monitoring devices may have occurred due to problems in placement, calibration or effects of the construction of upper layers. In addition, the difference in compaction schedules is expected to result in larger displacements towards the downstream face. To hold the construction technique responsible for the recorded incompatible data in the construction period would be thoroughly hypothetical.

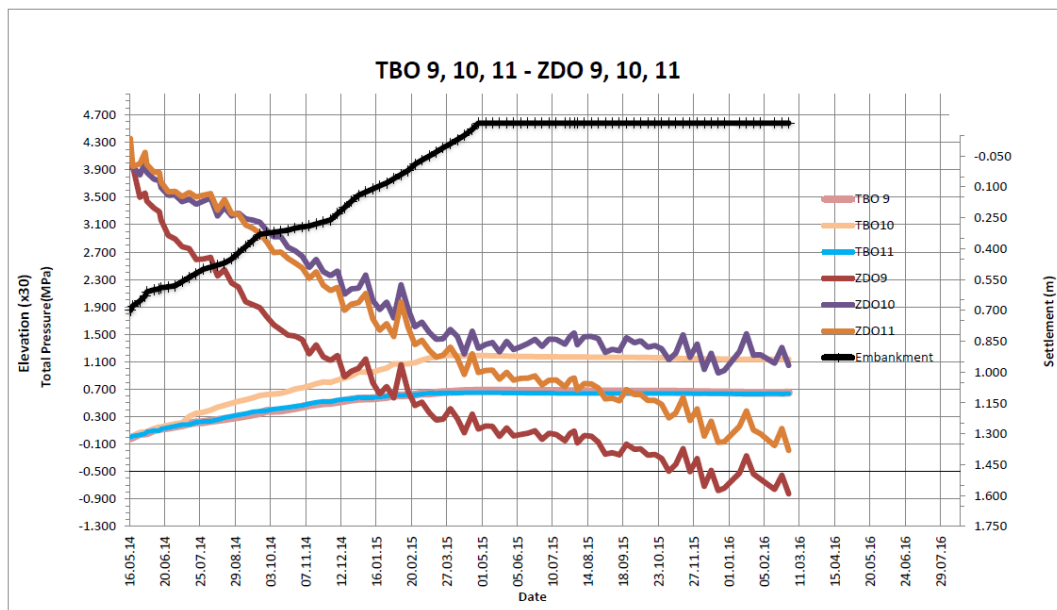


Figure 3.36. Settlement and Total Pressure Recordings on El.1180.0 at Km: 0+185

As given in the construction drawings, although the dam body section is approximately symmetrical about its vertical axis at Km: 0+185, other sections are

located above a stepped ground surface, resulting in different heights of embankment towards upstream and downstream faces; which may change the overall behavior of the dam body. The portion of the valley where the maximum section of Afşar Dam is located is especially narrow; with the elevation of the ground surface ascending in a steep slope on the north-south direction. According to the study of Escobar and Posada (2008), Afşar Dam can be classified to be located in a narrow valley, and significant effects of the valley shape are expected in the vicinity of the maximum section, diminishing towards the north bound edge of the dam body. Because the arching effect cannot be noticed by only the transverse section analyses, behavior of the dam body along the longitudinal axis should be investigated. It may be concluded that the most reliable analysis results for the deformation of Afşar Dam would be obtained by a three-dimensional analysis, to take into account both longitudinal and transverse effects of valley shape and dam zones.

Arching effect was defined by Terzaghi (1943) as the transfer of forces between a yielding mass and the remainder joint masses. Terzaghi (1943) explained the arching phenomenon referring to the displacement of a part of a rigid base below a soil mass. Displacement of the mass above the deforming rigid base is resisted by the induced shear stresses between the mass and the joint stationary masses. The induced shear stresses result in increased pressures at the base of the supporting masses while decreasing the pressure at the yielding mass. Obviously, the vertical pressure acting upon the base of the yielding mass remains unchanged, as the total weight of the mass. However, arching effect, including a vertical component of shear stresses, result in the transfer of a fraction of the total vertical pressure to the adjoint masses, increasing the intensity of stresses at the edges of these masses. Therefore, vertical deformation is observed at the deforming body, with lateral expansion towards the joint masses in the profile. It was also indicated that arching is universally encountered commonly both in laboratory and field. In the case of embankment dams, embankments placed in narrow valleys resembling a V-shape, undergo less vertical deformation compared to the embankments placed in wide valleys (ICOLD, 2004). This difference in behavior

occurs due to arching effect; which causes the vertical stresses to be transferred to supporting boundaries by induced shear stresses. Arching effect is more pronounced at lower elevations of an embankment body compared to its higher elevations when the longitudinal axis is investigated. Also, studies made on clay core rockfill dams show that the arching effect is significant at the lower elevations at the contact of core and fill zones (Adrian and Tschernutter, 2017). For the case with CFRDs, studies show that arching effect is more significant in embankments with an interlocked rock skeleton, supported by abutments on comparatively rigid bedrock (Cruz et al., 2010). Referring to the statistical studies carried out by Moradi et al (2014), the arching ratio (A_r) is calculated for a reference point as per the equation:

$$A_r = \left(1 - \frac{\sigma}{\gamma h}\right) \times 100$$

Where σ is the calculated total vertical stress at the point, γ is the unit weight of embankment material, and h is the height of the embankment above the point. The arching ratio of Afşar Dam calculated for the points considered are given in Figure 3.37. It was seen that at all reference points arching higher than 20% was present; therefore, it may be concluded that the valley shape caused a modification of vertical stress distribution.

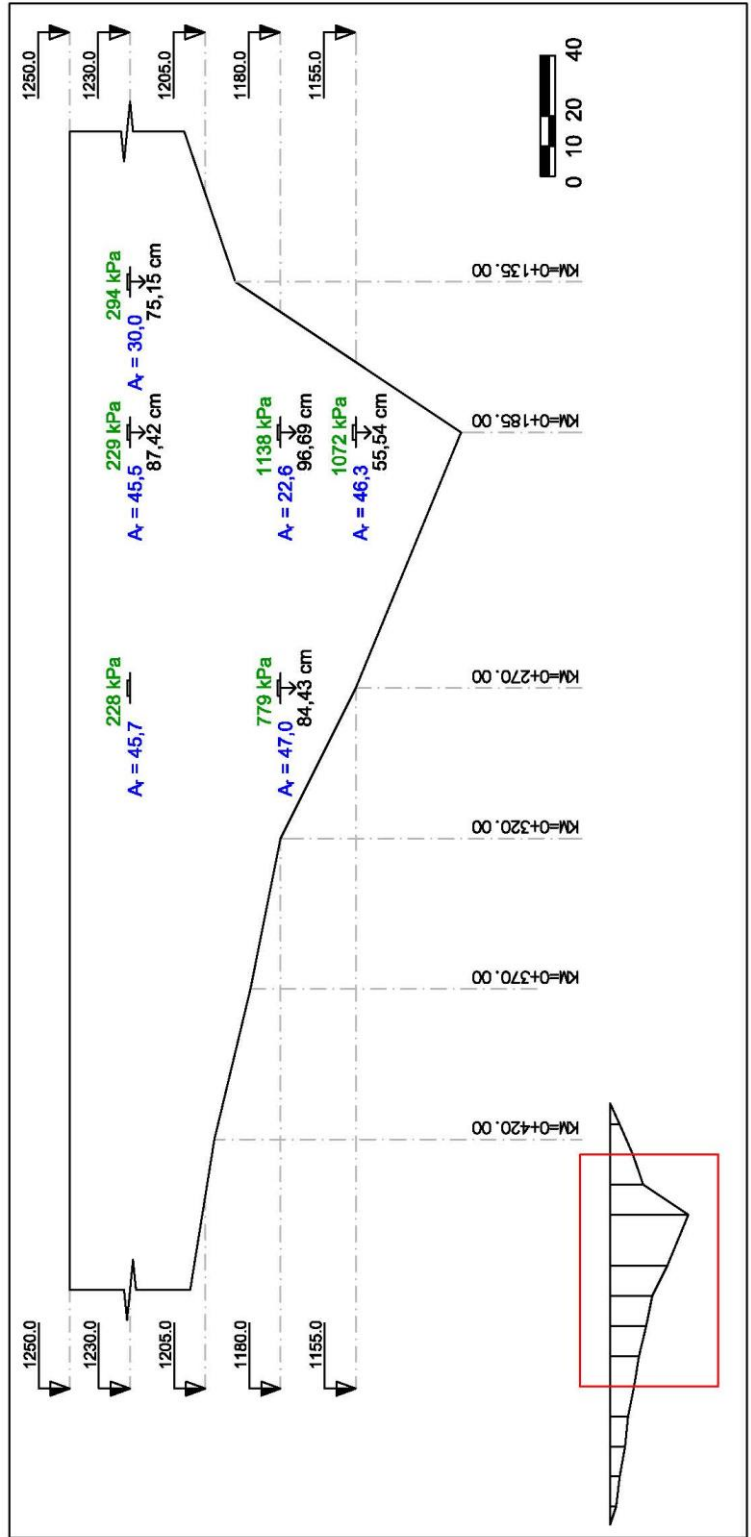


Figure 3.37. Monitored Total Vertical Stress and Settlement Values at the Axis of Afşar Dam

3.4.3. 3-D Analysis of Afşar Dam in Construction Period

Three-dimensional analyses of Afşar Dam were made on the cross sections given in the construction drawings at specified station kilometers, as given in Figure 3.38. Model boundaries were located 100 m away in each direction to provide adequate dissipation of stresses. As explained in the two-dimensional analyses, construction of the rockfill embankment was assumed to be formed by 5-m lifts, and zones 3B and 3C were constructed simultaneously, with the groundwater table further below the lowest elevation of the model. Zones 3B and 3C were included in the model with the estimated material parameters, in order to observe the effects of zoning. Analyses were carried out using constitutive model of Hardening Soil for materials, by the software Midas GTS NX. Three-dimensional element structure was modeled by joining two-dimensional cross sections of the bodies. Boundary conditions along the outer edges of bedrock were defined as simple supports, restraining the bedrock with total displacement fixities in x-direction at upstream and downstream ends, in y-direction at the edges of longitudinal axis, and in x, y, and z directions at the bottom of bedrock. Mesh generation was executed using a hexahedron-based mesh shape defined in the software as “Hybrid Mesh”, which forms elements combining pyramid shapes and tetrahedrons on a hexahedron base. Three-dimensional analyses of Afşar Dam were executed for both material parameter sets estimated for the given approaches; and the models were named as “Model-6”, and “Model-7”, respectively.

The results of three-dimensional analyses, given in Figures 3.40-3.43, show the effects of valley shape on the deformation behavior, where smaller settlements were calculated at each reference point. Comparing the differences in results among reference points, it was observed that the arching effect is more pronounced about the dam axis, with decreasing effectiveness towards upstream and downstream faces. Also, in Km: 0+185 section it was seen that due to the material property differences between zones 3B and 3C in addition to the arching effect, the point where the

maximum settlement was observed is upwards downstream from the mid-height center point in Model-6. For the results calculated in Model-7, the maximum settlement values were obtained at the same point both in two-dimensional and three-dimensional analyses. Since both in two-dimensional and three-dimensional analyses the same assumptions were made for the material parameters, observed differences in settlement results indicate the importance of three-dimensional behavior. Magnitudes of settlements differ by more than 30% in two- and three-dimensional analyses.

Table 3.10. Comparison of Settlement Results of 3-D Analyses at Km: 0+185

Instrument	Monitored(cm)	Model-6(cm)		Model-7(cm)	
		Result	Diff. (%)	Result	Diff. (%)
ZDO-19	87,42	24,54	-71,93	55,79	-36,18
ZDO-14	63,39	25,86	-59,20	82,94	30,84
ZDO-15	74,84	58,01	-22,49	86,89	16,10
ZDO-9	159,15	31,36	-80,29	80,34	-49,52
ZDO-10	96,69	54,23	-43,91	97,57	0,91
ZDO-11	138,03	55,70	-59,65	84,34	-38,90
ZDO-2	64,89	28,92	-55,43	64,08	-1,25
ZDO-3	55,54	43,30	-22,04	68,86	23,98
ZDO-4	39,80	42,84	7,64	64,29	61,53

Table 3.11. Comparison of Total Vertical Stresses of 3-D Analyses at Km: 0+185

Instrument	Monitored(kPa)	Model-6(kPa)		Model-7(kPa)	
		Result	Diff. (%)	Result	Diff. (%)
TBO-19	229	425	85,59	282	23,14
TBO-14	512	645	25,98	546	6,64
TBO-15	436	537	23,17	513	17,66
TBO-9	650	533	-18,0	663	2,0
TBO-10	1138	734	-35,50	876	-23,02
TBO-11	635	657	3,46	678	6,77
TBO-2	1305	745	-42,91	810	-37,93
TBO-3	1072	933	-12,97	1028	-4,10
TBO-4	857	849	-0,93	852	-0,58

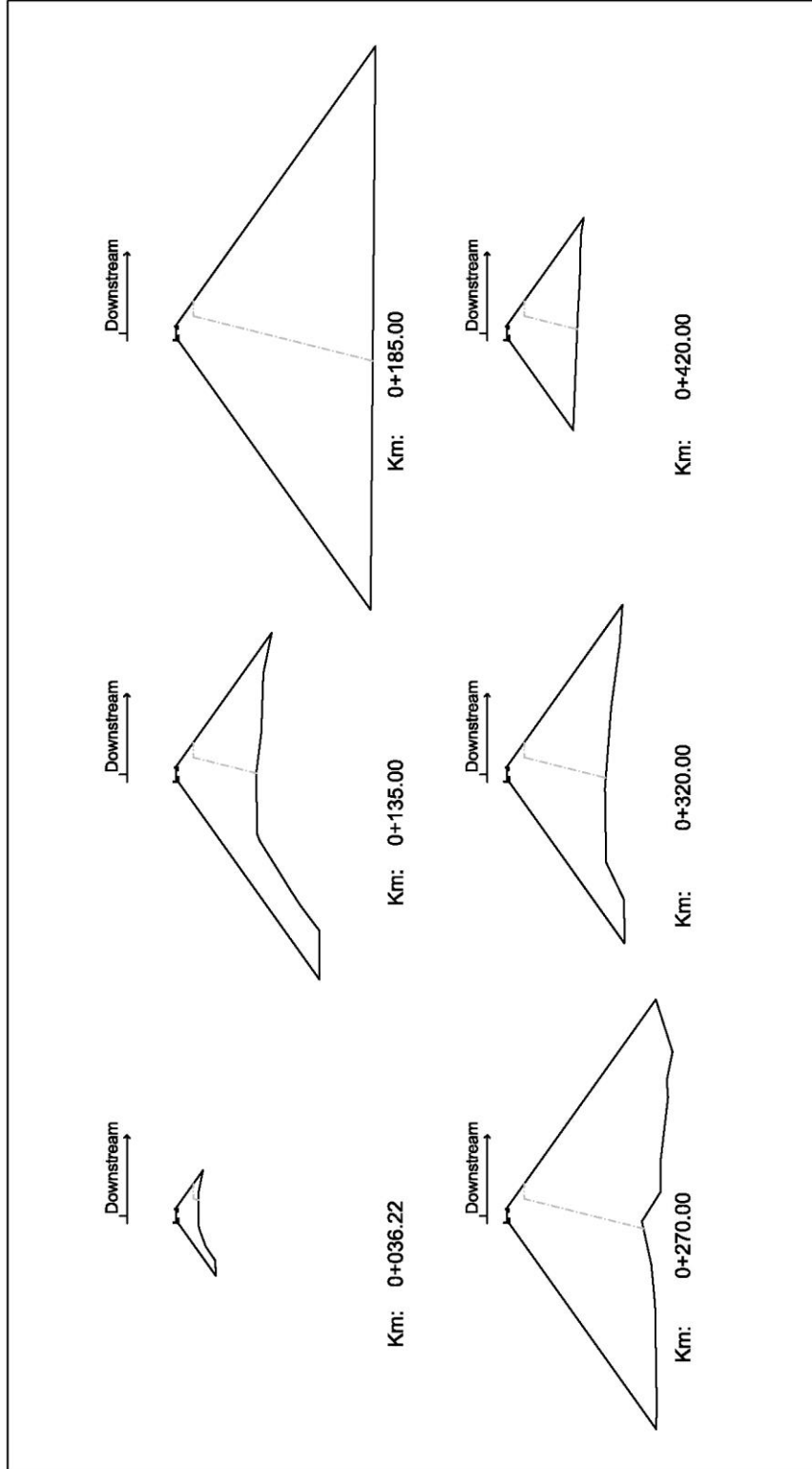


Figure 3.38. Defined Sections of Afşar Dam for 3-D Model

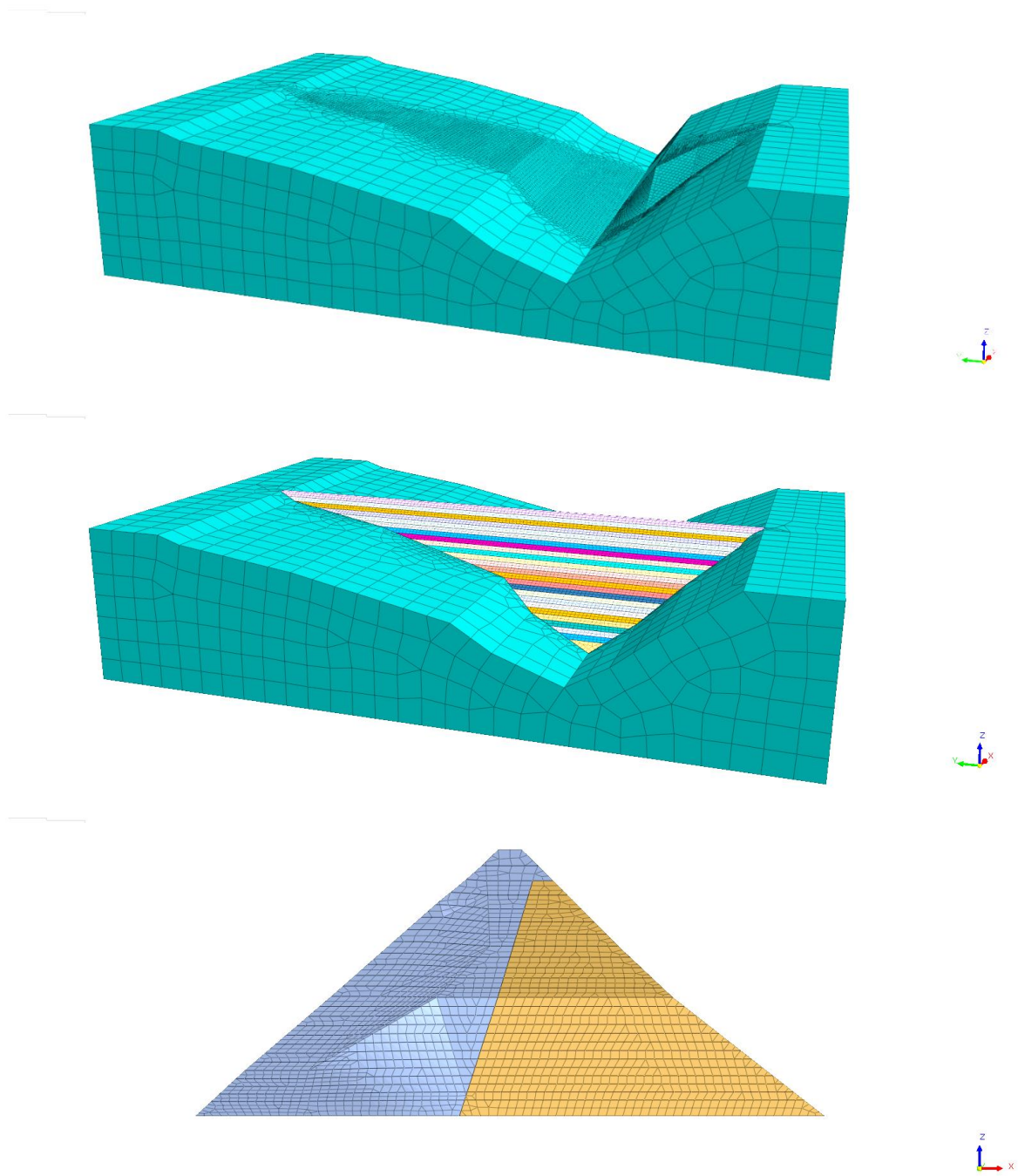


Figure 3.39. 3-D Views of Bedrock, Dam Body and Zoning

Table 3.12. Comparison of Settlement Results of 3-D Analyses at Km: 0+135

Instrument	Monitored(cm)	Model-6(cm)		Model-7(cm)	
		Result	Diff. (%)	Result	Diff. (%)
ZDO-16	43,86	12,88	-70,63	28,83	-34,27
ZDO-17	38,58	20,15	-47,78	34,57	-10,39
ZDO-20	75,15	15,38	79,53	28,72	-61,78

Table 3.13. Comparison of Total Vertical Stresses of 3-D Analyses at Km: 0+135

Instrument	Monitored(kPa)	Model-6(kPa)		Model-7(kPa)	
		Result	Diff. (%)	Result	Diff. (%)
TBO-16	494	597	20,85	633	28,14
TBO-17	506	594	17,39	290	-42,69
TBO-20	294	475	61,56	325	10,54

Table 3.14. Comparison of Settlement Results of 3-D Analyses at Km: 0+270

Instrument	Monitored(cm)	Model-6(cm)		Model-7(cm)	
		Result	Diff. (%)	Result	Diff. (%)
ZDO-6	83,68	18,68	-77,68	41,81	-50,04
ZDO-7	84,43	39,03	-53,77	61,75	-26,86
ZDO-8	94,48	34,45	-63,54	55,53	-41,23
ZDO-12	90,16	21,99	-75,61	48,06	-46,69
ZDO-13	94,19	43,73	-53,57	67,51	-28,33

Table 3.15. Comparison of Total Vertical Stresses of 3-D Analyses at Km: 0+270

Instrument	Monitored(kPa)	Model-6(kPa)		Model-7(kPa)	
		Result	Diff. (%)	Result	Diff. (%)
TBO-7	779	693	-11,04	803	3,08
TBO-8	1015	526	-48,18	582	-42,66
TBO-12	570	649	13,86	687	20,53
TBO-13	719	451	-37,27	571	-20,58
TBO-18	228	429	88,16	375	64,47

In addition to section Km: 0+185, settlement measurements were made at two more sections of the dam. These data were used to validate the results of three-dimensional analyses more accurately by considering these measurements. Settlements, vertical stresses calculated and the differences between calculated and monitored values at sections Km: 0+135 and Km: 0+270 are given in Tables 3.12-3.15. Comparing the calculated settlement results of the section at Km: 0+270 with the measured ones; it was seen that the results at downstream reference points in Model-7 are closer to the measurements than those obtained from Model-6. The higher stiffness of dam body materials combined with the arching effect provided by the bedrock resulted in lower settlements at Km: 0+270 reference points as well as those of at Km: 0+135.

The parameters estimated for Model-6 define a higher rigidity for the dam body, which resulted in a more pronounced effect of arching in the three-dimensional analyses, causing further decrease in the settlement values obtained compared to the two-dimensional analyses. Two-dimensional plane strain analysis yielded the maximum settlement value of 97,11 cm, whereas in three-dimensional analysis using the same material parameters a maximum settlement value of 58,0 cm was obtained. Because the arching effect is more pronounced at lower elevations, the maximum settlement value obtained in Model-6 was above the mid-height of dam body, whereas the maximum settlement in two-dimensional plane strain analysis was obtained at the mid-height center point.

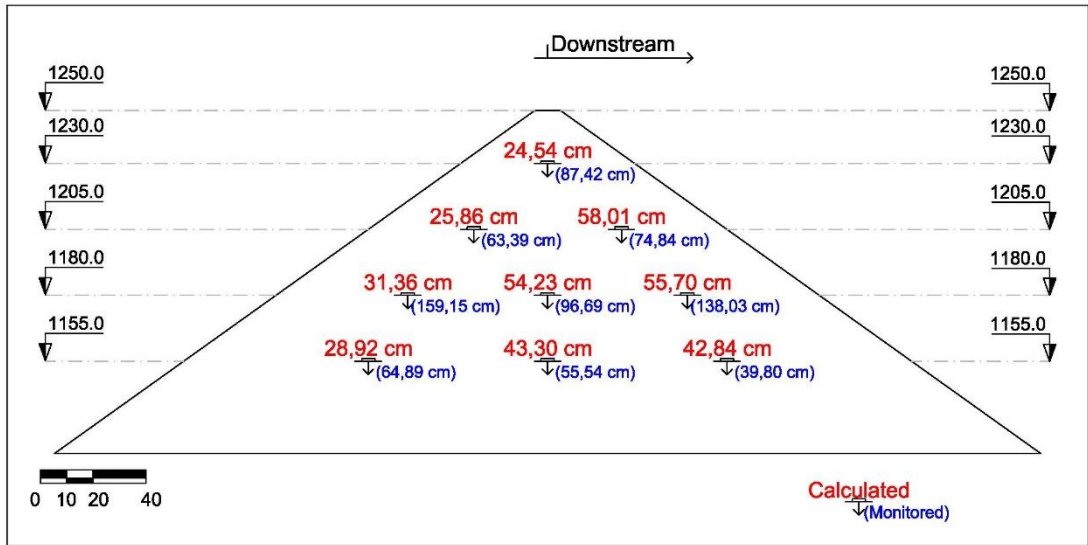


Figure 3.40. Settlement Results at Km: 0+185 at the End of Construction (Model-6)

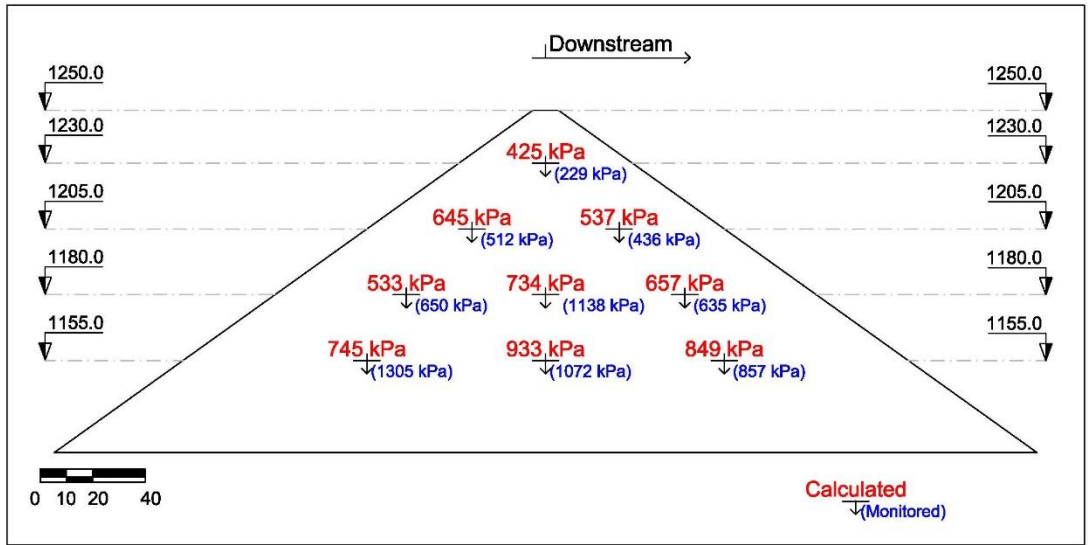


Figure 3.41. Total Vertical Stress Results at Km: 0+185 at the End of Construction (Model-6)

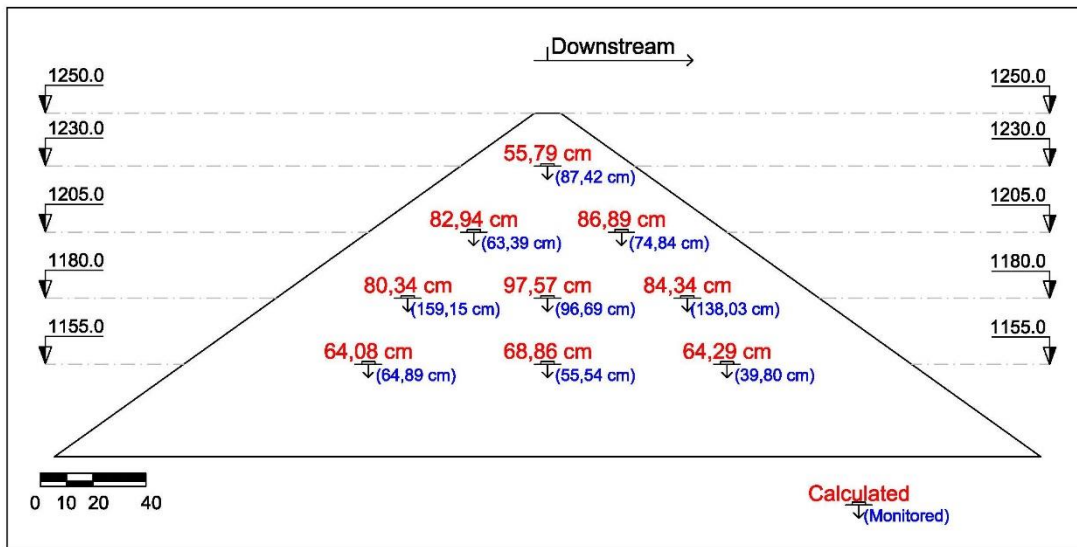


Figure 3.42. Settlement Results at Km: 0+185 at the End of Construction (Model-7)

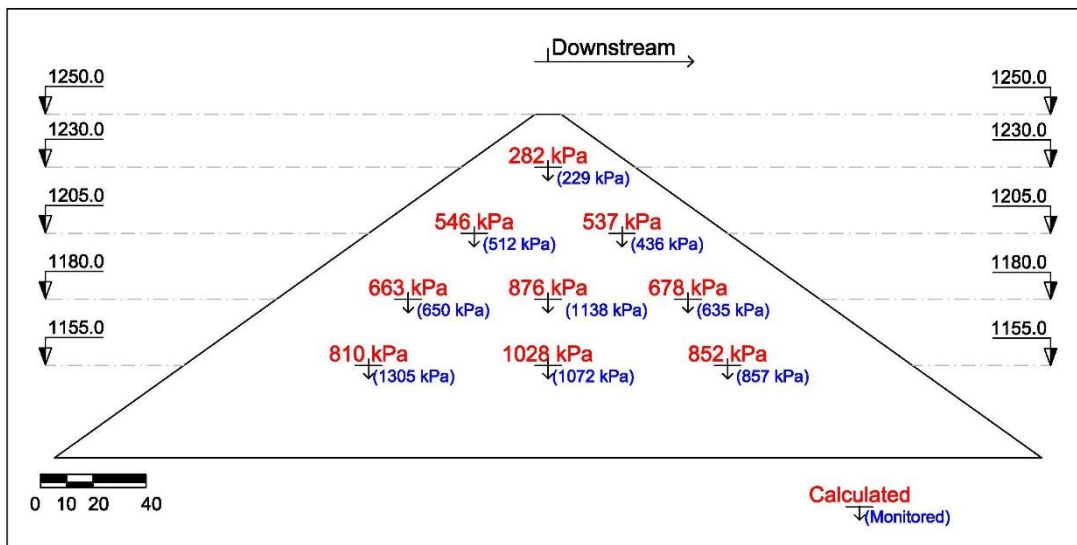


Figure 3.43. Total Vertical Stress Results at Km: 0+185 at the End of Construction (Model-7)

Although at certain points both two-dimensional and three-dimensional analyses did not yield the monitored values, the overall results obtained in Model-7 were closer to the monitored settlements. After careful examination of the above cited considerations

it may be concluded that the observed settlements on ZDO-9 and ZDO-11 can be neglected; as at these points monitoring errors may have occurred due to construction or calibration problems. The frequency distributions of settlements including the results of ZDO-9 and ZDO-11 are given in Figure 3.44, and the frequency distribution neglecting ZDO-9 and ZDO-11 results are given in Figure 3.45.

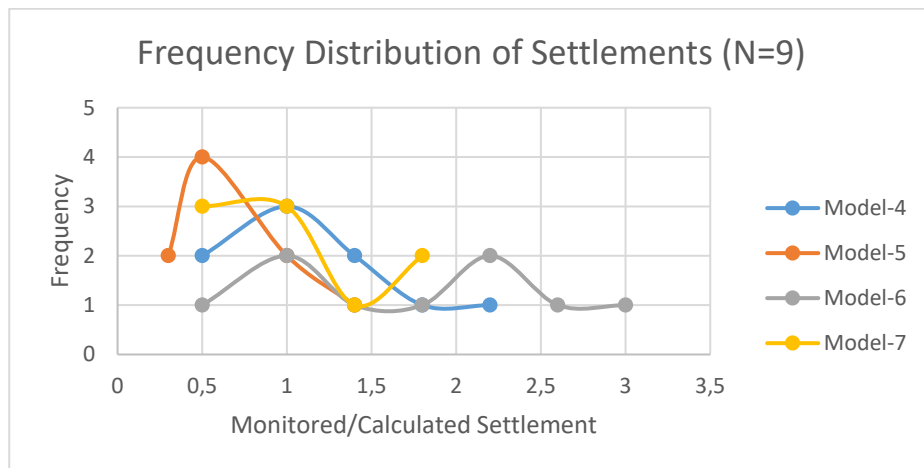


Figure 3.44. Frequency Distribution of Settlements Monitored to Calculated at Km: 0+185 (N=9)

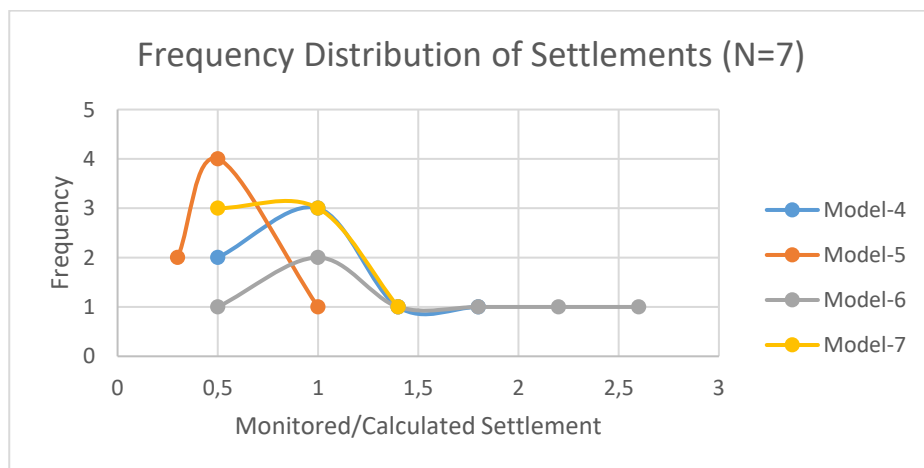


Figure 3.45. Frequency Distribution of Settlements Monitored to Calculated at Km: 0+185 (N=7)

Focusing on the calculated settlements at Km: 0+185, it was seen that the parameters used in Model-7 yielded results closer to the recorded values. It was observed that settlements obtained in Model-6 are even smaller than the values calculated in two-dimensional analysis with the same parameters (Model-4). The difference of settlement results between Model-4 and Model-6 also underlined the significance of arching effect on the deformations at this section. Calculated total vertical stresses were closer to the recorded values in Model-7, with smaller differences from monitoring results at all reference points. Comparing the settlements and total vertical stresses in Model-6 and Model-7 with monitoring results, it was observed that the behavior of Afşar Dam indicates a more deformable behavior than the estimations in Model-6. Therefore, the material parameters estimated for Model-7 may be selected to be more representative of the dam body.

3.4.4. Deformation Behavior of Afşar Dam at Reservoir Impoundment

The aim of construction of a concrete slab on the upstream face of a rockfill dam is to provide an impervious face required to retain the water. Because of the impermeability provided by the face slab, the body of the dam can be assumed to be dry. Therefore, for a properly constructed CFRD; embankment of which is placed in lifts of adequate depth, adding of water and compaction to prevent major post construction settlements that would cause cracks to develop in the concrete face; the impoundment mainly only results in hydrostatic loading on the face slab and rockfill body. In the project drawings of Afşar Dam, necessary preventive measures were taken with grout curtain applications in addition to the excavation of improper material. As a result of these data, deformation analysis of Afşar Dam in the impoundment period considers the hydrostatic pressure.

In the reservoir impoundment analysis, hydrostatic pressure was assumed to act normal upon the concrete face slab, with the reservoir filled up to elevation 1250.0,

which is 4 m below the top of the parapet wall. As the reservoir impoundment analysis was carried out following the construction stage analysis of Afşar Dam, to observe the effects of impoundment on the deformed body of the dam, the reservoir impoundment was simulated as a construction stage following the activation of the concrete face slab in the three-dimensional analysis model. The settlements and horizontal displacements that occur upon impoundment were observed, and deformations on the concrete face slab were evaluated. As previously mentioned, the reservoir impoundment analysis was carried out with the assumption of perfect bond between the concrete slab and dam body; simulating a total compatibility in deformations between the face slab and rockfill embankment.

Three-dimensional analyses of reservoir impoundment were studied for Model-7. Impoundment was simulated as an additional construction stage, and the water level was assumed to rise to the normal reservoir level in a single stage. As the data on impoundment period was not available in this study, only calculation results were presented. Settlement and total vertical stress distributions at the end of construction and reservoir impoundment are given in Figures 3.46-3.49. The major effect induced by the reservoir impoundment was the horizontal deflection and the shear stresses developed. With the shear stresses and horizontal deformations given in Figure 3.50-3.53, it was observed that the horizontal deformations induced by reservoir impoundment tend to be maximum about the upstream face, decreasing towards the downstream. It was observed that at the maximum section, Km: 0+185, the deformation due to reservoir impoundment decreases to approximately 1,7 cm about the downstream.

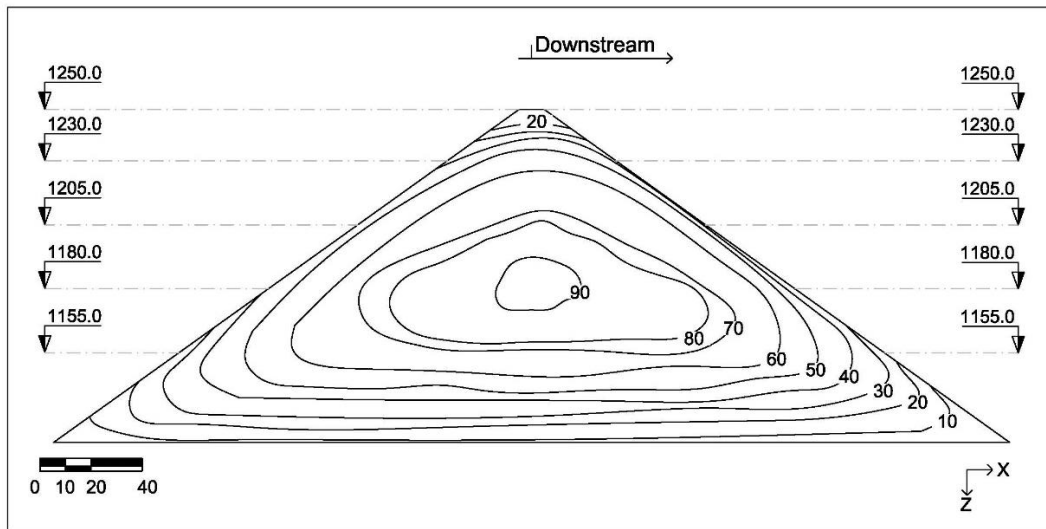


Figure 3.46. Settlement Results at Km: 0+185 at the End of Construction (Model-7)

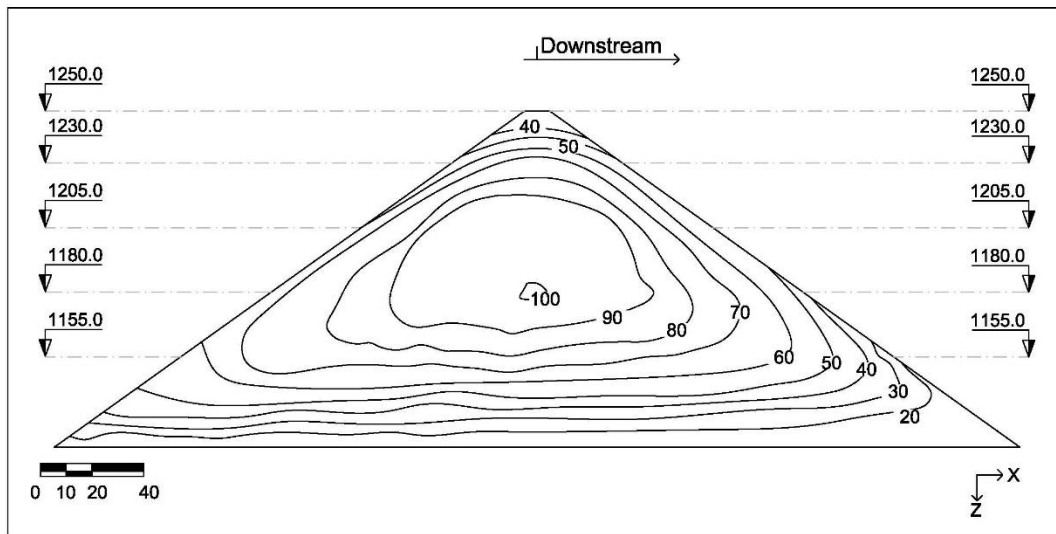


Figure 3.47. Settlement Results at Km: 0+185 at Reservoir Impoundment (Model-7)

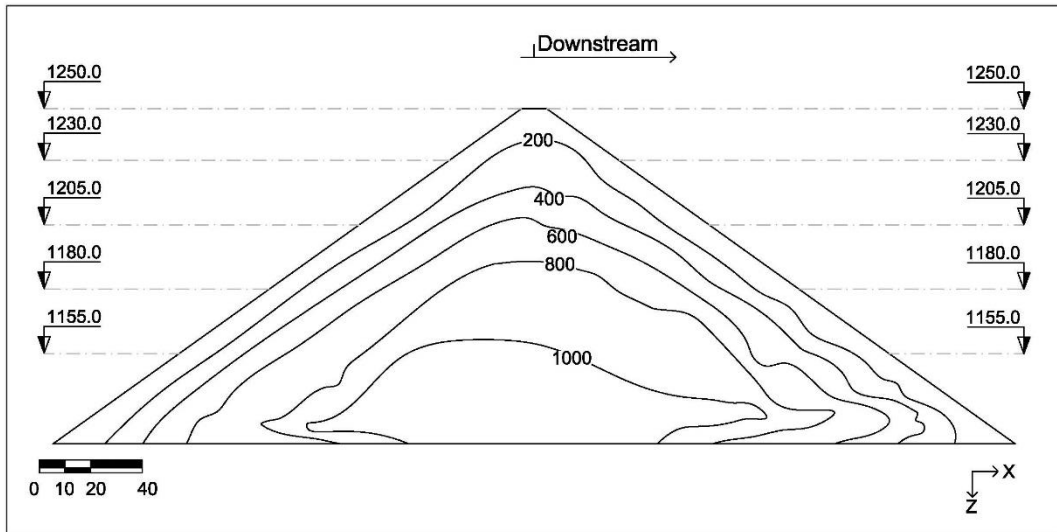


Figure 3.48. Total Vertical Stress Results at Km: 0+185 at the End of Construction (Model-7)

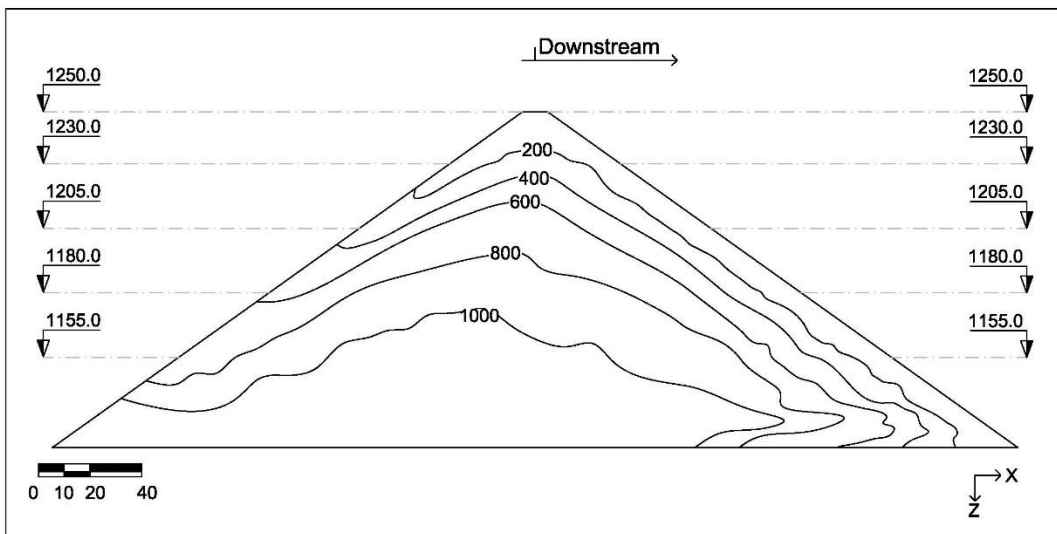


Figure 3.49. Total Vertical Stress Results at Km: 0+185 at Reservoir Impoundment (Model-7)

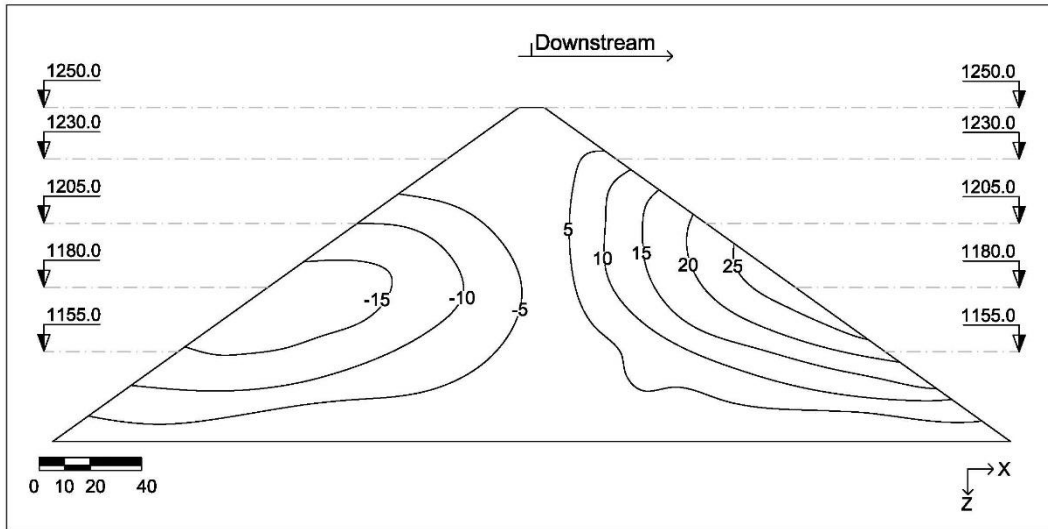


Figure 3.50. Horizontal Displacements at Km: 0+185 at the End of Construction (Model-7)

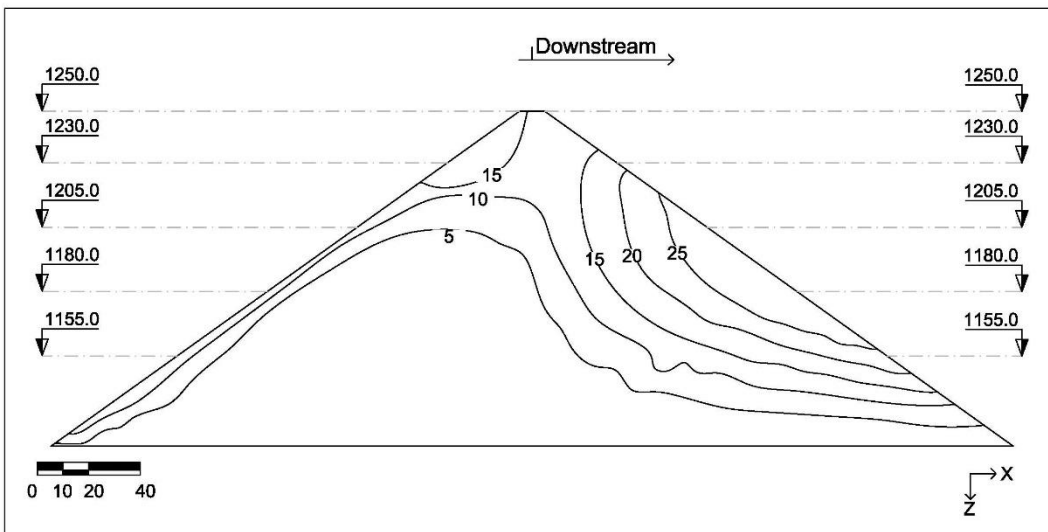


Figure 3.51. Horizontal Displacements at Km: 0+185 at Reservoir Impoundment (Model-7)

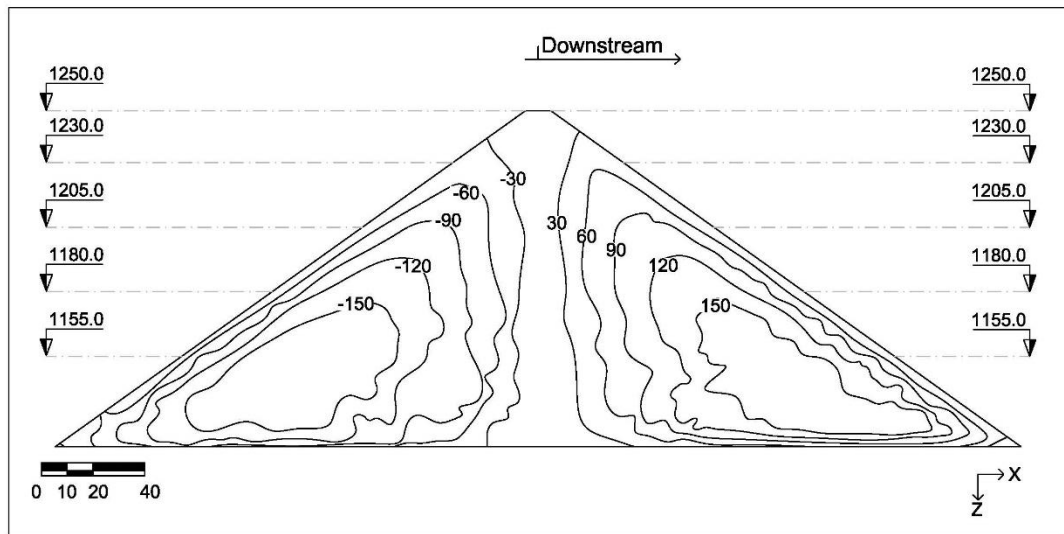


Figure 3.52. Shear Stresses at Km: 0+185 at the End of Construction (Model-7)

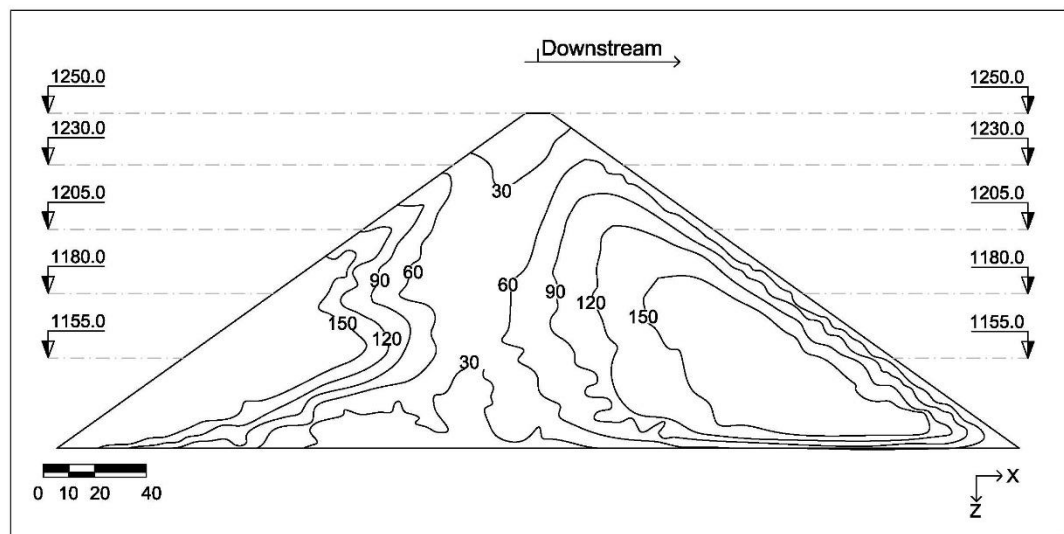


Figure 3.53. Shear Stresses at Km: 0+185 at Reservoir Impoundment (Model-7)

The three-dimensional analysis was evaluated for the three stations at which total pressure gages and hydraulic settlement cells were placed. At Km: 0+135, it was seen that the impoundment does not result in a considerable increase in settlements of the

dam body. The overall settlement to occur at Km: 0+135 was reached at the end of embankment construction, and the additional load due to face slab did not increase the settlement more than 1 cm. In the reservoir impoundment period, the maximum relative settlement was observed at upstream reference point, followed by the top center point. As expected, reservoir impoundment was observed to be of least significance towards the downstream. Calculated total vertical stresses were higher at all reference points at this section than the monitored values at the end of construction, and the reservoir impoundment caused significant vertical stress increase at the upstream of Km: 0+135. At the top-center point the calculated increase was approximately equal to the hydrostatic pressure applied. However, the settlement at Km: 0+270 indicated a different deformation behavior. Upstream total settlement values did not exceed 57 cm, while the downstream total settlement values reached 71,6 cm. As the arching effect was not as significant at Km: 0+270 compared to the maximum section at Km: 0+185, the settlement calculated on elevation 1180.0 center was higher (61,75 cm) in total than the upstream (41,81 cm) and downstream (55,53 cm) settlement values obtained at this elevation. The additional settlement due to reservoir impoundment at Km: 0+270 was observed to be decreasing from the upstream towards the downstream.

At Km: 0+185, the settlements due to reservoir impoundment was calculated to be larger than the results obtained at the sections Km: 0+135 and Km: 0+270. The weight of water to act upon this station caused higher settlement compared to other stations, with a maximum additional settlement of 13,57 cm at the mid-height upstream reference point. Considering the reservoir impoundment period, the upstream and center deformations at the bottom elevation reached similar values. It was observed that the deformation due to reservoir impoundment diminishes towards the downstream. Observing the deformations at the end of reservoir impoundment, smaller deformations were calculated in downstream Zone 3C than those of upstream Zone 3B, despite more deformable material characteristics. Settlement and total

vertical stress results are compared to the recordings in Tables 3.16, and 3.17; and the differences are indicated between the calculated and monitored values.

Table 3.16. Comparison of Settlement Results of 3-D Analysis Model-7 at Km: 0+185

Instrument	Monitored(cm)	Construction(cm)		Impoundment(cm)	
		Result	Diff. (%)	Result	Diff. (%)
ZDO-19	87,42	55,79	-36,18	71,16	-18,60
ZDO-14	63,39	82,94	30,84	96,51	52,25
ZDO-15	74,84	86,89	16,10	93,23	24,57
ZDO-10	96,69	97,57	0,91	102,67	6,18
ZDO-2	64,89	64,08	-1,25	72,96	12,44
ZDO-3	55,54	68,86	23,98	71,66	29,02
ZDO-4	39,80	64,29	61,53	65,72	65,13

Table 3.17. Comparison of Total Vertical Stresses of 3-D Analysis Model-7 at Km: 0+185

Instrument	Monitored(kPa)	Construction(kPa)		Impoundment(kPa)	
		Result /Ar(%)	Diff. (%)	Result	Diff. (%)
TBO-19	229	282 / 33	23,14	388	69,43
TBO-14	512	546 / 0	6,64	662	29,30
TBO-15	436	513 / 2	17,66	545	25,0
TBO-9	650	663 / 1	2,0	849	30,62
TBO-10	1138	876 / 40	-23,02	945	-16,96
TBO-11	635	678 / 0	6,77	702	10,55
TBO-2	1305	810 / 16	-37,93	1037	-20,54
TBO-3	1072	1028 / 49	-4,10	1091	1,77
TBO-4	857	852 / 12	-0,58	872	1,75

Özkuzukıran (2005) stated that, the behavior of the embankment body in reservoir impoundment was reported to be stiffer than in construction period; which was idealized in the analyses by multiplying the stiffness parameters by assumed coefficients to model the behavior. On the other hand, the data on reservoir impoundment period was not available for Afşar Dam, therefore, the analyses carried

out in this study did not follow this assumption, because of the varying deformation behavior monitored. Due to the total contact defined between the concrete face slab and the dam body, no tension stresses occurred in the concrete face; except the lowest point of the valley where the face slab is connected to both bedrock and the dam body.

Considering the horizontal deflections that occur along the concrete face, it was observed that at the end of construction period, the horizontal deformation induced by the settlement of the rockfill body caused the impervious membrane to deform towards the upstream near the maximum section. This deformation pattern was reversed by the reservoir impoundment, resulting in deformation towards the downstream; with maximum values near the crest of the maximum section. On the other hand, maximum settlements of the concrete face slab occurred near the mid-height of the maximum section. Relative horizontal deformation of 14,02 cm was calculated during the reservoir impoundment; and maximum relative vertical deflection of 34,4 cm was calculated for the concrete face slab. Rockfill body and bedrock were taken as perfectly bonded during calculations, so this may result in larger stresses in the concrete face slab. In addition, remembering the stiffness of the rockfill embankment during impoundment period, it may be concluded that the horizontal and vertical deformations of the concrete face slab may be smaller than the calculation results.

CHAPTER 4

SUMMARY AND CONCLUSIONS

4.1. Conclusions

This research was oriented toward the investigation of the deformation behavior of Konya Afşar concrete faced rockfill dam. A review of the literature and case studies were presented, and the analysis methods concerning the embankment construction were evaluated. Initially, the parameters to represent the rockfill characteristics were estimated considering the previous research in the field; followed by preliminary analyses which were carried out for the calibration of material parameters to be used in the study. The reliability of two-dimensional analyses was investigated in comparison to three-dimensional analyses, to observe the effects of valley shape on the overall behavior of a rockfill embankment.

The assumptions made in the various steps of this study can be listed as:

- Hardening Soil model was used for both two-dimensional and three-dimensional analyses of the dam body.
- The foundation below the dam body at the maximum section at Km: 0+185 was assumed to be level, and the bedrock was assumed to be infinitely rigid.
- The lift heights to be assumed in construction stages were studied as 10-m per lift and 5-m per lift; and the final analyses were carried out assuming 5-m lifts for each construction stage of the embankment.
- Concrete face slab was assumed to be impervious and crack propagation which may occur in the construction and impoundment was neglected. As a result, it was assumed that no leakage occurred through the dam body.
- Concrete face slab and rockfill embankment was assumed to be perfectly bonded, having full compatibility in deformations.

- Model material parameters determined from previous studies were made use of to represent the actual deformation results monitored at main points of concern in the two-dimensional analyses and three-dimensional analyses are carried out using the parameters estimated in the preliminary analyses.

In this study it is observed that in the deformation analyses of a CFRD, factors such as assumed lift height, material parameters, valley shape effects, as well as zoning assumptions, should be taken into account.

Idealization of the rockfill embankment body in a single zone results in a symmetrical behavior, which failed to represent the actual settlement and stress values. More compatible results are obtained by utilizing different material parameters for the major zones. Comparing the calculation results of the two-dimensional plane strain analyses with the three-dimensional analyses, the significance of arching effect is also pointed out. It may be concluded that a steep and narrow valley may result in lower settlements, whereas the arching effect may deviate along a stepped valley with varying slopes.

Comparing the calculated deformations with monitored settlements, it is found that the upstream and downstream settlements recorded on elevation 1180.0 are higher than the central settlement value on this elevation. It may be concluded that the difference of the settlement results occurred due to monitoring errors or local property differences which may be present in the rockfill material. Both two-dimensional and three-dimensional analyses yield results proving the unlikelihood of this settlement distribution.

Reservoir impoundment analyses were carried out, and it is observed that the effect of reservoir impoundment diminishes towards the downstream. Because the impoundment data were not available, an increase of stiffness of the dam body was neglected in the analysis, however, the calculated settlement and horizontal deformations were observed to be in acceptable range, referring to the previous studies on CFRD performance. Hydrostatic pressure induced by the reservoir impoundment

was calculated to cause larger deformations at deeper sections; but the bottom points were observed to be where smallest deformations occur, among the central reference points. This result may be attributed to the valley shape effect, providing more considerable resistance to deformations that may occur at lower elevations. In addition, as the reservoir impoundment was not yet realized at the time of this study, the impoundment analyses were carried out to reach predictions regarding the performance of the CFRD in reservoir impoundment stage. It is concluded that the dam body at reservoir impoundment is expected to provide satisfactory performance given the measurements during the construction period.

Considering the deformation analyses in this study, it may be concluded that when evaluating the performance of an embankment body in an asymmetrical, or relatively narrow valley; two-dimensional plane strain analysis may be inadequate to reach reliable results. Although the general characteristics of distribution of stresses and deformations are maintained even in extraordinary cases; valley shape, and material characteristics as well as the different zones may cause different embankment behavior that may not be observed with two-dimensional analyses.

4.2. Recommendations

For future studies, detailed parametric comparisons between the two-dimensional and three-dimensional analyses may be carried out to enhance the available arching effect assumptions that can be used for simpler analyses. Material parameters may be varying within a dam body, as continuum assumptions have shortcomings considering rockfill embankments; therefore, statistical approaches in combination with FEM/DEM may be used in further rockfill embankment modelling. Finally, the analyses carried out must be compared with reliable data for validation. Therefore, quality control is essential in geological instrumentation; especially for a structure type as empirical in design as concrete faced rockfill dams.

REFERENCES

- Adrian, K., & Tschernutter, P. (2017). Embankment behavior: prediction of arching and cracking potential.
- Arı, O. (2016). *Development of a decision support system for optimal instrumentation of concrete faced rockfill dams* (Ph.D.). METU.
- Arici, Y. (2011). Investigation of the cracking of CFRD face plates, *Comput Geotech*, Vol. 38, 905-916.
- Arici, Y. (2013). Behaviour of the reinforced concrete face slabs of concrete faced rockfill dams during impounding. *Structure and Infrastructure Engineering*, 9(9), 877-890.
- Ayvaz, E.O. (2008). *Static analysis of concrete faced rockfill dams and Dim dam application* (M.Sc.). Eskişehir Osmangazi University.
- Bayraktar, A., Kartal, M. E., & Basaga, H. B. (2009). Reservoir water effects on earthquake performance evaluation of Torul Concrete-Faced Rockfill Dam. *Water Science and Engineering*, 2(1), 43-57.
- Burgess, P. J., Sarabia, D., Small, J., Poulos, H. G., & Sinha, J. (2007). Settlement behavior of a major dam. *ANCOLD Bulletin*, 137, 91.
- Chen, S. S., Fu, Z. Z., Wei, K. M., & Han, H. Q. (2016). Seismic responses of high concrete face rockfill dams: A case study. *Water Science and Engineering*, 9(3), 195-204.
- Cooke, J.B. (1960). Symposium on Rockfill Dams. Transactions, ASCE, vol. 104.

- Cooke, J.B. (1984). Progress in Rockfill Dams., (18th Terzaghi Lecture). *Geotech.Engrg.*, ASCE, Vol. 110, Issue 10, 1381-1414.
- Cooke, J.B., & Sherard, J. L. (1987). Concrete-Face Rockfill Dam: I. Assessment, *Geotech. Engrg.*, ASCE, Vol. 113, Issue 10, 1096-1112.
- Cooke, J.B., and Sherard, J. L. (1987). Concrete-Face Rockfill Dam: II. Design, *Geotech. Engrg.*, ASCE, Vol. 113, Issue 10, 1113-1132.
- Cruz, P. T., Materón, B., & Freitas, M. (2010). Concrete face rockfill dams. CRC Press.
- Cundall, P. A., & Strack, O. D. (1979). A discrete numerical model for granular assemblies. *Geotechnique*, 29(1), 47-65.
- Da Silva, A.F. & Assis, A. (2014). Effect of the valley shape on the embankment behavior of concrete face rockfill dams. *Journal of Software Engineering*. 19. 1855-1862.
- Deluzarche, R., & Cambou, B. (2006). Discrete numerical modelling of rockfill dams. *International journal for numerical and analytical methods in geomechanics*, 30(11), 1075-1096.
- DGSI – Vented settlement cells (2018). Retrieved 5 August 2018, from <https://durhamgeo.com/product/vented-settlement-cells/>
- Dorador, L., Anstey, D., & Urrutia, J. (2017). Estimation of geotechnical properties on leached coarse material. *70th Canadian Geotechnical Conference, GeoOttawa*, Ottawa, ON, Canada.

Dorador, L., & Urrutia, J. (2017). Geotechnical characterisation of coarse-grained soils containing weak and strong particles mixtures. *70th Canadian Geotechnical Conference, GeoOttawa*, Ottawa, ON, Canada.

DSI (2014). Baraj ölçüm cihazları teknik şartnamesi. State Hydraulic Works (DSI).

DSI – Afşar Hadimi Barajı İnşaatında %75 fiziki gerçekleşme seviyesine ulaşıldı. (2016). Retrieved 5 March 2017, from <http://www.dsi.gov.tr/haberler/2016/07/29/af%C5%9Far-hadimi-baraj%C4%B1-i-n%C5%9Faat%C4%B1nda-75-fiziki-ger%C3%A7ekle%C5%9Fme-seviyesine-ula%C5%9F%C4%B1ld%C4%B1>

Einav, I. (2007). Breakage mechanics-part 2: modelling granular materials. *Journal of the Mechanics and Physics of Solids*, 55(6), 1298-1320.

Elmi, D., & Mirghasemi, A. A. (2013). Effects of arching on measurement of embedded pressure cell in embankment dam. *7th International Conference on Case Histories in Geotechnical Engineering*, Missouri.

Emiroglu, M. E. (2008). Influences on selection of the type of dam. *International Journal of Science & Technology*, 3(2), 173-189.

Erdoğan, E.E. (2012). *Investigation of the effect of soil structure interaction on the behavior of concrete faced rockfill dams and assessment of current analysis methodologies* (M.Sc.). METU.

Escobar, C., & Posada, A. (2008). Recent Experience on Design, Construction and Performance of CFRD Dams. *International Conference on Case Histories in Geotechnical Engineering*, 1–9.

Fragaszy, R. J., Su, W., & Siddiqi, F. H. (1990). Effects of oversize particles on the density of clean granular soils. *Geotechnical Testing Journal*, 13(2), 106-114.

Gamboa, C. J. N. (2011). *Mechanical behavior of rockfill materials-Application to concrete face rockfill dams* (Ph.D.). École Centrale Paris.

Galloway, J.D. (1939). Symposium - The Design of Rockfill Dams. *Transactions*, ASCE, 104, 1-92.

Gardarsson, S. M., Gunnarsson, A., Tomasson, G. G., & Pfister, M. (2015). Karahnjúkar dam spillway: Comparison of operational data and results from hydraulic modelling.

Gong, W.Q. (2005). The feasibility study stage of Sujiahekou hydropower station: the test study report of weathered materials and rock-fill in location. Kunming: the scientific research branch of Kunming investigation and design institute, Hydrochina Kunming Engineering Corporation.

Gurbuz, A., Peker, I. (2016). Monitored Performance of a Concrete Faced Sand Gravel Dam. *ASCE Journal of Performance of Constructed Facilities* 10.1061/(ASCE)CF.1943-5509.0000870, 04016011.

Guyer, P. (2018). An introduction to rockfill dams. Guyer Partners.

Hoek, E. (2000). Practical rock engineering. Rocscience.

Hoek, E., Carranza-Torres, C., & Corkum, B. (2002). Hoek-Brown failure criterion 2002 edition. *Proceedings of NARMS-Tac*, 1(1), 267-273.

- Hunter, G., & Fell, R. (2003). Rockfill modulus and settlement of concrete face rockfill dams. *Journal of Geotechnical and Geoenvironmental Engineering*, 129(10), 909-917.
- ICOLD, I. (2004). Concrete Face Rockfill Dams-Concepts for Design and Construction. International Commission on Large Dams, Committee on Materials for Fill Dams (Draft).
- Indraratna, B., Wijewardena, L. S. S., & Balasubramaniam, A. S. (1993). Large-scale triaxial testing of greywacke rockfill. *Geotechnique*, 43(1), 37-51.
- Keskin, M., Korkmaz, K., Çarhoğlu, A., & Helvacı, D. (2009). Dim Barajının Deprem Güvenliğinin Dinamik Analizlerle İncelenmesi. *Tübvav Bilim Dergisi*, 2(2), 128-137.
- Korkmaz, S. (2009). *Evaluation of Concrete Face Rockfill Alternative for Dam Type Selection: A Case Study on Gökçeler Dam* (M.Sc.). METU.
- Lade, P. V. (2005). Overview of constitutive models for soils. *Geo-Frontier 2005*.
- Laura, K., & Figene, A. (2008). Dams with impervious membrane of asphalt concrete. *BALWOIS*, 27-31 May 2008, Ohrid, 01-07.
- Likitlersuang, S., Surarak, C., Kim, S., Balasubramaniam, A., Oh, E., & Wanatowski, D. (2013). Duncan-Chang - Parameters for Hyperbolic Stress Strain Behaviour of Soft Bangkok Clay. *Proc. 18th International Conference on Soil Mechanics and Geotechnical Engineering*, 2-7 September 2013, Paris, 381–384. <https://doi.org/10.13140/2.1.3744.8966>
- Lollino, P., Cotecchia, F., Zdravkovic, L., & Potts, D. M. (2006). Numerical analysis and monitoring of Pappadai dam. *Canadian Geotechnical Journal*, 42(6), 1631–1643. <https://doi.org/10.1139/t05-079>

- Lu, M., & McDowell, G. R. (2007). The importance of modelling ballast particle shape in the discrete element method. *Granular Matter*, (9), 69-80.
- Lubliner, J., & Moran, B. (1992). Plasticity Theory. *Journal of Applied Mechanics*, 59(1), 245. <https://doi.org/10.1115/1.2899459>
- Luding, S. (2008). Introduction to discrete element methods: basic of contact force models and how to perform the micro-macro transition to continuum theory. *European Journal of Environmental and Civil Engineering*, 12(7-8), 785-826.
- Ma, H., & Cao, K. (2007). Key technical problems of extra-high concrete faced rock fill dam. *Science in China Series E: Technological Sciences*, 50(1), 20-33.
- Ma, G., Zhou, W., Chang, X. L., & Zhou, C. B. (2011). 3D mesoscopic numerical simulation of triaxial shear tests for rockfill. *Chinese Journal of Geotechnical Engineering*, 33(5), 746-753.
- Ma, H., & Chi, F. (2016). Technical Progress on Researches for the Safety of High Concrete-Faced Rockfill Dams. *Engineering*, 2(3), 332–339. <https://doi.org/10.1016/J.ENG.2016.03.010>
- Marachi, N. D., Chan, C. K., & Seed, H. B. (1972). Evaluation of properties of rockfill materials. *Journal of the Soil Mechanics and Foundations Division*, 98(1), 95-114.
- Marandi, S. M., VaeziNejad, S. M., & Khavari, E. (2012). Prediction of Concrete Faced Rock Fill Dams Settlements Using Genetic Programming Algorithm. *International Journal of Geosciences*, 03(03), 601–609. <https://doi.org/10.4236/ijg.2012.33060>
- Marsal, R.J. (1973). Mechanical properties of rockfill. *Embankment dam engineering, Casagrande volume*, 109-200.

- Materon, B. (1985). Alto Anchicaya dam – ten years performance. *Proceedings, ASCE Symposium, Detroit USA.*
- Materon, B. (2008). Design, construction and behavior of slabs of the highest concrete-faced dams. *CFRD World*, v.2, n.1, CFRD International Society and HydrOu China.
- Modares, M., & Quiroz, J. E. (2015). Structural Analysis Framework for Concrete Faced Rockfill Dams. *International Journal of Geomechanics*, 16(1), 04015024. [https://doi.org/10.1061/\(asce\)gm.1943-5622.0000478](https://doi.org/10.1061/(asce)gm.1943-5622.0000478)
- Mori, T., (1999). Deformation and cracks in concrete face rockfill dams. *Proc. 2nd Symp. on CFRD, Florianopolis*, 49-61.
- Özel, H.F. (2012). *Comparison of the 2D and 3D analyses methods for CFRDs* (M.Sc.). METU.
- Özkan, M.Y. (1998). A review of considerations on seismic safety of embankments and earth and rock-fill dams. *Elsevier*, 17, 439-458.
- Özkuzukıran, R. S. (2005). *Settlement Behaviour Of Concrete Faced Rockfill Dams: A Case Study* (M.Sc.). METU.
- Qian, C. (2008). Immediate development and future of 300 m high CFRD. *CFRD World*, Journal of CFRD International Society, v.2, n.1.
- Plaxis ver. 7- Material Models Manual.
- Resende, F., Materon, B. (2000). Ita method – new construction technology for the transition zone of CFRDs. *Proceedings, International Symposium on Concrete Faced Rockfill Dams, Beijing.*

- Reynolds, O. (1885). LVII. On the dilatancy of media composed of rigid particles in contact. With experimental illustrations. *The London, Edinburgh, and Dublin Philosophical Magazine and Journal of Science*, 20(127), 469-481.
- Roctest – PW series vibrating wire piezometer (2017). Retrieved 5 April 2017, from <https://roctest.com/en/product/pw-series-vibrating-wire-piezometer>
- Roctest – TPC total pressure cell (2016). Retrieved 5 March 2017, from <https://roctest.com/en/product/tpc-total-pressure-cell>
- Rowe, P. W. (1962). The stress-dilatancy relation for static equilibrium of an assembly of particles in contact. *Proceedings of the Royal Society of London. Series A. Mathematical and Physical Sciences*, 269(1339), 500-527.
- Schanz, T., & Vermeer, P.A. (1996). Angles of friction and dilatancy of sand. *International Journal of Rock Mechanics and Mining Sciences and Geomechanics Abstracts*, Vol. 8, No. 33, 349A.
- Schanz, T., Vermeer, P.A., & Bonnier, P.G. (1999). The hardening soil model: formulation and verification. *Beyond 2000 in comp. geotechnics*, 281-296.
- Schofield, A., & Wroth, P. (1968). *Critical state soil mechanics* (Vol. 310). London: McGraw-Hill.
- Shao, L., Chi, S.C., Zhou, L.J., & Wang, Y.Z. (2013). Discrete element simulation of crushable rockfill materials. *Water Science and Engineering*, 6(2), 215-229.
- Siddiqi, F.H. (1984). *Strength evaluation of cohesionless soils with oversize particles* (Ph.D.). University of California, Berkeley.
- Sowers, G.F., & Gore, C.E. (1961). Large Scale Preconstruction Tests of Embankment Materials for an Earth-rockfill Dam. *5th International Conference on Soil Mechanics and Foundation Engineering*, Vol. 2, 717-720.

- Sukkarak, R., Pramthawee, P., & Jongpradist, P. (2017). A modified elasto-plastic model with double yield surfaces and considering particle breakage for the settlement analysis of high rockfill dams. *KSCE Journal of Civil Engineering*, 21(3), 734–745. <https://doi.org/10.1007/s12205-016-0867-9>
- Szostak-Chrzanowski, A., Massiera, M., & Deng, N. (2009). Concrete face rockfill dams-new challenges for monitoring and analysis. *Reports on Geodesy, (génie civil)*, 381–390.
- Tabibnejad, A. (2017). *Evaluation of Collapse Deformation Behavior of a Rockfill Material Using Large Scale Triaxial Tests*. (Ltd), 373–384. <https://doi.org/10.3217/978-3-85125-564-5-051>
- Terzaghi, K. V. (1920). Old earth pressure theories and new test results. *Engineering News Record*, 85(14), 632-637.
- Terzaghi, K.V. (1943). *Theoretical soil mechanics*. (9th ed.). London: John Wiley and Sons.
- Ti, K. S., Gue, S. S., Bujang, B. K. H., Noorzaei, J., & Jaafar, M. S. (2009). A review of basic soil constitutive models for geotechnical application. *Electronic Journal of Geotechnical Engineering*, 18. <https://doi.org/10.4317/medoral.19033>
- Timoshenko, S., & Goodier, J. N. (1951). *Theory of elasticity*. New York: McGraw Hill.
- Tosun, H., Batmaz, S., & Ayvaz, E.O. (2007). CFRD practice in Turkey. *International Water Power and Dam Construction*. 59. 22-23+25.

- Tütüncübaşı Tosun, T. (2015). *Deformation Analysis of Concrete Faced Aydın Karacasu Dam* (M.Sc.). METU.
- TS500, (2000). Requirements for Design and Construction of Reinforced Concrete Structures. Turkish Standards Institution (TSE).
- USBR, (2008). *El Vado Dam Middle Rio Grande Project, New Mexico*, EVMAA-8668460-2008-1, Technical Service Center, U.S. Bureau of Reclamation, Denver, Colorado.
- Wang, L. B., & Yan, Q. (2010). Analyze on development prospects of 300m level ultra-high CFRD from Shuibuya high CFRD. *2010 Asia-Pacific Power and Energy Engineering Conference*, 1-4.
- Wang, Z., Liu, S., Vallejo, L., & Wang, L. (2014). Numerical analysis of the causes of face slab cracks in Gongboxia rockfill dam. *Engineering Geology*, 181, 224–232. <https://doi.org/10.1016/j.enggeo.2014.07.019>
- Xiao, Y., Liu, H., Zhang, W., Liu, H., Yin, F., & Wang, Y. (2016). Testing and modeling of rockfill materials: A review. *Journal of Rock Mechanics and Geotechnical Engineering*, 8(3), 415–422. <https://doi.org/10.1016/j.jrmge.2015.09.009>
- Yang, Z.Y., & Juo, J.L. (2001). Interpretation of sieve analysis data using the box counting method for gravelly cobbles. *Canadian Geotechnical Journal*, 38(6), 1201-1212.
- Yanmaz, A.M. (2006). *Applied Water Resources Engineering* (3rd ed.). Ankara: METU Press.

Yenigün, K., & Yüzgöl, F. (2013). Baraj Güvenliği Açısından Tip Seçimi: ÖYBK Barajlarda Etkin Faktörler ve Ilisu Barajı Örneği. 3. *Bursa Uluslararası Su kongresi ve Sergisi*, 22-24.

Zeller, J., & Wullimann, R. (1957). The shear strength of the shell materials for the Göschenentalp Dam, Switzerland. *4th International Conference on Soil Mechanics and Foundation Engineering*, 399–404.

Zhou, W., Hua, J., Chang, X., & Zhou, C. (2011). Settlement analysis of the Shuibuya concrete-face rockfill dam. *Computers and Geotechnics*, 38(2), 269–280. <https://doi.org/10.1016/j.compgeo.2010.10.004>

Zhou, X., Ma, G., & Zhang, Y. (2018). Grain size and time effect on the deformation of rockfill dams: a case study on the Shuibuya CFRD. *Géotechnique*, (September), 1–14. <https://doi.org/10.1680/jgeot.17.p.299>